ANALYSES OF ECOSYSTEM-PRIMARY PRODUCTION INTERACTIONS IN THE NORTHERN LEVANTINE BASIN

A THESIS SUBMITTED TO
INSTITUTE OF MARINE SCIENCES
OF
MIDDLE EAST TECHNICAL UNIVERSITY

BY

ELİF YILMAZ

IN PARTIAL FULFILMENT OF THE REQUIREMENTS
FOR
THE DEGREE OF MASTER OF SCIENCE
IN
THE DEPARTMENT OF OCEANOGRAPHY

AUGUST 2016

Approval of the thesis:

ANALYSES OF ECOSYSTEM-PRIMARY PRODUCTION INTERACTIONS IN THE NORTHERN LEVANTINE BASIN

Submitted by **ELİF YILMAZ** in partial fulfillment of the requirements for the degree of Master of Science in Oceanography Department, Middle East Technical University by,

Prof. Dr. Ahmet Erkan Kıdeyş _____
Director, Institute of Marine Sciences
Prof. Dr. Süleyman Tuğrul _____
Head of Department, Oceanography
Assoc. Prof. Dr. Barış Salihoğlu_____
Supervisor, Oceanography Dept., METU

Examining Committee Members:

Prof. Dr. Zahit Uysal _____
Marine Biology and Fisheries Dept., METU
Assoc. Prof. Dr. Barış Salihoğlu _____
Oceanography Dept., METU
Assist. Prof. Dr. Ekin Akoğlu _____
Marine Biology and Fisheries Dept., METU

29.08.2016

I hereby declare that all information in this document has been obtained and presented in accordance with academic rules and ethical conduct. I also declare that, as required by these rules and conduct, I have fully cited and referenced all material and results that are not original to this work.

Name, Last name : Elif Yılmaz

Signature:

ABSTRACT

ANALYSES OF ECOSYSTEM-PRIMARY PRODUCTION INTERACTIONS IN THE NORTHERN LEVANTINE BASIN

Yilmaz, Elif

M.S., Department of Oceanography

Supervisor: Assoc. Prof. Dr. Barış Salihoğlu

August 2016

Three areas of different ecosystem characteristics in the Northern Levantine Basin is compared using a 1-D multicomponent lower trophic level ecosystem model developed by SALIHOĞLU, B. et al. (2009) (NAGEM). Main focus was to analyze and compare the carrying capacity (PP) and regulatory mechanisms of the nutrients on lower trophic levels. 26 years' of historical data obtained from METU-IMS data inventory and CORIOLIS was used to form a climatology, to introduce boundary conditions to the model as well as to carry out model skill analyses. At the three sites (Erdemli Times Series, that represents a coastal system, Mersin Bay, that represent offshore waters and Rhodes upwelling area) vertical mixing in winter and stratification in summer are found to play a major role in the distribution of nutrients in the water column resulting shift in ecosystem structure. Furthermore, model results suggest distinct mechanisms that control phytoplankton biomass in each region. In Rhodes upwelling area, highest annual primary production values calculated due to nutrient-rich, deep water carried into the euphotic zone throughout the year. On the other hand,

the strongest and deepest spring bloom occurred at Erdemli coasts which are attributed to increasing riverine input to the area in early spring.

Offshore waters of Mersin Bay have the lowest productivity throughout the year with minor pulses during winter and spring seasons. The model also suggests alterations on limiting nutrients due to changing nutrient budgets among sites. Even though all areas are found to be limited by phosphate, offshore waters of Mersin Bay are also co-limited by nitrogen for autotrophic eukaryotes and diatoms in the summer season. This limitation also occurs in ETS station for diatom species.

Keywords: Eastern Mediterranean, Levantine Basin, primary production, nutrient limitation, ecosystem modeling

ÖZ

KUZEY LEVANT DENİZİ'NDE EKOSİSTEM – BİRİNCİL ÜRETİM ETKİLEŞİMLERİNİN İNCELENMESİ

Yilmaz, Elif
Yüksek Lisans, Oşinografi Bölümü
Tez yöneticisi: Assoc. Prof. Dr. Barış Salihoğlu

Ağustos 2016

Kuzey Levant Baseni'nde değişik ekosistem özelliklerine sahip 3 bölgenin birincil üretimi ve bu bölgelerdeki besin tuzlarının alt trofik seviye üzerindeki kontrol mekanizmalarını analiz etmek ve birbiriyle karşılaştırmak için, SALIHOĞLU, B. et al (2009) (NAGEM) tarafından geliştirilen tek boyutlu, çok değişkenli alt trofik seviye ekosistem modeli kullanılmıştır. ODTÜ DBE veri envanterinden edinilen yaklaşık 26 yıllık data, üzerinde klimatoloji çalışması yapılarak, model sınır koşulları olarak ve model sonuçlarının doğrulanması için kullanılmıştır. Kışın gerçekleşen dikey karışım ve yazın oluşan tabakalaşmanın besin tuzlarının su kolonundaki dağılımı ve dolayısıyla ekosistem yapısındaki değişimlerde çok büyük bir rol oynadığı görülmüştür. Dahası, model sonuçları, her bölgede fitoplankton biokütlesini kontrol eden farklı mekanizmalar olduğunu göstermektedir. Rodos yukarı taşınım bölgesinde yıl boyunca besin tuzu açısından zengin derin suların ışıklı tabakaya taşınmasına bağlı olarak en yüksek yıllık birincil üretim değerleri hesaplanmıştır. Diğer taraftan, bahar ayındaki fitoplankton artışının en güçlü ve en derin olarak

Erdemli kıyılarında gerçekleşmesi, bu bölgede bahar ayında artmakta olan nehir girdileriyle ilişkilendirilmiştir. Kış ve ilkbahar sezonlarında ufak artışlar gösterse de Mersin Körfezi açık suları en düşük birincil üretim değerlerine sahiptir. Model sonuçları, bölgeler arasında değişkenlik gösteren besin tuzu bütçeleri sebebiyle bölgelerdeki birincil üretimi sınırlayıcı besin tuzlarında da değişiklikler olabileceğini göstermektedir. 3 alanda da fosfat, birincil üretimi sınırlayıcı besin tuzu olarak bulunsa da, yaz sezonunda Mersin Körfezi açık sularında diatomlar ve ototrofik ökaryotlar için azotun da eş sınırlayıcı besin tuzu olabileceği görülmüştür. Benzer bir sınırlama yaz aylarında Erdemli kıyılarındaki diatomlar için de geçerlidir.

Anahtar Kelimeler: Doğu Akdeniz, Levant Denizi, birincil üretim, sınırlayıcı besin tuzları, ekosistem modellemesi

To My Family

ACKNOWLEDGMENTS

I wish to express my deepest gratitude to my supervisor Assoc. Prof. Dr. Barış Salihoğlu for his guidance, advice, criticism, encouragement and insight throughout the research. I also would like to thank him for introducing me such an interesting subject.

I would also like to thank Prof. Dr. Zahit Uysal for his valuable suggestions and comments during this study and revisions during finalization of this thesis.

Also, comments of Assoc. Prof. Dr. Mustafa Koçak and Assist. Prof. Dr. Devrim Tezcan were much valuable for this study.

I am grateful to V. Çağlar Yumruktepe, who helped me during the initial configuration process of the model and to Volodymyr Myroshnychenko for providing me with the data used in this study from the IMS-METU database, whenever I need.

I would like to thank the examining committee member Assist. Prof. Dr. Ekin Akoğlu for his revision and advices on my thesis.

I sincerely to thank Anıl Akpınar for his support, especially at hard times.

I always cherished with the friendship and spiritual support of Beybin İlhan, I thank her for her patient and being such a great friend.

I thank Ceren Güraslan for the friendship since the day I arrived at the IMS-METU.

Finally, I would like to thank my family for their endless love, constant support and encouragement all my life.

This study was supported by The Scientific and Technological Research Council of Turkey (TÜBİTAK) in framework of the project with title “Doğu Akdeniz’de Mevcut Farklı Ekosistemlerin – Upwelling Bölgeleri, Açık Deniz ve Kıta Sahanlığı Suları – Dinamikleri, Bakteriyel ve Birincil Üretim Potansiyelleri, Üst Trofik Seviyelere Yansımaları” and with number 111Y023, and by DEKOSİM Project (Deniz Ekosistem ve İklim Araştırmaları Merkez, Project Code BAP-08-11-DPT.2012K120880) financed by the Ministry of Development of Turkey.

The data used in this study is obtained by several project cruises including:

-Development of forecast system for the Cilician Basin (TÜBİTAK 102Y056)
-Researches on the Circulation, Transport and Eutrophication Characteristics on the Coastal Basin of Cilician Basin (TÜBİTAK 104Y277)
-Programme for the Assessment and Control of Pollution in the Mediterranean Region, Phase III (MedPol)
-Impact of phosphorus and nitrogen variations in Northeastern Med. coastal waters to the phytoplankton composition (TÜBİTAK 102Y057)
-Southern European Seas: Assessing and Modeling Environmental Changes (SESAME)
-Urban wastewater management along coastal areas of Turkey: reidentification of hot spots and sensitive areas, determination of assimilation capacities by monitoring and modeling and development of sustainable urban wastewater investment plans (TARAL-SINHA) (TÜBİTAK 107G066)
-TÜBİTAK MAM
-Mediterranean National Monitoring
-Programme for the Assessment and Control of Pollution in the Mediterranean Region, Phase II (MedPol)
-Programme for the Assessment and Control of Pollution in the Mediterranean Region, Phase IV (MedPol)
-Investigation of changes in small pelagic fish stock in the Northeastern Mediterranean (TÜBİTAK 108O566)
-Investigations on the changing impacts on Kızılliman Marine Protected Area and responses of the ecosystem (TÜBİTAK 104Y028)

-Researches in Gulf of Mersin on improvement of fishery by using size-selective trawls (TÜBİTAK 109O684)

-Dynamics and bacterial and primary production potential of distinct ecosystems composed of upwelling regions, shelf and offshore waters in the eastern Mediterranean, reflections on higher trophic levels (TÜBİTAK 111Y023)

-POEM BC

-Dredging Applications and Environmental Management of Dredge Material (DİPTAR)

- The data which were collected and made freely available by the Coriolis project and programmes that contribute to it (http://www.coriolis.eu.org).

TABLE OF CONTENTS

LIST OF TABLES

TABLES

LIST OF FIGURES

FIGURES

CHAPTER 1

INTRODUCTION

1.1. Overall Description of Study Area

1.1.1. Geography and Bottom Topography

Mediterranean Sea is a mid-latitude, semi-enclosed sea which covers 2.523×10^6 km^2 area and has 3.708×10^6 km^3 volume (Lionello et al., 2006). It is connected to the Atlantic Ocean via the Strait of Gibraltar and to the Black Sea via Dardanelles – Marmara – Bosphorus system. The Levantine Basin, which is connected to the Ionian Basin through Cretan Archipelago, is one of the 2 major basins of the Eastern Mediterranean with a volume of 7.5×10^5 km^3 and the maximum depth of 4300m. Northern Levantine Basin apart from the southern part by 34N latitude. It is bounded by Turkish coasts from the north, Cyprus from the south, Rhodes Island from the west and Syria and Iskenderun from the east. It's estimated total area of 111000 km^2 (Ludwig, Dumont, Meybeck, & Heussner, 2009)

Bottom topography of the Northern Levantine Basin has various features. From the east, Gulf of Iskenderun has an exceptionally wide continental shelf. There is a narrow channel between Cyprus and Gulf of Iskenderun with 700m depth which Lattakia and Cilician Basins communicate. Northern Levantine continental slope rapidly steepens through the west till the northwestern part of the Cyprus. In the west part, the continental shelf is narrow and 200 m depths are reached within 10 – 20 km. The depth reaches its maximum at Rhodes Trough (4500 m). Other major troughs are Antalya (2000 – 2500 m), Cilicia (1000 m) and Lattakia (1000 – 1500 m) Basins.

Another significant bottom structure is the Anaximander Seamount (1500 m) which locates between Rhodes and Antalya Basins.

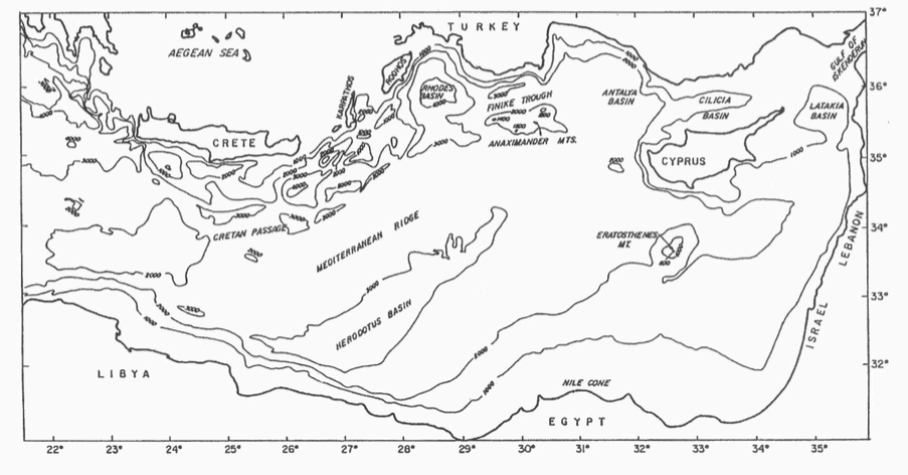

Figure 1. The bottom topography and geography of the Levantine Basin (Özsoy, 1991)

Rhodes Basin, one of the study areas, is located in northwest corner of the Northeastern Levantine Sea between latitudes 35.5 N – 36.5 N and longitudes 27.5 E – 29 E. This basin reaches 4400 m depth and constitutes the deepest part of the eastern Mediterranean between southwest Turkey coasts and east of the Rhodes Island with very steep continental slope. The bathymetry shallows more gradually and reaches the Eastern Mediterranean Ridge (about 2500 m) to the south and Anaximander Seamounts (1500 m) to the east. The Basin is interconnected to Aegean and Cretan Seas through Rhodes Strait (~15 km width, ~850 m sill depth) between Rhodes Island and Asia Minor, and Karpathos Strait (~40 km width, ~850 m sill depth) between Karpathos and Rhodes Islands.

Together with the current systems and climatic conditions, the bottom topography here is thought to have an important role in the formation of Rhodes Cyclonic Gyre whose center takes place at about 36 N, 28.5 E, with a diameter of about 300 km (Milliff & Robinson, 1992).

The second study area is Mersin Bay which lies in the northeast part of the Cilician Basin, between Göksu Delta in the southwest and the Seyhan-Tarsus-Ceyhan Delta in the northeast, covering an area of nearly 1150 km^2 of the continental shelf. With

the discharge of Göksu, Lamas, Seyhan, Ceyhan and Asi Rivers, there is a high volume of fresh water input to the area. However, these waters are mostly trapped in near coasts affected by the circulation patterns in the area.

The depth of the bay is shallow in the northeast and gradually becomes deeper in the southwest. The continental shelf is very wide in this area, and the continental slope is flattened. Near Erdemli from the coastline to 50 m contour the sea-floor slopes approximately 1 degrees, then it even flattens to 0.6 degrees between 50 and 200 m (Ediger, Evans, & Ergin, 1997).

1.1.2. Atmospheric Conditions

Meteorology of the region displays seasonal variability, and it is known to play an important role on the seasonal character of the Eastern Mediterranean circulation. In winter, wind stress follows east – west direction and enters the Levantine basin through the Straits of Sicily. Extratropical cyclones, Poyraz and Sirocco winds form the winter wind regime. Cold and dry Poyraz winds are the major source of LIW formation of the Turkish coastal waters during late winter. It is intensified as it flows through the river valleys and gaps in the Taurus mountains and reaches coastal waters and causes the rapid cooling and buoyancy loss (Özsoy, Hecht, & Ünlüata, 1989). Sirocco winds blow through north African/Arabian deserts carrying warm and dry air to the Northern Levantine Basin and reveals as humid air.
In their review, Malanotte-Rizzoli & Hect (1988) included wind pattern alterations among seasons in Eastern Mediterranean (Figure 2). In summer wind pattern is flattened, blowing through Europe towards Africa, in northwest – southeast direction. Accompanied with mid – latitude Westerlies, Northerly Etesians reaches the southern Aegean and forms the west-northwesterly winds in the Levantine Basin.

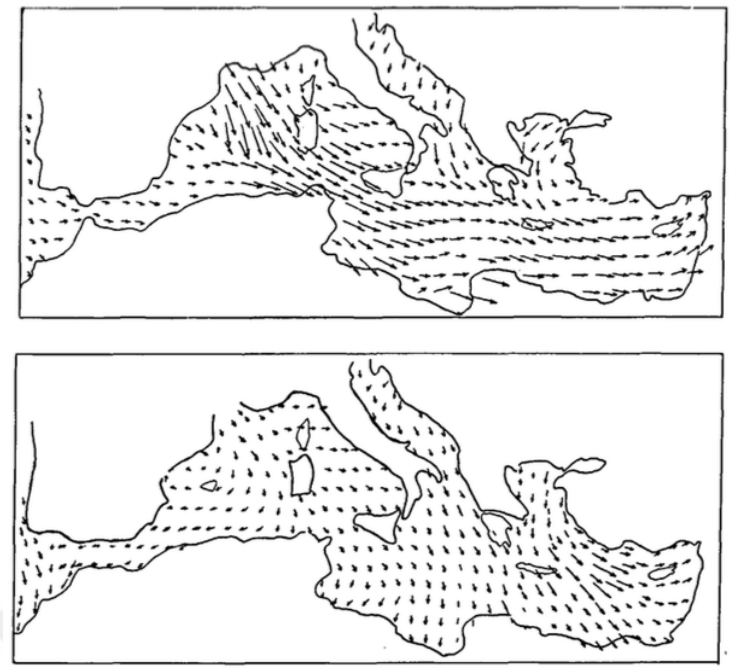

Figure 2. Large-scale properties of the Eastern Mediterranean: a review (Malanotte-rizzoli & Hecht, 1988)

1.1.3. Water Masses and Circulation

The general circulation of the Eastern Mediterranean Sea is a complex system occurring at different spatial scales, consists of permanent and recurrent eddies, gyres and jets, arising from different driving forces like topography, seasonal changes, and internal dynamical processes. Below the general structure of the main study area is discussed, namely Northeastern Levantine Basin (Rhodes Basin and Mersin Bay).

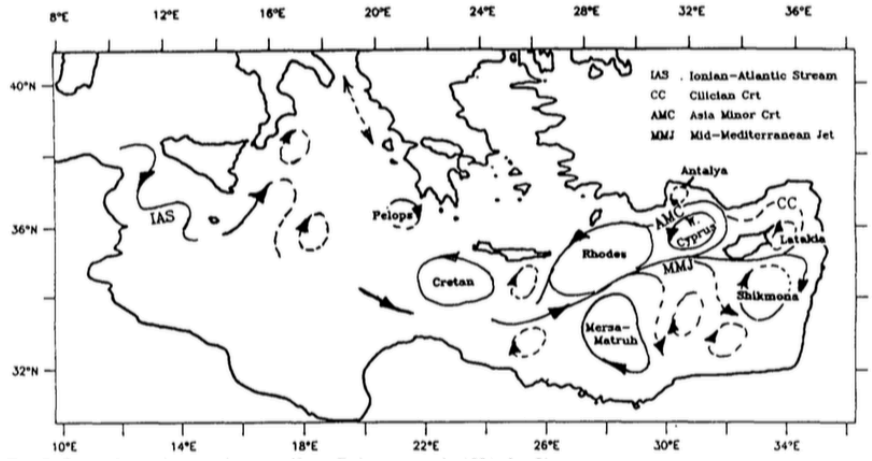

Figure 3. General Circulation of the Eastern Mediterranean (Robinson et al., 1992)

In the Mediterranean Sea, the total evaporation exceeds the precipitation and river runoff (Carter, 1956). To conserve the mass and salinity, there is a continuous water exchange between the North Atlantic Ocean and the Mediterranean Sea through the Strait of Gibraltar. Even though the Eastern Mediterranean isn't directly connected to the Strait of Gibraltar, its circulation and water masses are highly affected by this the two-layered flow regime. Inflow in the upper 150m consists of Atlantic water (AW) with a salinity of about 36.15 ppt ($x10^{-3}$) and temperature 15˚C, whereas outflowing water consists of Western Mediterranean Deep Water and Levantine Intermediate Water (LIW) takes place in the bottom layer with a salinity about 39.1 ppt and temperature about 15˚C.

In winter, there is a net outflux from Mediterranean to North Atlantic (Carter, 1956). As intense mixing events occur upper layer diminishes resulting the AW to mix through the water column and becomes less distinctive than in summer (Hect, 1986). In summer, Mediterranean waters expose more heat and reaches higher evaporation rates resulting in a net influx of AW into the Mediterranean with the contribution of westerlies. Also, summer conditions create an upper hot and saline surface layer that helps AW to maintain its low salinity values and can be observed as a salinity minimum below the Levantine Surface Waters (LSW). AW are named Modified Atlantic Water (MAW) as they arrive in Eastern Mediterranean since they interact with upper and the lower layer waters and slightly loses its properties. They reach southeastern offshore waters of Turkey with a salinity of 38.6 ppt (Özsoy et al. 1981).

Entering the Gibraltar, Ovchinnikov (1966) states that AW reaches the African coast and then carried by the North African current to the Eastern Mediterranean. After passing the Cretan Passage, the northern branch of it continues as a free jet isolated the effects of the coasts and named as Central Levantine Basin Current by Özsoy et al. (1989) and Mid-Mediterranean Jet by Robinson et al. (1992). It bifurcates after passing between the Rhodes and Mersa-Matruh Gyres, branches are flowing in the north and encircles the Rhodes Gyre, in the south, joins the Mersa-Matruh Gyre. Core flow moves eastward and bifurcates again in the southwest of Cyprus. Remaining waters pass from the south of the Cyprus and reach the eastern boundary

of Northern Levantine Basin. Near the Israel coasts, MMJ flows through the south. Özsoy et al. (1993) observed that only a small portion of it moves northwards and enters the Cilician Basin and feeds the Cilician Current then flows westwards parallel to the shoreline of the Mersin Bay and then joins Asian Minor Current. Thanks to the blocking effect of the coastline topography, few number of fluctuating weak eddies occupies Mersin Bay (Ünlüata, Oguz, & Özsoy, 1983). The flow patterns of the Cilician Basin pictured by Collins and Banner (1979), based on the study conducted by combining ERTS imagery and secchi depths, geostrophic computations which are modified from Engel (1967) and hydrographic observations of Akyüz (1957). They also stated the existence of quasi – permanent cyclonic flow along the Mersin Bay.

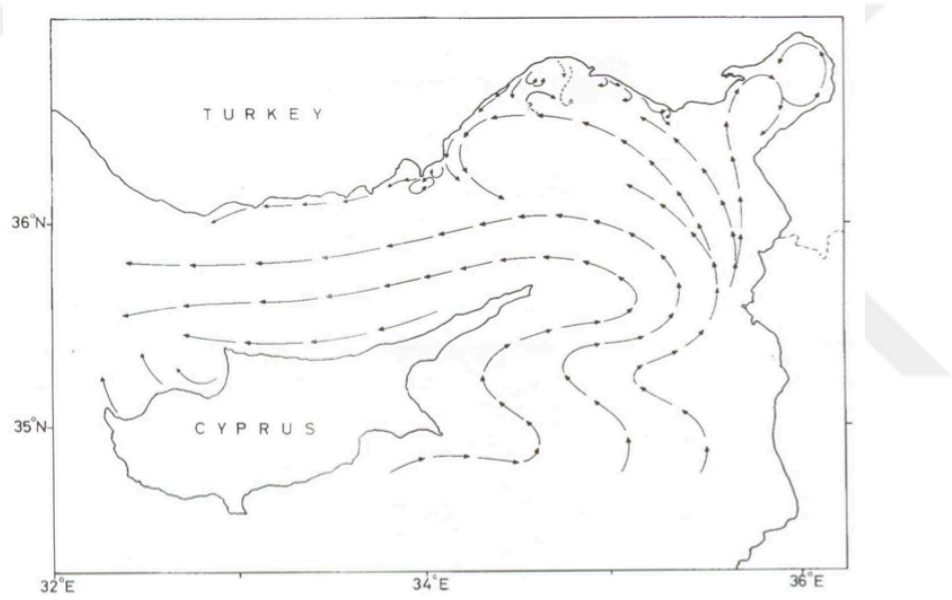

Figure 4. General Circulation Patterns of the Cilician Basin (Collins & Banner, 1979)

Asia Minor Current flows westward by meandering and joining some permanent and quasi-permanent gyres and eddies on the southern coasts of Turkey. Significant of these are persistent anticyclonic Anaximander eddy located between the Anaximander Seamounts and Anatolian coast, anticyclonic Antalya eddy located in the western part of the Cilician Basin and West Cyprus cyclonic eddy located in the west of the Cyprus Island (Onken & Yuce, 2000; Özsoy et al., 1993). AMC then joins the permanent cyclonic Rhodes Gyre and eventually flows westwards along the southwest Anatolian coast.

Because of high surface temperature and evaporation rates, Levantine Surface Water (LSW) is characterized by a high temperature (~ 28˚C) salinity (> 39 psu). It is thought to play an important role in the formation of Levantine Intermediate Water (LIW). LIW has one of the most important water masses in the Eastern Mediterranean since it is produced in the Northeastern Levantine, especially in Rhodes Basin and has a great impact on the general thermohaline circulation of the Mediterranean Sea as it spread from the formation regions (Wüst, 1961, Özsoy, 1981).

Ovchinnikov and Plakhin (1984) suggest that formation of LIW is a thermohaline process that requires a couple of conditions including a thin surface layer at the center of the cyclonic gyre, relatively warm and salty waters in the intermediate layer. With the help of intrusion of cold and dry air masses, LSW gets intensely cool; it becomes denser than the intermediate layers and convective mixing occurs. Özsoy and Ünlüata (1983) observed that these events coincide with Poyraz events. LIW comprises approximately 26% of the net water volume of the Mediterranean Sea (Ovchinnikov, 1984). It can be observed below MAW with an increase in salinity (38.95 – 39.05 psu) between depths 200 m and 600 m. After its formation, it flows through west and finally exits from Gibraltar Strait.

Below LIW, Eastern Mediterranean Deep Water (EMDW) exist. The origin of EMDW was a debate if it is formed in the Aegean Sea (Nielsen, 1912) or the southern part of the Adriatic Sea (Pollak,1951). Lascaratos, Williams, & Tragou (1993) support the idea that it is originated in the Adriatic Sea, then flows eastward through the Ionian Basin and reaches the Eastern Mediterranean Sea with his modeling study. In 1994, Roether et al. used tritium and ^{3}He to trace the origins, prove Pollak's (1951) results This thermohaline cell is completed by the return of these waters that are upwelled in Eastern Mediterranean. (Roether, Roussenov, & Well, 1994)

1.1.4. Nutrients, Biology, and Production

Mediterranean Sea is widely known as the most oligotrophic ocean in the world with low nutrient low chlorophyll concentrations (LNLC). The nutrient inputs are limited

in both internal and external sources, resulting in extremely low amounts of primary production about 109.4 $gCm^{-1}yr^{-1}$. Primary production decreases further through the Eastern part of the Mediterranean and has been observed as low as 86.8 $gCm^{-1}yr^{-1}$ in the Northern Levantine Basin (Antoine & Morel, 1995)

The main reason for poor nutrient conditions are attributed to anti-estuarine circulation, that is as balancing the water budget of the Mediterranean Sea, nutrient depleted Atlantic surface water enters the basin and in return, relatively nutrient-enriched intermediate and deep waters are carried out to the North Atlantic by the two-layer flow regime of the Strait of Gibraltar (Béthoux & Copin-Montégut, 1986; Bethoux, Morin, Madec, & Gentili, 1992; Krom, Emeis, & Van Cappellen, 2010). Atlantic inflow with a volume of $53x10^{12}$ m^3 yr^{-1} exceeds the volume of the outflow of Mediterranean waters, $50.5x10^{12}$ m^3 yr^{-1} with a difference of $2.5x10^{12}$ m^3 yr^{-1}. Mean P concentration of Mediterranean outflowing waters estimated to be ~ 0.28 µmol L^{-1} and Atlantic inflow with ~ 0.05 µmol L^{-1} whereas the N concentration was 6 µmol L^{-1} and < 1 µmolL^{-1} respectively resulting nutrient poor conditions in the Mediterranean Sea.

Bethoux and Montegut (1986,1988) estimated the nutrient budget by calculating the water exchanges through the Straits of Gibraltar, terrestrial inputs and river runoffs and found that Atlantic inflow supplies only 20% of the nutrients that flow out of the Mediterranean. Also, nitrogen concentrations are very high in the Mediterranean Sea. They hypothesized that this unexpected values of N budget arise from high rates of N_2 fixation with the highest contribution of *Posidonia* species. Historical and recent evaluations support that Mediterranean has a high N concentration. Very high molar ratio of N/P (> 16:1) has been calculated with an increasing trend from west to east which implies the phosphate limitation on primary production. N/P ratio is calculated for the whole Mediterranean as ~ 21-23 (Bethoux et al., 1992) whereas for the Eastern Mediterranean as ~ 28 in the deep waters (Krom, N., & L.I., 1991; Yilmaz & Tugrul, 1998). However, as a contradiction to Bethoux &Montegut (1986,1988); Krom (2010) claims that during N budget estimations, Bethoux didn't include atmospheric deposition of N and P. Based on a few recent evidence, he states that N_2 fixation and denitrification rates in Eastern Mediterranean is relatively very low and that the high N/P ratios is mainly resulted from atmospheric depositions

(N/P=117:1), with the contribution of riverine discharges that have N/P ratios significantly higher than the Redfield Ratio. Ludwig et al. (2009) support that the riverine inputs are phosphorus limited and also adds the dissolved silica components is controlled by water discharge. Recent climate change and dam construction reduces the discharge of fresh water and also Si input. Ludwig hypothesized that this reduction might limit the production of diatoms and cause a shift in primary production to nonsiliceous species at coastal areas in the future.

In his work, Koçak et al. (2010), analyzing dry and wet atmospheric and riverine data sampled from Erdemli, Turkey, states that the atmospheric depositions dominate the N and P fluxes of the Northern Levantine Basin and accounts for ~ 90% of N and ~ 60% of P input, whereas Si input was highly originated by riverine runoff (~ 90%). He also calculated N/P ratios of the atmosphere and riverine as ~ 233:1 and 28:1 respectively, concluding that this input may even provoke more phosphorus deficiency. To observe the coastal water ecosystem and assess the riverine nutrients, Doğan-Sağlamtimur & Tuğrul (2004) conducted a case study on Erdemli and observed signs of eutrophication in coastal waters of Mersin Bay. Inshore waters influenced by Lamas River which has fluctuated but has high N/P ratio most of the year. Lamas River is modified in May by rainfall that includes dust from Saharan Desert with high phosphate content. Primary Production is co-limited by N and P Mersin Bay showing seasonal variations (Yücel, 2013; Zohary et al., 2005). River input and mixing in winter also reduces the light attenuation and limits the primary production especially in coastal areas. The ending of the winter mixing and increasing light availability gives rise to phytoplankton bloom. Inshore waters have mean chlorophyll concentrations varying between 0.066 – 2.49 µg/L and offshore varies between 0.014 – 0.38 µg/L. The primary production varied between 0.024 – 14.42 and 0.007 – 1.48 $mgCm^{-3}h^{-1}$ in the shelf and offshore waters respectively (Yüce, 2013). In oligotrophic oceans like Mediterranean Sea, especially in high temperatures primary production is highly dominated by picoplankton *Synechococcus* (Uysal & Koksalan, 2010). In shelf waters of Mersin Bay (near Erdemli), the highest biomass of phytoplankton is observed during winter with the dominance of diatoms contributing ~ 90% of the annual average total phytoplankton biomass. During summer, however, the most abundant species is *Synechococcus* (Uysal & Köksalan, 2006). Phytoplankton biomass decreases significantly from

coast to offshore waters. In their study between 2004 and 2006, Zenginer and Beşiktepe (2010) calculated the zooplankton abundance in the coastal areas was about ten times higher than offshore waters. Zooplankton abundance in the Mediterranean Sea has two maxima in a year, one in late winter or early spring and the other in autumn.

Other than anthropogenic, riverine and atmospheric inputs in the Mediterranean, the most input of nutrient needed for primary production is internally supplied by winter mixing that introduces nutrient-rich deep waters to the biogenic layer. Especially in the center of cyclonic gyres, with upwelling from the deep layers, nutrients are carried to the euphotic zone (Salihoğlu et al., 1990; Yilmaz & Tugrul, 1998). One example of such region, Rhodes Gyre is known as the most productive area in Northern Levantine Basin with annual primary production ~97 gCm^2yr^{-1} (Napolitano, Oguz, Malanotte-Rizzoli, Yilmaz, & Sansone, 2000)

1.2. Objectives

Modeling 3 separate areas that show distinct characteristics to determine:

- The carrying capacity (PP) and its transfer to the upper trophic levels
- The governing factors of the primary productivity
- The effects of upwelling on lower trophic level ecosystem and primary production
- The effect of limiting nutrients on ecosystem dynamics
- The effect of the river and terrestrial inputs on ecosystem dynamics (coastal ecosystem)

CHAPTER 2

MODEL STRUCTURE

To analyze the ecosystem dynamics, one-dimensional multicomponent lower trophic level ecosystem model (Salihoglu et al., 2008) developed for oligotrophic and mesotrophic oceans (NAGEM) adapted to specific conditions of these three areas. Since the study area contains both oligotrophic and mesotrophic regions, the model structure was ideal to address the research questions of the thesis. Also, model has the capacity to address phosphate and nitrate limitations on the growth of algal groups and the suppression of Silicate on diatom growth. The model has necessary equations to consider the limitations which differs among these three regions while estimating the primary production.

2.1. Model compartments and flow

Five algal groups included in the model are cyanobacteria group (Low and High Light adapted *Prochlorococcus*, *Synechococcus*) with cell size ~ 0.9μm, autotrophic eukaryotes ~ 2.5 μm, and diatoms ~ 15 μm . As shown in Figure 5, Nitrogen, Phosphorus and Silicate are uptaken from the nutrient pool by photosynthetic species and included into their cell structure, and dissolved oxygen is released into the water. While nitrogen and phosphorus are used by all algal groups, silicate is only used by diatoms. Losses from the algal group are via natural mortality and zooplankton grazing. Through mortality, phytoplankton biomass with small particles slowly sink forming slow sinking detritus. As these particles sink, they aggregate, get heavier and form fast sinking detritus.

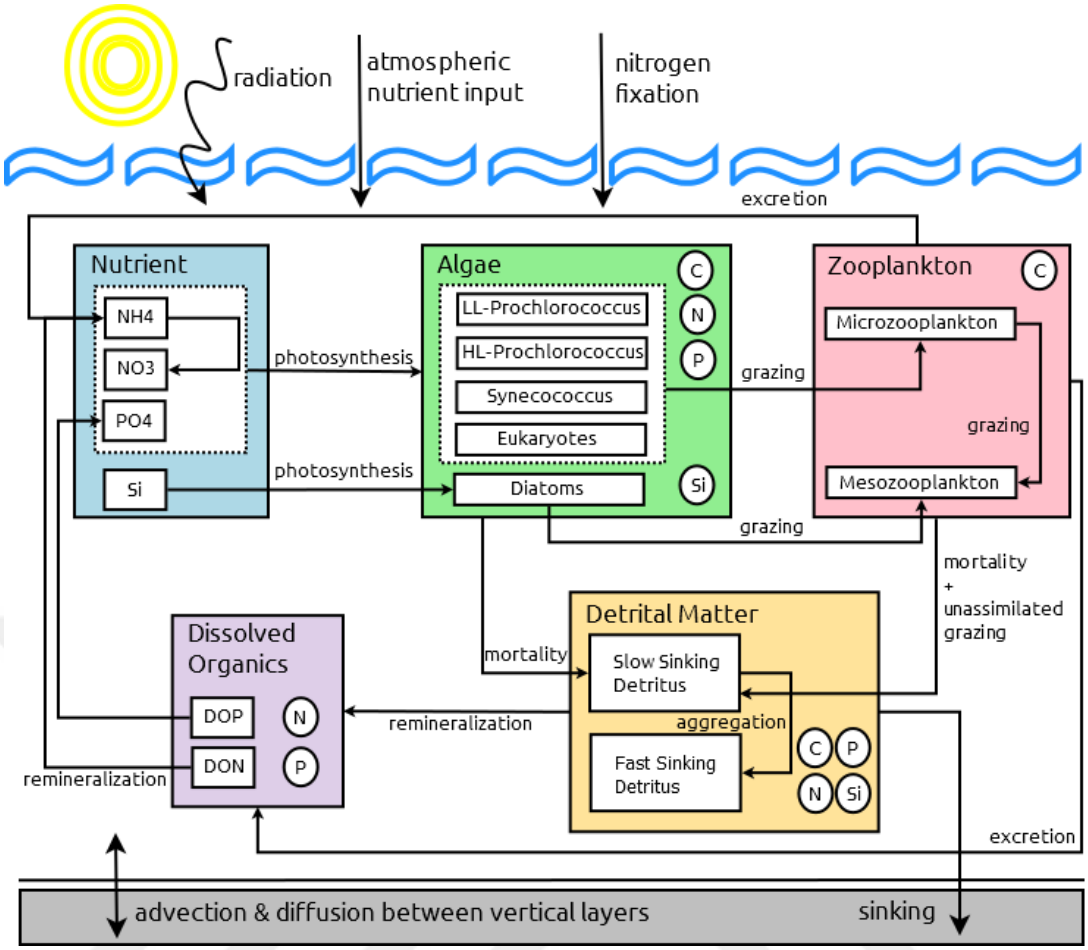

Figure 5. Model flow chart

Zooplankton group is divided into 2 groups as microzooplankton that pass 200 µm mesh and mesozooplankton with size 200 – 2000 µm. Microzooplankton is grazing on cyanobacteria group and autotrophic eukaryotes whereas mesozooplankton are fed on diatoms and microzooplankton. Fecal pellets of zooplankton group join the dissolved organic matter and nutrient pools. Organic material arising from zooplankton mortality and unassimilated grazing mixes with detritus. Some part of detrital matter dissolves in the water column where other part sinks and is buried deep inside sediment. Dissolved Organic Phosphorus (DOP) and Nitrogen (DON) join nutrient pool as PO_4 and NH_4 respectively. Other than regenerated nutrients, atmospheric nutrient input and nitrogen fixation are other nutrient sources. Light attenuation under the surface and the simulation of underwater light field is obtained by coupling a bio-optical model which is explained by Salihoglu (2005) in detail. These material and light transfers occurring at certain rates and functions are

determined by various studies and the ones used for this model are explained in next section.

2.2. Model Equations

2.2.1. Phytoplankton State Equations

The phytoplankton dynamics are expressed as following equation:

$$\frac{\partial AG_i}{\partial t} + w\frac{\partial AG_i}{\partial z} - \frac{\partial}{\partial z}K_z\frac{\partial AG_i}{\partial z} = \left[\min\left(\mu_{ll_i}, \mu_{nul_i}\right)\right]AG_i - m_i AG_i - I_{AG_i}Z_{s+l} \qquad for\ i = 1{,}5 \tag{1}$$

The left side of the equation stands for time variations (t), vertical (z) advection (w) and vertical diffusive flux (K_z). In the right side of the equation includes light (μ_{ll_i}) and nutrient (μ_{nul_i})limited growth, natural mortality (m_i) and grazing pressure of micro and mesozooplankton (Z_{s+l}) on algal groups. All processes are expressed in terms of carbon. The definitions and units used in equations are given in Table 1.

The net growth rate is calculated based on least available resource theory and is the minimum of light and nutrient-limited growth rates which are determined from temperature and is of the form:

$$\mu_{mt_i}(z,t) = \mu_{m_i} exp^{0.0633(T(z)-27)} \tag{2}$$

where μ_{m_i} is the maximum growth rate at 27°C and μ_{mt_i} is the temperature dependent maximum growth rate for each algal group.

Table 1 Definitions and units of variables or parameters used in the equations that describe the dynamics of phytoplankton particulate carbon, nitrogen, phosphorus, and silicon for each algal group(Details and references can be found in (Salihoglu, Garçon, Oschlies, & Lomas, 2008)

Symbol	Definition	Units
μ_{ll}	Light-limited carbon-specific growth rate	h^{-1}
μ_{nul}	Nutrient-limited carbon-specific growth rate	h^{-1}
m	Phytoplankton-specific death rate	h^{-1}
μ_{mt}	Maximum, temperature-dependent carbon-specific growth rate	h^{-1}
μ_m	Maximum, 24 h, carbon-specific growth rate at 27 °C	d^{-1}
g_{AG}	Phytoplankton-specific grazing coefficient	d^{-1}
Λ	Ivlev coefficient of grazing	$(mmol\,C\,m^{-3})^{-1}$
$\rho_{NO_3^-}$	Absolute nitrate transport flux	$\mu mol\,N\,l^{-1}\,d^{-1}$
$\rho_{NH_4^+}$	Absolute ammonium transport flux	$\mu mol\,N\,l^{-1}\,d^{-1}$
$\rho_{PO_4^{3-}}$	Absolute phosphate transport flux	$\mu mol\,P\,l^{-1}\,d^{-1}$
ρ_{Si}	Absolute silicate transport flux	$\mu mol\,Si\,l^{-1}\,d^{-1}$
$K_{sNO_3^-}$	Half saturation constant for nitrate uptake	$\mu mol\,NO_3^-\,l^{-1}$
ψ	Nitrate uptake repression exponent	$(\mu mol\,NH_4^+\,l^{-1})^{-1}$
$K_{sNH_4^+}$	Half saturation constant for ammonium uptake	$\mu mol\,NO_3^-\,l^{-1}$
$K_{sPO_4^{3-}}$	Half saturation constant for phosphate uptake	$\mu mol\,PO_4^{3-}\,l^{-1}$
K_{sSi}	Half saturation constant for silicate uptake	$\mu mol\,Si\,l^{-1}$
$\bar{\mu}$	Growth rate at maximum cellular nutrient concentrations	d^{-1}
K_{QN}	Subsistence quota for nitrogen-limited growth	$\mu mol\,N\,(\mu mol\,C)^{-1}$
Q_N	Cellular nitrogen status of the algal group	$\mu mol\,N\,(\mu mol\,C)^{-1}$
K_{QP}	Subsistence quota for phosphorus-limited growth	$\mu mol\,P\,(\mu mol\,C)^{-1}$
Q_P	Cellular phosphorus status of the algal group	$\mu mol\,P\,(\mu mol\,C)^{-1}$
K_{QSi}	Subsistence quota for silicate-limited growth	$\mu mol\,Si\,(\mu mol\,C)^{-1}$
Q_{Si}	Cellular silicate status of the algal group	$\mu mol\,Si\,(\mu mol\,C)^{-1}$
QN_{max}	Maximum allowed nitrogen to carbon ratio in each algal group	$\mu mol\,N\,(\mu mol\,C)^{-1}$
QP_{max}	Maximum allowed phosphorus to carbon ratio in each algal group	$\mu mol\,P\,(\mu mol\,C)^{-1}$
QSi_{max}	Maximum allowed silicate to carbon ratio in each algal group	$\mu mol\,Si\,(\mu mol\,C)^{-1}$

Light-limited growth is given as the following formulation, whose details are not mentioned here but could be found at Salihoglu&Hoffmann (2007)

$$\mu_{ll_i}(z,t) = tanh\left[\frac{\alpha_i(E_0(z)-E_0cp_i)}{\mu_{mt_i}(z,t)}\right]\left[\frac{\alpha_i(E_0(z)-E_0cp_i)}{\mu_{mt_i}(z,t)}\right]e^{-dr_i(E_0(z)-E_0inb_i)}\mu_{mt_i}(z,t), \quad for\ i = 1{,}5 \tag{3}$$

where $E_0(z)$ is the scalar irradiance at depth z, E_0cp_i is compensation irradiance and E_0inb_i is the inhibiting light level.

Zooplankton grazing on algal groups are given by Franks et al. (1986):

$$I_{AG_i} = g_{AG_i}\Lambda AG_i(1 - e^{-\Lambda AG_i}) \tag{4}$$

where the maximum grazing rate of zooplankton interpreted as g_{AG_i} and the Ivlev coefficient for zooplankton grazing denoted by Λ. The phytoplankton particulate nitrogen, phosphorus, and silicate is given as a set of equations:

$$\frac{\partial AGN_i}{\partial t} + w\frac{\partial AGN_i}{\partial z} - \frac{\partial}{\partial z}K_z\frac{\partial AGN_i}{\partial z} = \rho_{NO_{3_i}} + \rho_{NH_{4_i}} - m_i AGN_i - I_{AGN_i}Z_{s+l}$$
$$\frac{\partial AGP_i}{\partial t} + w\frac{\partial AGP_i}{\partial z} - \frac{\partial}{\partial z}K_z\frac{\partial AGP_i}{\partial z} = \rho_{PO_{4_i}} - m_i AGP_i - I_{AGP_i}\left[Z_s\left(\frac{P}{C}\right)_{Z_s} + Z_l\left(\frac{P}{C}\right)_{Z_l}\right]$$
$$\frac{\partial AGSi_5}{\partial t} + w\frac{\partial AGSi_5}{\partial z} - \frac{\partial}{\partial z}K_z\frac{\partial AGSi_5}{\partial z} = \rho_{Si_5} - m_5 AGSi_5 - I_{AGSi_i}Z_l \quad (5)$$

Physical processes are expressed on the left side of the equation whereas on the right side, ρ denotes uptake of nutrient, second term natural mortality and third term, grazing by microzooplankton (Z_s) and mesozooplankton (Z_l). Uptake rate of phosphorus by each algal group are explained via Monod function based on the ambient phosphate concentration which is of the form:

$$\rho_{PO_4^{3-}{}_i}(z,t) = \mu_{mt_i}(z,t)AGP_i\left[\frac{PO_4^{3-}}{K_{sPO_4^{3-}{}_i} + PO_4^{3-}}\right] \quad (6)$$

in the right side of the μ_{mt_i} term is for temperature-dependent-specific growth rate and $K_{sPO_4^{3-}{}_i}$ is the half saturation constant for phosphate uptake which is phosphate concentration at which one-half the maximum rate is obtained.

The equation for nutrient-limited growth rate is as follows:

$$\mu_{nul_i}(z,t) = \bar{\mu}_i(z,t)\left[1 - \frac{K_{QN_i}}{Q_{N_i}(z,t)}\right]\left[1 - \frac{K_{QP_i}}{Q_{P_i}(z,t)}\right]\left[1 - \frac{K_{QSi_5}}{Q_{Si_5}(z,t)}\right] \quad (7)$$

Algal group actual particulate nitrogen to carbon, particulate phosphorus to carbon and particulate silicon to carbon ratios are represented by $Q_{N_i}(z,t)$, $Q_{P_i}(z,t)$ and

Q_{Si_3}(z,t) and shown in equation (7) respectively. At maximum ratios of these, algal group growth rate is denoted as $\bar{\mu}_i(z,t)$. The subsistence ratios are given by K_{QN_i} , K_{QP_i} , and K_{QSi_5} at points zero growth rate occurs.

$$Q_{N_i}(z,t) = \frac{AGN_i}{AG_i}\,, \qquad Q_{P_i}(z,t) = \frac{AGP_i}{AG_i}, \qquad Q_{Si_5}(z,t) = \frac{AGSi_5}{AG_i} \tag{8}$$

When the particulate matter ratios reached to a maximum, excess nitrogen and phosphorus are released as DON and DOP, and uptake of silicate stops. The formulation of maximum growth rate that is calculated upon maximum particulate ratios is given below

$$\bar{\mu}_i(z,t) = \mu_{mt_i}(z,t)\left[1 - \frac{K_{QN_i}}{QN_{max_i}}\right]^{-1}\left[1 - \frac{K_{QP_i}}{QP_{max_i}}\right]^{-1}\left[1 - \frac{K_{QSi_5}}{QSi_{max_5}}\right]^{-1} \tag{9}$$

Table 2 Values of parameters used in the equations describing the dynamics of each algal group (Details and references can be found in Salihoğlu et. al. 2008)

Parameter	*AG1*	*AG2*	*AG3*	*AG4*	*AG5*
m	0^{1}	0^{1}	0^{1}	0^{1}	0.15^{1}
μ_m	$0.58^{2,3}$	$0.56^{2,3}$	$0.8^{2,4,5}$	1.8^{6}	1.0^{6}
g_{AG}	$4^{7,8}$	$4^{7,8}$	$4^{7,8}$	$4^{7,8}$	$5^{9,10}$
$E_o$cp	1.0^{2}	6^{2}	6^{2}	$10^{11,12}$	8^{11}
dr	0.1^{13}	0.001^{13}	—	—	—
$E_o$inb	40^{2}	105^{2}	—	—	—
ϕ_m	0.0833^{3}	0.0833^{3}	0.0833^{14}	0.0833^{14}	0.0833^{14}
K_{sNO_3}	0.1^{15}	0.1^{15}	0.167^{16}	0.417^{16}	2.29^{17}
ψ	1000^{16}	1000^{16}	6.5^{16}	2.6^{16}	1.462^{18}
K_{sNH_4}	0.05^{15}	0.05^{15}	0.083^{16}	0.208^{16}	2.18^{17}
K_{sFe}	0.01^{16}	0.01^{16}	0.01^{16}	0.02^{6}	$0.12^{19,20}$
K_{sSi}	—	—	—	—	1.2^{21}
K_{QN}	0.18^{5}	0.18^{5}	0.18^{5}	$0.07^{11,22,23,24}$	0.06^{25}
K_{QFe}	$2 \times 10^{-3^{6}}$	$2 \times 10^{-3^{6}}$	$2 \times 10^{-3^{6}}$	$3.0 \times 10^{-3^{6}}$	$5.5 \times 10^{-3^{6}}$
K_{QSi}	—	—	—	—	0.18^{26}
QN_{max}	0.29^{5}	0.29^{5}	0.29^{5}	$0.18^{11,22,23,24}$	0.16^{25}
QFe_{max}	$31 \times 10^{-3^{6}}$	$31 \times 10^{-3^{6}}$	$31 \times 10^{-3^{6}}$	$50 \times 10^{-3^{6}}$	$50 \times 10^{-3^{6}}$
QSi_{max}	—	—	—	—	0.315^{26}

Superscripts refer to the references that provide the source for the parameter value given in the table, and the citation is provided below. The parameters that are not required by a particular algal group are indicated by —. [1]Leonard *et al.* (1999); [2]Moore *et al.* (1995); [3]Partensky *et al.* (1993); [4]Cuhel and Waterbury (1984); [5]Kana and Glibert (1987a); [6]Sunda and Huntsman (1995); [7]Landry *et al.* (1995); [8]Verity *et al.* (1996); [9]Dam *et al.* (1995); [10]Roman and Gauzens (1997); [11]Richardson *et al.* (1983); [12]Sakshaug *et al.* (1987); [13]Bissett *et al.* (1999b); [14]Sakshaug *et al.* (1991); [15]Harrison *et al.* (1996); [16]See text for calculations; [17] Zhang and Zou (1997); [18]Wroblewski (1977); [19]Coale *et al.* (1996b); [20]Fitzwater *et al.* (1996); [21]Nelson and Treguer (1992); [22]Laws and Bannister (1980); [23]Sakshaug *et al.* (1989); [24]Flynn *et al.* (1994); [25]Geider *et al.* (1998); [26]Takeda (1998).

2.2.2. Zooplankton State Equations

Microzooplankton governing equation is given as:

$$\frac{\partial Z_s}{\partial t} + w\frac{\partial Z_s}{\partial z} - \frac{\partial}{\partial z}K_z\frac{\partial Z_s}{\partial z} = \sum_{i=1}^{2} \lambda^* I_{AG_i} Z_s - I_{Z_s} Z_l - e_s Z_s - m_{Z_s} Z_s \tag{10}$$

The left side of the equation implies the changes of zooplankton in space and time, where on the right side these changes are expressed. The first term is assimilated ingestion of grazed phytoplankton biomass with an efficiency λ^*. The second term is the grazing of mesozooplankton grazing on microzooplankton explained by Franks et

al. (1986) with microzooplankton-specific grazing rate $g_{Z_{s_i}}$ and Ivlev constant g_{AG_i}. The term e_s stands for microzooplankton excretion rate and m_{Z_s} is the microzooplankton mortality rate.

The equation explaining mesozooplankton dynamics is similar to microzooplankton equation

$$\frac{\partial Z_l}{\partial t} + w\frac{\partial Z_l}{\partial z} - \frac{\partial}{\partial z}K_z\frac{\partial Z_l}{\partial z} = \lambda^* I_{AG_3} Z_l + \lambda^* I_{Z_s} Z_l - e_l Z_l - m_{z_l} Z_l \tag{11}$$

Grazing on diatoms and microzooplankton are the source of increase in phytoplankton biomass whereas excretion and mortality are the loss terms. Excreted nitrogen and phosphorus by microzooplankton and mesozooplankton joins DON and DOP respectively.

2.2.3. Nutrient State Equations

Inorganic nitrogen is composed of recycled nitrogen, ammonium and new nitrogen, nitrate. Nitrate dynamics are explained following state equation

$$\frac{\partial NO_3^-}{\partial t} + w\frac{\partial NO_3^-}{\partial z} - \frac{\partial}{\partial z}K_z\frac{\partial NO_3^-}{\partial z} = \partial NO_3^- - \sum_{i=1}^{5}\rho_{NO_3^-{}_i} + nitr + \delta(z)(FN + Nfix) \tag{12}$$

The only loss term of nitrate is the uptake by algal groups, where nitrate is gained by nitrification (nitr), atmospheric deposition (FN) and nitrogen fixation (Nfix). The atmospheric nitrogen deposition and nitrogen fixation take place only at the surface, and they are mixed vertically.

The gain and loss terms of ammonium are expressed as

$$\frac{\partial NH_4^+}{\partial t} + w\frac{\partial NH_4^+}{\partial z} - \frac{\partial}{\partial z}K_z\frac{\partial NH_4^+}{\partial z} = \sum_{i=1}^{5}\left(-\rho_{NH_4^+\,i}\right) - nitr + 0.5e_sZ_s\left(\frac{N}{C}\right)_{Z_s} + 0.5e_lZ_l\left(\frac{N}{C}\right)_{Z_l} + c_aDe_sN + c_aDe_lN \tag{13}$$

The uptake of phytoplankton species and nitrification leads to consumption of ammonium in the water column whereas it is accumulated with excretion by microzooplankton and mesozooplankton and remineralization of small De_sN and large detrital nitrogen De_lN. To estimate the nitrogen amount in zooplankton excretion, carbon pools of zooplankton groups are converted to nitrogen. The remineralization rate of DON to ammonium is assumed to be a function of temperature as

$$c_a(z) = c_a^* T_{func}(z) \tag{14}$$

T_{func} is obtained from Moore (2012), where remineralization rate of detrital nitrogen is set to 30°C, and T(z) is the water temperature at depth z.

$$T_{func} = e^{\left(-4000*\left[\left(\frac{1}{T(z)+273.15}\right)-\left(\frac{1}{303.15}\right)\right]\right)} \tag{15}$$

The phosphate dynamics are governed by

$$\frac{\partial PO_4^-}{\partial t} + w\frac{\partial PO_4^-}{\partial z} - \frac{\partial}{\partial z}K_z\frac{\partial PO_4^-}{\partial z} = -\sum_{i=1}^{5}\rho_{PO_4^{3-}\,i} + c_aDe_sP + c_aDe_lP \tag{16}$$

The change of phosphate in the water column is affected by uptake by phytoplankton and remineralization of large and small detritus.

The governing equation of silicate which is only used by diatoms is

$$\frac{\partial Si}{\partial t} + w\frac{\partial Si}{\partial z} - \frac{\partial}{\partial z}K_z\frac{\partial Si}{\partial z} = -\rho_{Si_3} + c_{Si}De_l Si \tag{17}$$

With the uptake of silicate by diatom, the concentration of this element decreases and dissolution of large detritus to silicon leads to increase. The detrital silicon is assumed to dissolve at rate c_{Si} that changes according to T_{func}

2.2.4. DOM State Equations

DOM composed of DON and DOP which are considered to include both labile and semi-labile pools. The only difference between DON and DOP equations is DON pool contains only 50% of the zooplankton excretions whereas DOP pool contains all portion of them.

$$\frac{\partial DON}{\partial t} + w\frac{\partial DON}{\partial z} - \frac{\partial}{\partial z}K_z\frac{\partial DON}{\partial z} = 0.5e_s Z_s\left(\frac{N}{C}\right)_{Z_s} + 0.5e_l Z_l\left(\frac{N}{C}\right)_{Z_l} + c_{DON}De_s + c_{DON}De_l + c_a DON \tag{18}$$

$$\frac{\partial DOP}{\partial t} + w\frac{\partial DOP}{\partial z} - \frac{\partial}{\partial z}K_z\frac{\partial DOP}{\partial z} = e_s Z_s\left(\frac{P}{C}\right)_{Z_s} + e_l Z_l\left(\frac{P}{C}\right)_{Z_l} + c_{DOP}De_s + c_{DOP}De_l + c_a DOP \tag{19}$$

Terms on the right side of the equations represent excretions of microzooplankton and mesozooplankton, remineralization of small and large detrital material and remineralization of DOM respectively. To estimate the nitrogen and phosphorus amounts in zooplankton excretion, carbon pools of zooplankton groups are converted to nitrogen.

2.2.5. Detritus State Equations

The dynamics of small detrital carbon is explained as following equation

$$\frac{\partial De_s}{\partial t} + (w + sc_{des})\frac{\partial De_s}{\partial z} - \frac{\partial}{\partial z}K_z\frac{\partial De_s}{\partial z} = \sum_{i=1}^{5}\left[m_i P_i + (1-\lambda^*)I_{P_i}Z_s\right] + m_{Z_s}Z_s + (1-\lambda^*)\left(I_{P_3} + I_{Z_s}\right)Z_l + m_{Z_l}Z_l - c_c De_s - aggDe_s \quad (20)$$

The left side of the equation explains the spatial and temporal changes, where sinking of the small detritus is considered to be at a constant rate. Small detritus gaining terms are unassimilated grazed fractions of phytoplankton which are grazed by zooplankton groups and microzooplankton which are grazed by mesozooplankton, mortality of phytoplankton groups, microzooplankton and mesozooplankton. Loss terms are aggregation to fast sinking detritus and demineralization of small detritus. Remineralization of small detritus carbon is assumed to dissolve at the rate c_c that changes according to T_{func}. The governing equation that explains large detrital carbon loss and gaining terms is of the form

$$\frac{\partial De_l}{\partial t} + (w + sc_{del})\frac{\partial De_l}{\partial z} - \frac{\partial}{\partial z}K_z\frac{\partial De_l}{\partial z} = aggDe_s - c_c De_l \quad (21)$$

Where input is gained by aggregation of slow sinking detritus and loss occurs via remineralization which is assumed to be the same as small detrital carbon.
DON bottom value is estimated by Pujo-Pay et al. (2011) for Eastern Mediterranean biogenic layer as 4.7±0.7 μmol, and it is stated that this value did not change significantly for whole Eastern Mediterranean. Also DON:DOP ratio is found as 50:1 by Krom et al. (2005). These results are implemented into the model equations.

Table 3 Definitions, values, and units of the parameters used in the zooplankton, nutrient, and detritus governing equations. (Details and references can be found in Salihoğlu et. al. 2008)

Symbol	Definition	Value	Units
Λ	Ivlev coefficient of grazing	1[1]	$(\text{mmol C m}^{-3})^{-1}$
e_s	Mesozooplankton excretion rate	0.1[2,3,4]	d^{-1}
m_{Z_s}	Mesozooplankton death rate	0.6	d^{-1}
e_l	Microzooplankton excretion rate	0.1[2,3,4]	d^{-1}
m_{Z_l}	Microzooplankton death rate	0.5	d^{-1}
λ^*	Zooplankton assimilation efficiency	0.75[1]	Unitless
g_{Z_s}	Mesozooplankton-specific grazing coefficient	15[5,6]	d^{-1}
nitr	Nitrification rate of ammonium to nitrate	0.05[7]	d^{-1}
FN	Aeolian nitrogen deposition at the surface	Estimated	$\mu\text{mol N m}^{-2}\,\text{d}^{-1}$
Nfix	Nitrogen fixation	Estimated	$\mu\text{mol N m}^{-2}\,\text{d}^{-1}$
c_a^*	Remineralization rate of DON to ammonium	0.018[8]	d^{-1}
c_P^*	Remineralization rate of DOP to phosphate	0.018[8,9,10]	d^{-1}
c_{Si}^*	Dissolution rate of detritus to silicate	0.1[11]	d^{-1}
c_{DON}^*	Remineralization rate of detritus to DON	0.16[8,12]	d^{-1}
c_{DOP}^*	Remineralization rate of detritus to DOP	0.16[8,9,10]	d^{-1}
sc_{des}	Small detritus sinking rate	2[8]	m d^{-1}
sc_{del}	Large detritus sinking rate	30[8]	m d^{-1}
agg	Aggregation rate of small detritus to large detritus	0.01[13]	d^{-1}
c_c^*	Remineralization rate of detritus to carbon	0.1[8]	d^{-1}

Superscripts refer to the references that provide the source for the parameter value and the citations are as follows: [1]Leonard et al. (1999); [2]Landry et al. (1996); [3]Hutchins and Bruland (1995); [4]Steinberg et al. (2000); [5]Dam et al. (1995); [6]Roman et al. (2002); [7]see text for calculations; [8]Laws et al. (2000); [9]Karl and Bjorkman (2002); [10]Benitez-Nelson (2000); [11]Nelson et al. (1995); [12]Bronk (2002); [13]Jackson and Burd (1998).

CHAPTER 3

DATA & MODEL SETUP

Climatology analysis has been conducted to simulate the one-year ecosystem dynamics by taking monthly averages of ~ 26 years' data. 1992 data excluded from the data set since in this year extreme cooling event occur in the troposphere with significant temperature drops of 1-2 °C, data characteristics are not a good estimator of the remaining structure (Malanotte-rizzoli, Paola, 1998). The depth for model implementation is chosen as 200 m from the surface thinking that this depth is below the euphotic zone, and so the primary production remains in the range of the chosen water column. For 1 year run, temperature and mixed layer depth are forced as physical values whereas initial nutrients calculated for several depths then interpolated for each depth. Bottom nutrients for every month is calculated and interpolated for each day. Also sea surface net solar radiation is given as initial value to the model. After implementing the model initial and boundary conditions, in the model run, 6-year spin-up is conducted for the model to reach the steady-state level. FORTRAN90 is used for solving model equations, MATLAB and SURFER are used for climatology analysis, visualize and evaluate the model results and Ocean Data View is used to monitor the historical data set.

3.1. Temperature & Mixed Layer Depth

Erdemli Time Series (ETS) data obtained with biweekly cruises to 3 stations between 1997 – 2002 by METU-IMS. After 2013 with wider time steps, similar data has been started to collect. This data set contains temperature (°C) and salinity (PSU) values obtained via CTD profilers.

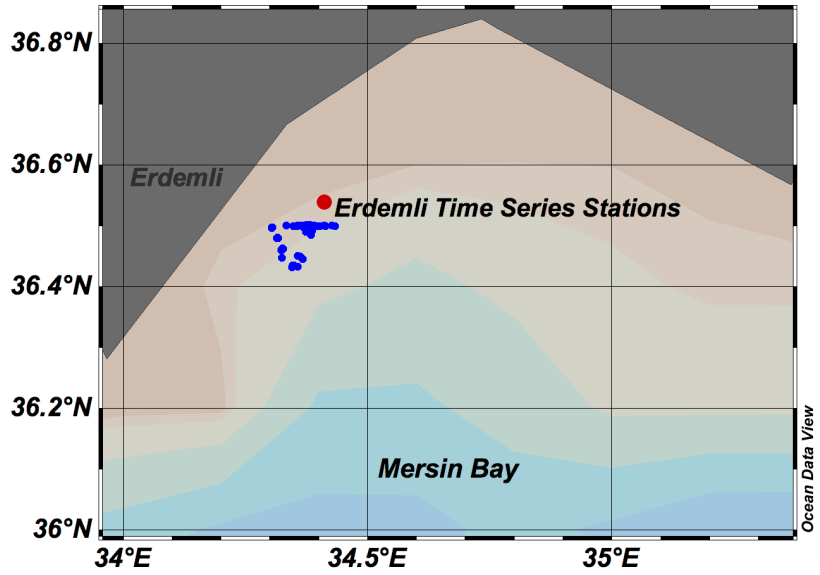

Figure 6. ETS stations map

Deepest station of ETS where the bottom depth reaches 200 m is chosen for this study. Totally 274 CTD profiles are used. Monthly distribution of these stations are shown in Table 4

Data for offshore waters of the Mersin Bay between years 1988 - 2014 is obtained from METU-IMS data inventory that contains various project cruises station data is obtained.

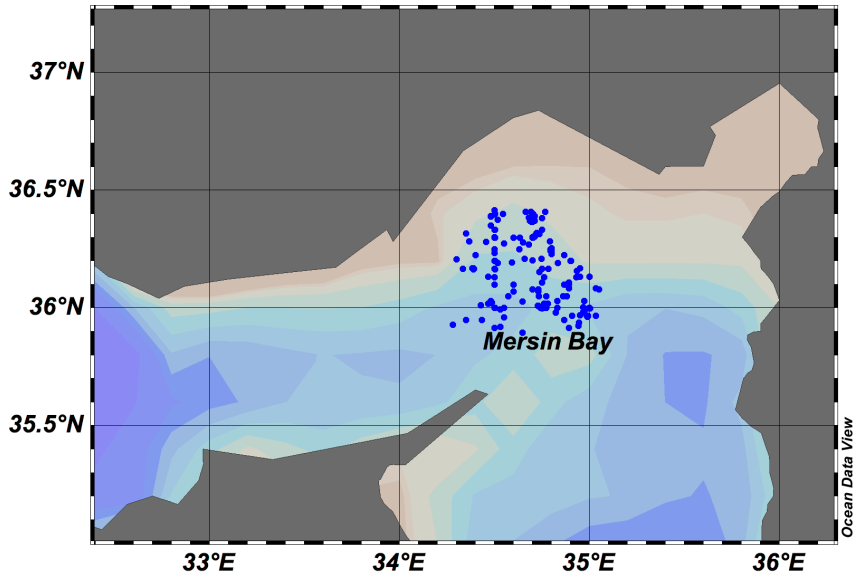

Figure 7. Mersin Bay Offshore stations map

326 CTD profiles that include temperature (°C) and salinity (PSU) parameters used for Mersin Bay. Their monthly variation is given in Table 4.

As in the Mersin Bay, data is provided from METU-IMS for Rhodes Basin. Stations were scarce especially for January and February due to harsh weather conditions in this area, so additional data from CORIOLIS, (these data were collected and made freely available by the Coriolis project and programs that contribute to it (http://www.coriolis.eu.org) is obtained and used. Since the center of the Rhodes Gyre is aimed to study, the location of the cyclonic gyre is retained with reference of a modelling study conducted by Marullo et al (2003) where TOPEX/Poseidon altimeter data (sea level anomalies) were used to observe the changes of the dimension and position of the Rhodes cyclone.

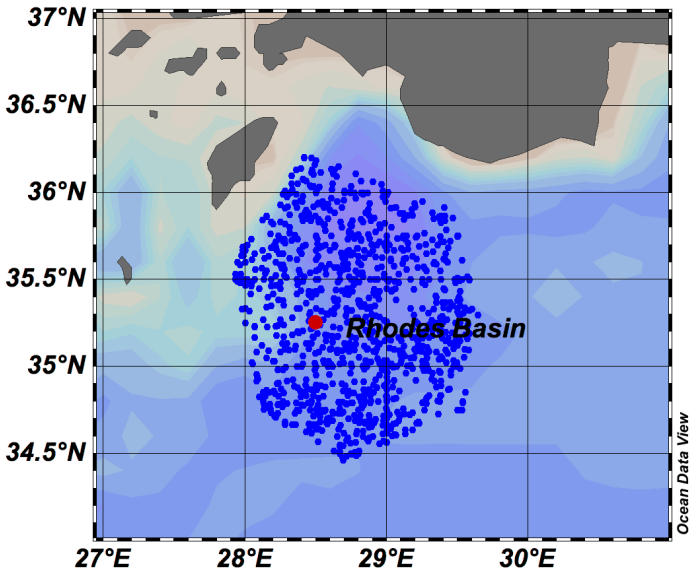

Figure 8. Rhodes Basin stations map

1153 CTD stations used with the same parameters and they are spread among months as in Table 4.

Table 4 Number of CTD profiles used in each region.

#of CTD stations	*ETS*	*Mersin Bay*	*Rhodes Basin*
January	*17*	*8*	*65*
February	*21*	*18*	*73*
March	*24*	*43*	*86*
April	*31*	*27*	*84*
May	*41*	*45*	*94*
June	*29*	*41*	*46*
July	*21*	*44*	*88*
August	*20*	*20*	*111*
September	*15*	*37*	*97*
October	*21*	*14*	*162*
November	*13*	*29*	*177*
December	*21*	*11*	*70*

One-year data for 1m resolution is constructed using temperature values obtained by taking monthly averages of the historical data for each depth and interpolating as hourly time intervals. The resulting temperature distribution for ETS, Mersin Bay, and Rhodes Basin are plotted as in Figure 9.

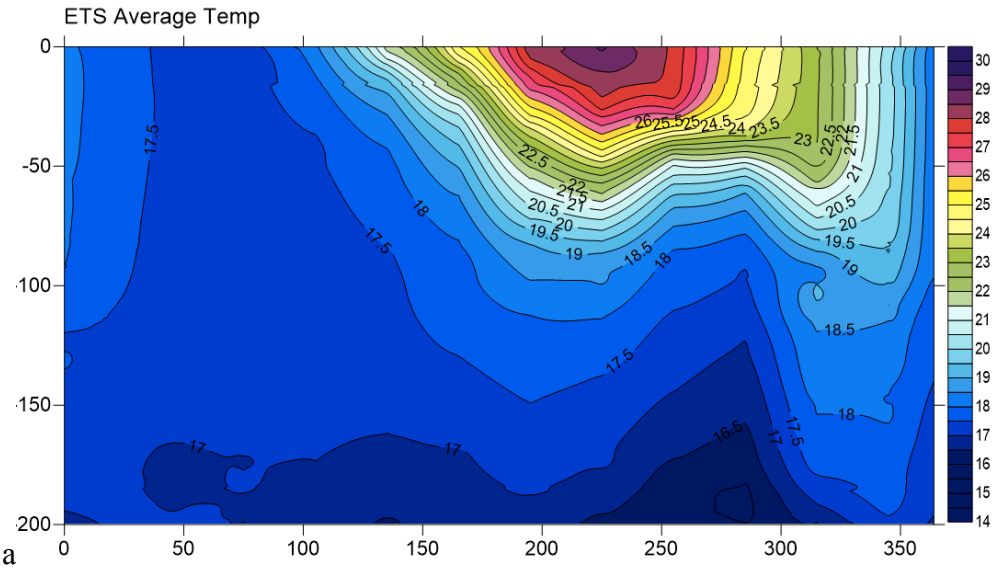

a

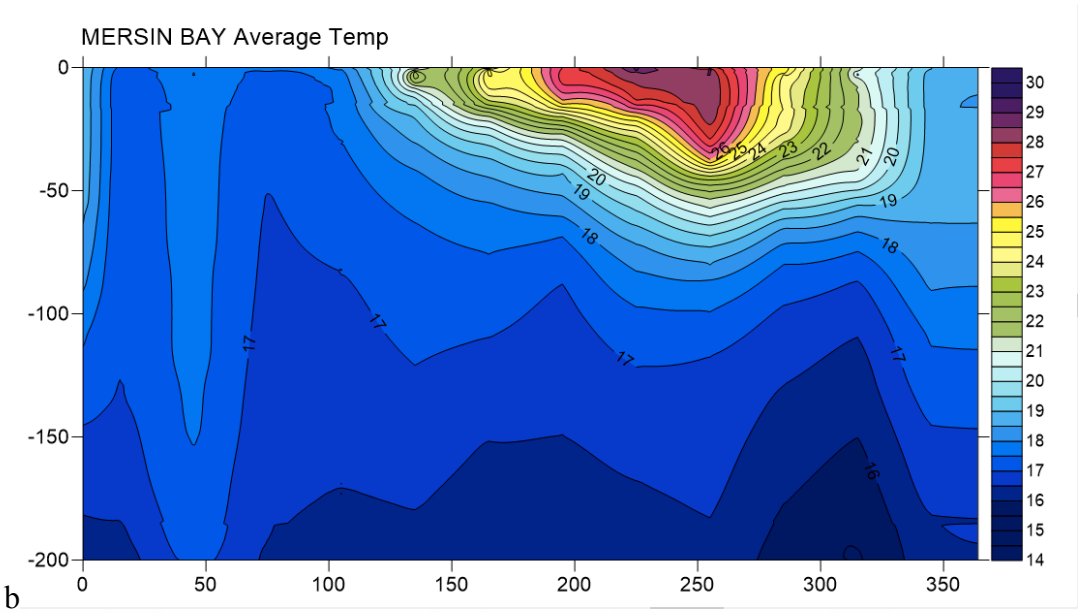

b

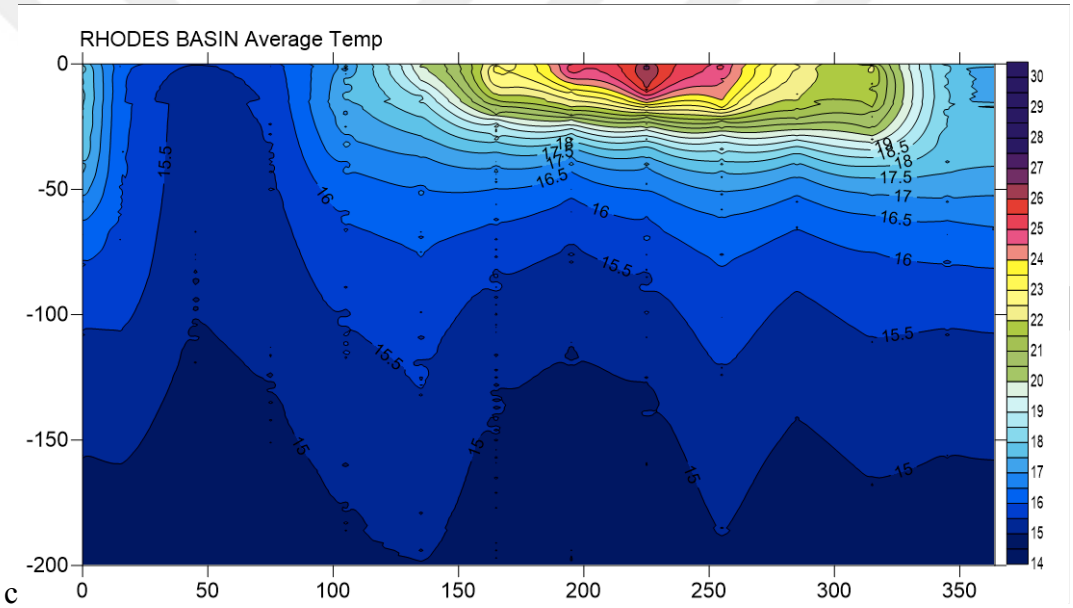

c

Figure 9. Distribution of temperature along the water column during one year.

Mixed Layer Depth is assigned to the depth that is 0.5°C lower than 10 m from the surface (D'ortenzo et al. 2005).

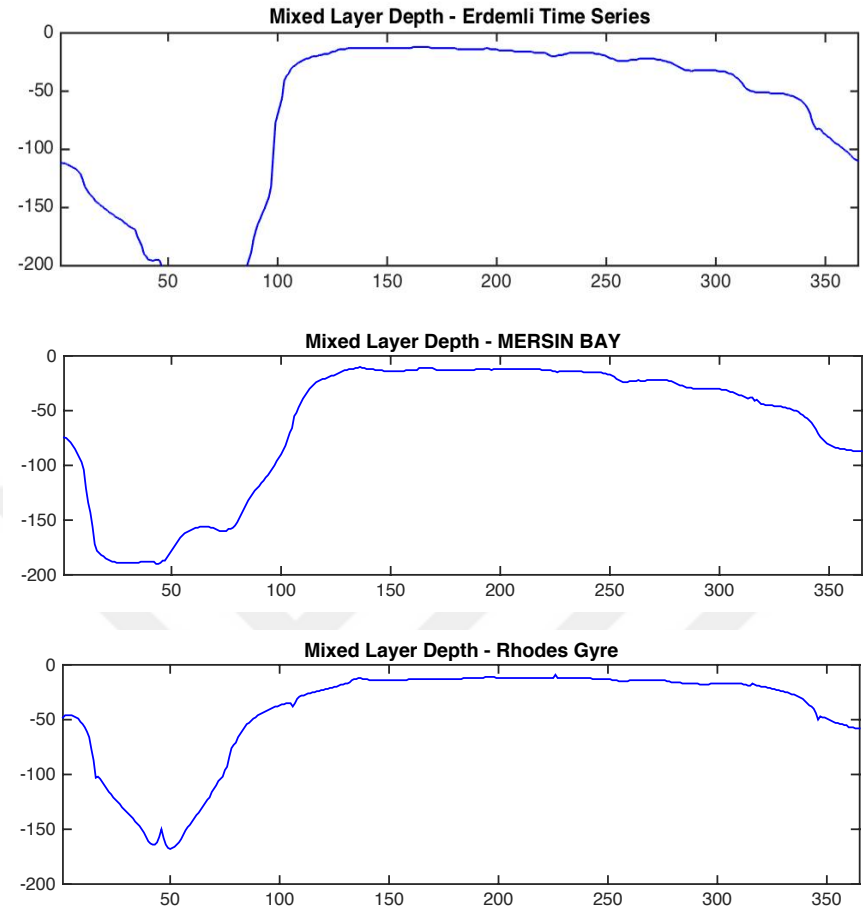

Figure 10. Mixed Layer Depth Estimations

3.2. Nutrients

The point of stations is the same as stated for CTD profilers. From the water samples collected in different depths, in laboratory experiments nitrate (NO_3_N_NO_2_N (µmol/L)), phosphate (PO_4 (µmol/L)), silicate (Si (µmol/L)) and Chl-a (µg/L) values are measured. Totally 200 nutrient stations measurements and 203 Chl-a stations measurements used for ETS region and their monthly distribution is as follows

Table 5 Number of nutrient and chl-a samples for Erdemli stations

Erdemli #of stations	*Nutrients*	*Total Chl-a*
January	*11*	*11*
February	*12*	*12*
March	*22*	*22*
April	*17*	*17*
May	*22*	*22*
June	*21*	*21*
July	*20*	*21*
August	*12*	*15*
September	*13*	*17*
October	*15*	*16*
November	*18*	*12*
December	*17*	*17*

Initial values for nutrients are calculated 25 m depth interval since data abundance were measured highest in these depths. Then these initial values were interpolated to 200 m for each depth. Bottom nutrients were calculated as monthly averages on 200 m and interpolated as 1-hour time interval.

Table 6 Initial boundary nutrients for Erdemli stations

Depth	*NO_3*	*PO_4*	*Si*
0	*0.19*	*0.042941*	*1.40*
25	*0.18*	*0.04*	*1.37*
50	*0.17*	*0.04*	*1.24*
75	*0.29*	*0.04*	*1.31*
100	*0.22*	*0.03*	*1.46*
125	*0.34*	*0.02*	*1.35*
150	*0.52*	*0.03*	*1.46*
175	*1.01*	*0.03*	*1.82*
200	*1.48*	*0.07*	*2.31*

Table 7 Bottom boundary nutrients for Erdemli stations

Days	***Depth***	***NO_3***	***PO_4***	***Si***
1	*200*	*0.96*	*0.07*	*2.22*
15	*200*	*1.29*	*0.06*	*1.76*
45	*200*	*0.48*	*0.06*	*2.02*
75	*200*	*0.76*	*0.03*	*1.69*
105	*200*	*0.88*	*0.04*	*1.94*
135	*200*	*2.05*	*0.05*	*2.27*
165	*200*	*2.16*	*0.03*	*2.49*
195	*200*	*1.64*	*0.03*	*2.36*
225	*200*	*1.29*	*0.05*	*1.66*
255	*200*	*3.17*	*0.07*	*3.99*
285	*200*	*2.83*	*0.06*	*3.27*
315	*200*	*2.17*	*0.05*	*2.73*
345	*200*	*0.96*	*0.07*	*2.22*
375	*200*	*1.29*	*0.06*	*1.76*

186 nutrient stations and 286 Chl-a stations used for Mersin Bay. The parameters are the same that used for ETS stations, and their monthly distribution is shown in Table 8.

Table 8 Number of nutrient and chl-a samples for Mersin Bay stations

Mersin #of stations	***Nutrients***	***Total Chl-a***
January	*6*	*8*
February	*9*	*13*
March	*27*	*45*
April	*11*	*22*
May	*19*	*26*
June	*13*	*30*
July	*22*	*34*
August	*13*	*17*
September	*20*	*33*
October	*12*	*19*

November	*24*	*27*
December	*10*	*12*

Initial and bottom nutrient values calculated as mentioned above and given as Table 9

Table 9 Initial boundary nutrients for Mersin Bay stations

Depth	***NO_3***	***PO_4***	***Si***
0	*0.09*	*0.02*	*1.65*
25	*0.11*	*0.03*	*1.82*
50	*0.08*	*0.02*	*1.80*
75	*0.00*	*-*	*-*
100	*0.34*	*0.02*	*1.71*
125	*0.13*	*0.02*	*1.55*
150	*0.69*	*0.02*	*1.88*
175	*-*	*-*	*-*
200	*1.12*	*0.03*	*2.13*

Table 10 Bottom boundary nutrients for Mersin Bay

Days	***Depth***	***NO***	***PO***	***Si***
-15	*200*	*1.12*	*0.03*	*2.13*
15	*200*	*0.30*	*0.03*	*1.12*
45	*200*	*0.60*	*0.03*	*1.09*
75	*200*	*1.01*	*0.04*	*2.16*
105	*200*	*0.88*	*0.04*	*1.64*
135	*200*	*1.73*	*0.05*	*1.95*
165	*200*	*1.10*	*0.04*	*1.63*
195	*200*	*1.98*	*0.09*	*1.74*
225	*200*	*0.59*	*0.05*	*1.69*
255	*200*	*1.49*	*0.05*	*1.98*
285	*200*	*1.90*	*0.07*	*2.30*
315	*200*	*1.77*	*0.02*	*2.79*
345	*200*	*1.12*	*0.03*	*2.13*
375	*200*	*0.30*	*0.03*	*1.12*

200 nutrient stations and 91 Chl-a stations used for Rhodes Basin with the same parameters and their monthly distribution is as Table 11.

Table 11 Number of nutrient and chl-a samples for Rhodes Basin stations

Rhodes #of stations	***Nutrients***	***Total Chl-a***
January	*-*	*-*
February	*14*	*7*
March	*30*	*7*
April	*10*	*4*
May	*17*	*9*
June	*14*	*3*
July	*32*	*13*
August	*7*	*7*
September	*13*	*5*
October	*46*	*26*
November	*8*	*4*
December	*9*	*6*

Initial and bottom nutrients for Rhodes Basin is calculated in the same manner and as follows:

Table 12 Initial boundary nutrients for Rhodes Basin

Depth	***NO_3***	***PO_4***	***Si***
0	*-*	*0.06*	*-*
25	*0.20*	*0.07*	*1.20*
50	*0.20*	*0.07*	*1.50*
75	*-*	*0.06*	*-*
100	*4.71*	*0.11*	*4.40*
150	*4.95*	*0.14*	*5.52*
200	*5.15*	*0.17*	*6.09*

Table 13 Bottom boundary nutrients for Rhodes Basin

Days	***Depth***	***NO***	***PO***	***Si***
-15	*200*	*5.15*	*0.17125*	*6.09*
45	*200*	*4.89*	*0.16*	*6.98*
75	*200*	*3.95*	*0.21*	*4.62*
135	*200*	*3.55*	*0.14*	*4.09*
195	*200*	*4.77*	*0.20*	*5.36*
225	*200*	*4.98*	*0.15*	*5.35*
255	*200*	*3.43*	*0.13*	*4.68*
285	*200*	*4.08*	*0.13*	*5.23*
315	*200*	*4.13*	*0.15*	*5.21*
345	*200*	*5.15*	*0.17*	*6.09*
375	*200*	*4.89*	*0.16*	*6.98*

3.3. Net Solar Radiation at the Surface

Sea surface radiation (Watt/m^2) with 3-hour time intervals was retrieved from European Centre for Medium-Range Weather Forecasts (ECMWF), Era-Interim data set. These data then were transformed to PAR. Because ETS Station and offshore of Mersin Bay is so close, same PAR data used for both study areas. Below, SSR data was plotted with using maximum radiation values per day. As expected, solar radiation increases in spring and reaches its maximum at summer months, and then decreases in autumn, attains its lover values in winter**.**

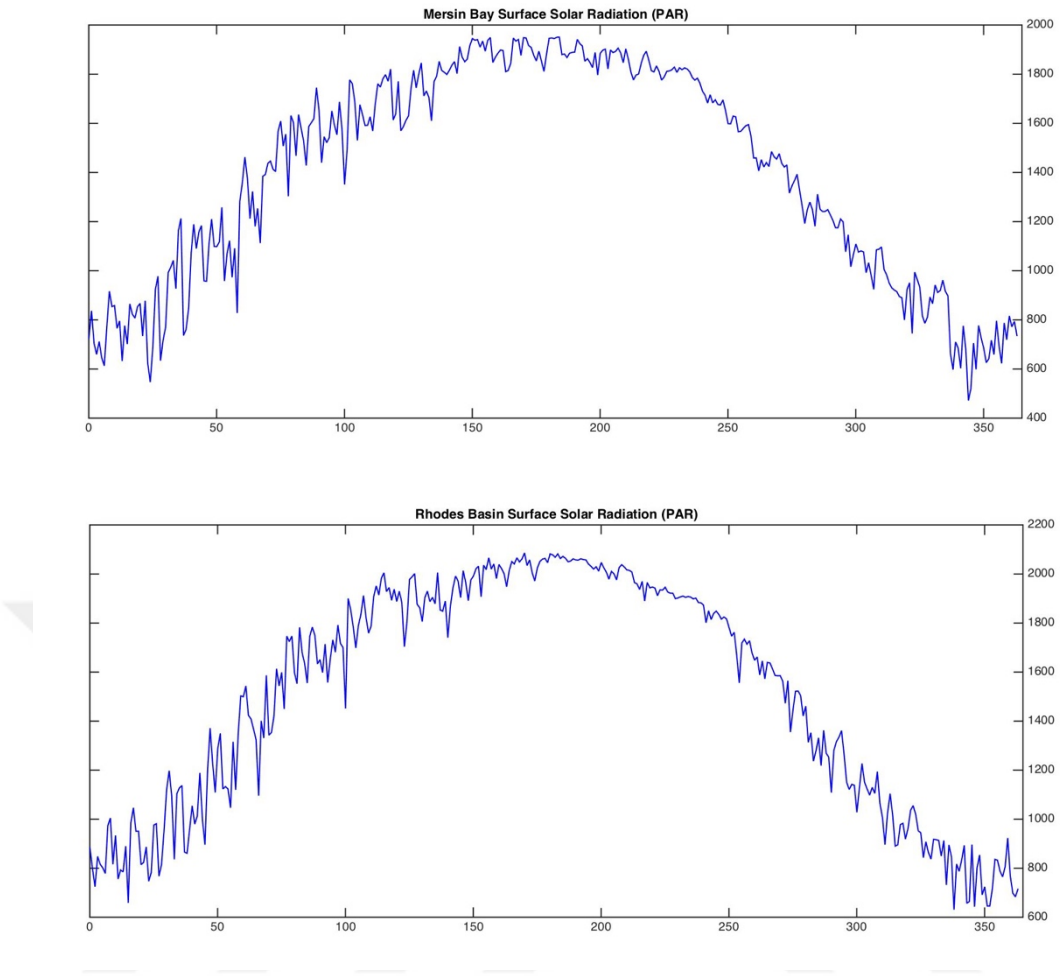

Figure 11. The net surface solar radiation (Watt/m2)

CHAPTER 4

RESULTS & DISCUSSION

In this chapter, key drivers of ecosystems are examined based on model results. Transfer of nutrients between compartments is distinguished by sensitivity analyses and testing scenarios by turning on/off relevant process in the model to determine the objectives of this work described in Chapter 1. Also, simulations of seasonal NO_3, PO_4, Si and Chl-a profiles are compared with in-situ data for model skill assessment. Then light field estimated by the model is compared to in-situ PAR data. Resulting from above sections, following parts are dedicated to analyzing the species composition, nutrient limitations on species and PP via the final run.

4.1. Nutrient Cycling

4.1.1. Initial DON and DOP inputs

Model is tuned and adapted to the specific conditions of Cilician Basin shelf waters (represented by ETS), Mersin Bay offshore waters and Rhodes Upwelling area. In this first run, DON and DOP in the water column are introduced as initial, and bottom boundary conditions. These values are based on available literature (Krom et al., 2005; Pujo-Pay et al., 2011) for eastern Mediterranean upper layer water column as 4.7 and the bottom layer (~ 200 m) 3.5 μg/L and DOP=DON:50. However, when the model is forced with these values, vast amount of DON and DOP accumulates in the water column, especially in deep layers of ETS and Mersin Bay regions. DOP in Rhodes Basin was also highly overestimated, which indicated that these values were high for these areas. Simulated DON and DOP depth-time distributions are displayed in Figure 12.

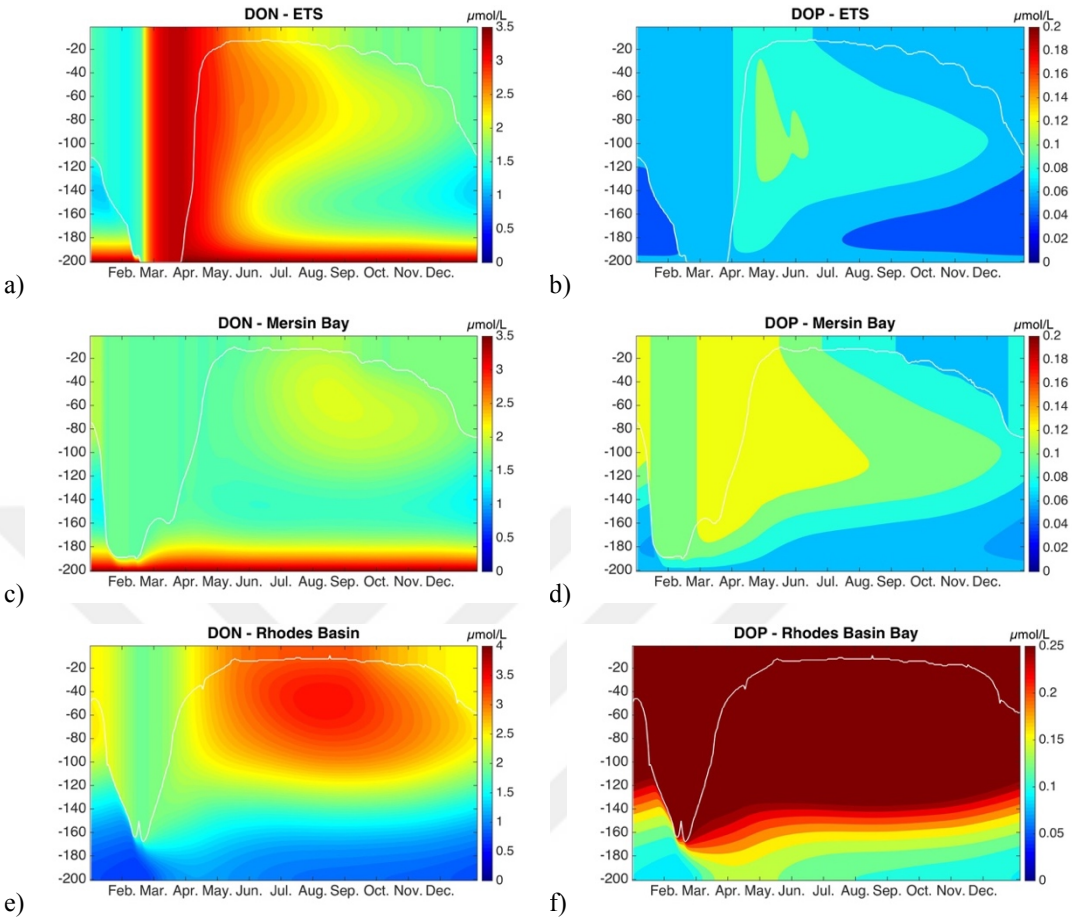

Figure 12. Depth-time distribution of model simulations for DON and DOP values, for ETS (a, b), Offshore waters of Mersin Bay (c, d), Rhodes Upwelling region (e, f) – white line indicates the mixed layer depth

When the dissolved organic material in the water column was elevated, an excess amount of NO_3 and PO_4 were transferred from DON pool to the system. Since the system is P-limited, when extra PO_4 was added a rapid growth of certain species occurred, and large amount of PO_4 was utilized. Also, diatom species proliferated resulting in a strong decrease in Silicate values. In the comparison with the in-situ data with the model results for Mersin Bay, an increase in PO_4 concentrations took place in bottom layers. This increase was also enhanced by the mortality and excretion inputs from overproduced species into the DON and DOP pools. Similar pattern was produced by the model for Erdemli coasts and Rhodes Basin.

To overcome this problem, the intrusion of bottom values of DON into the model was switched off while the DON and the system were expected to balance itself with a 6-year spin up. This resulted in a more realistic model output Figure 13. Another problem was the accumulation of nutrients in the deeper parts of the water column that still exists below ~ 100-120 m.

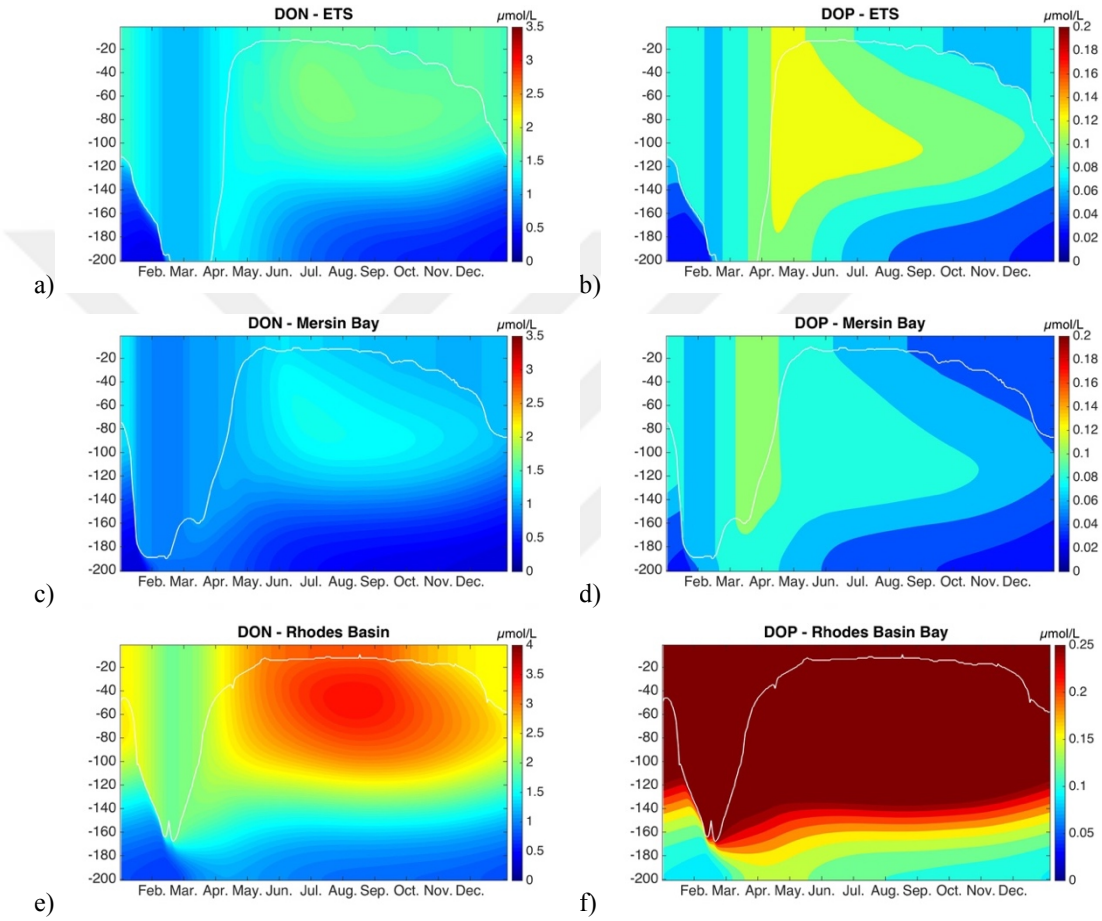

Figure 13. Depth-time distribution of model simulations for DON and DOP values, for ETS (a, b), Offshore waters of Mersin Bay (c, d), Rhodes Upwelling region (e, f), – white line indicates mixed layer depth

4.1.2. Temperature Dependent Remineralization Rates at Depth

Remineralization rates from the detrital pool to dissolved organic matter and then to nutrients were characterized by a temperature dependent function however with a parameterization that differs for different nutrients (e.g. remineralization rate of phosphate from DOM was higher than that of ammonium, each can be seen in Table

3 in Chapter 2). Bacterial utilization of dissolved organic matter varied through different oceans significantly. Bacterial loop dynamics is not explicitly resolved in NAGEM, however, to illustrate the remineralization done by bacteria explained by temperature dependent function. To set the appropriate remineralization rates, 2 temperature-dependent remineralization functions were tested. T-func1 is default in model equations, following Christian and Karl (1995), from their observational study (Subtropical & equatorial Pacific Ocean, polar environment). Since this function was weak to mimic the transfer, similar function which was estimated by a model study conducted by Moore et al. (2002) (Several Oceans – 9 sites) was tested. Using the temperature profiles of each region as input, plotted functions are given in Figure 14 for Mersin Bay, Figure 15 for Erdemli coasts and Figure 16 for Rhodes Basin.

$$\mathrm{Tfunc1} = e^{(0.967*(t(z)-25))}$$

$$\mathrm{Tfunc2} = e^{-4000*\left(\left(\frac{1}{t(z)+273.15}\right)-\left(\frac{1}{303.15}\right)\right)}$$

where T(z) is the temperature (ºC) at depth z

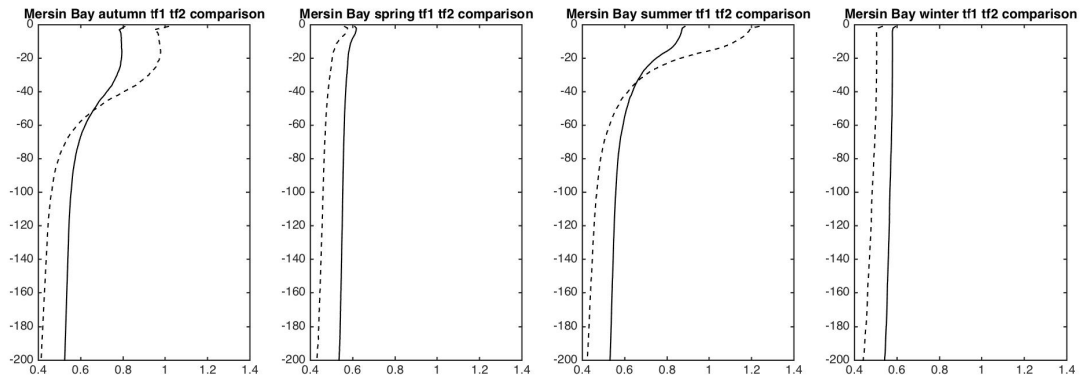

Figure 14. Comparison of 2 different temperature-dependent remineralization functions in Mersin Bay. Solid line denotes Tfunc1 and dashed line denotes Tfunc1

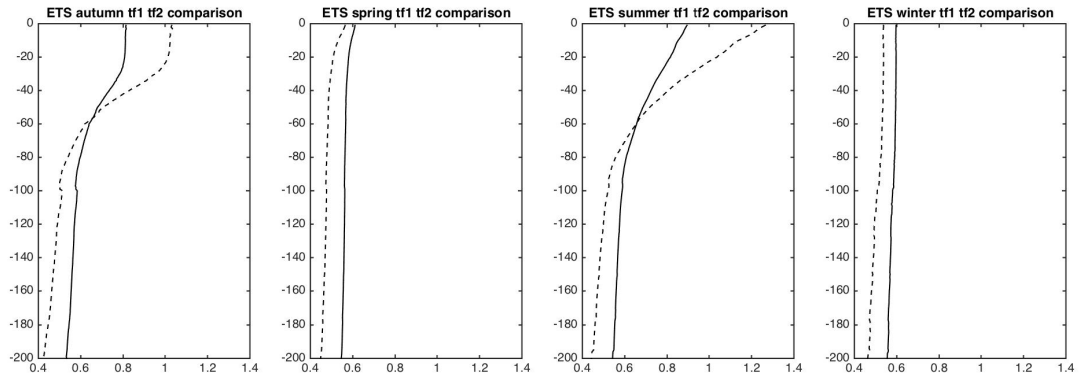

Figure 15. Comparison of 2 different temperature-dependent remineralization function on ETS. Solid line denotes Tfunc1 and dashed line denotes Tfunc1

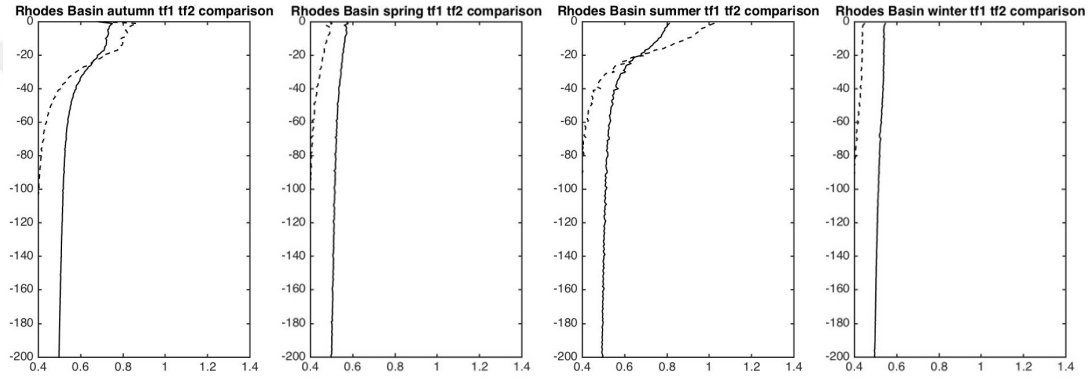

Figure 16. Comparison of 2 different temperature-dependent remineralization function on Rhodes Basin. Solid line denotes Tfunc1 and dashed line denotes Tfunc1

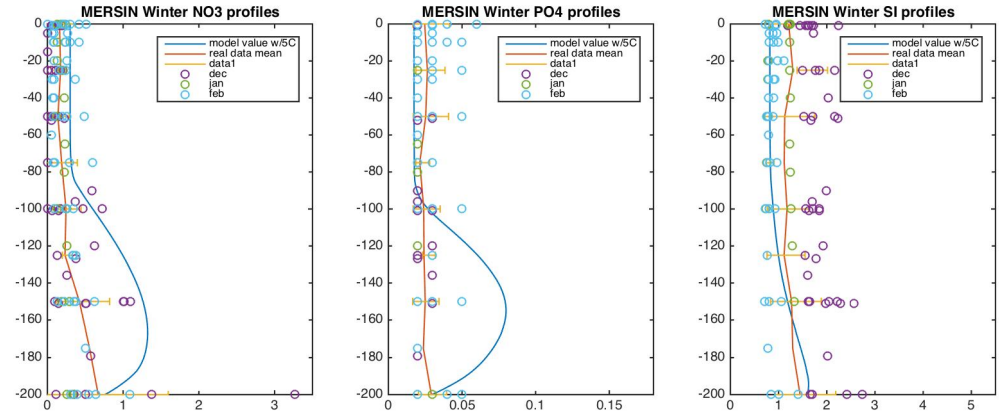

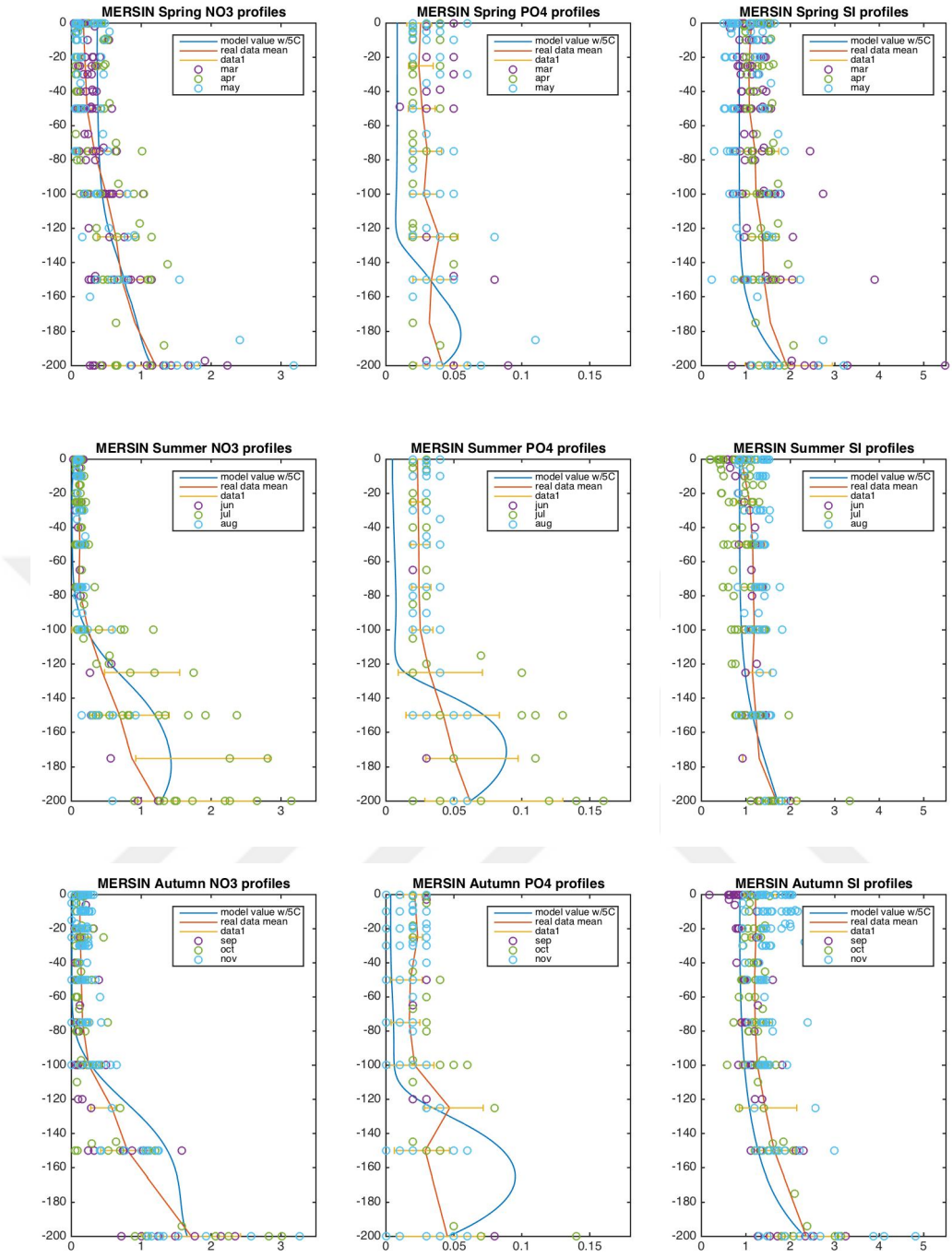

Figure 17. Comparison of model results vs data of Mersin Bay, using T-func2 (yellow horizontal lines indicate error bars)

Remineralization rate increased with temperature at the surface and decreased with the depth due to the cooling of the water column. In summer and autumn, remineralization above the thermocline differed highly from the deeper layers, where this difference decreased when thermocline layer vanishes in winter and spring. Model results responded well to such seasonal variability. However, for both

seasons, model-data misfit occurred due to remineralization algorithms. At the surface layers, remineralization rates were low whereas with depth it results in high remineralization increase. These rates resulted in an overestimation of nutrient profiles by model, resulting slightly higher values than the actual ones at deep waters and underestimation in surface waters (Figure 17). Comparing to Si, this change was more pronounced for NO_3 and PO_4 because, in model calculations, remineralization process is more complex for these minerals and goes through several levels and in every step the effect of this small calculation error increases.

In model equations, material transfer is through remineralization from large and small detrital phosphorus to DOP and then again through remineralization of PO_4 for phosphorus. For nitrogen, one part of the transfer is via remineralization of small and large detrital nitrogen DON and then NH_4. Also, zooplankton excretion added to ammonium and, with nitrification of the ammonium, NO_3 is transferred to the medium. For silicate, however, the only input to Si pool is remineralization from small and large detritus to silicate.

Despite these small errors, model results calculated with 2nd remineralization function showed high skill reproducing the data regarding seasonal variations and magnitude. Therefore, this function is used to describe the temperature dependent remineralization rate and rest of the model results are based on this structure. The model skill for ETS and Rhodes Basin were similar (Figure 18, Figure 19).

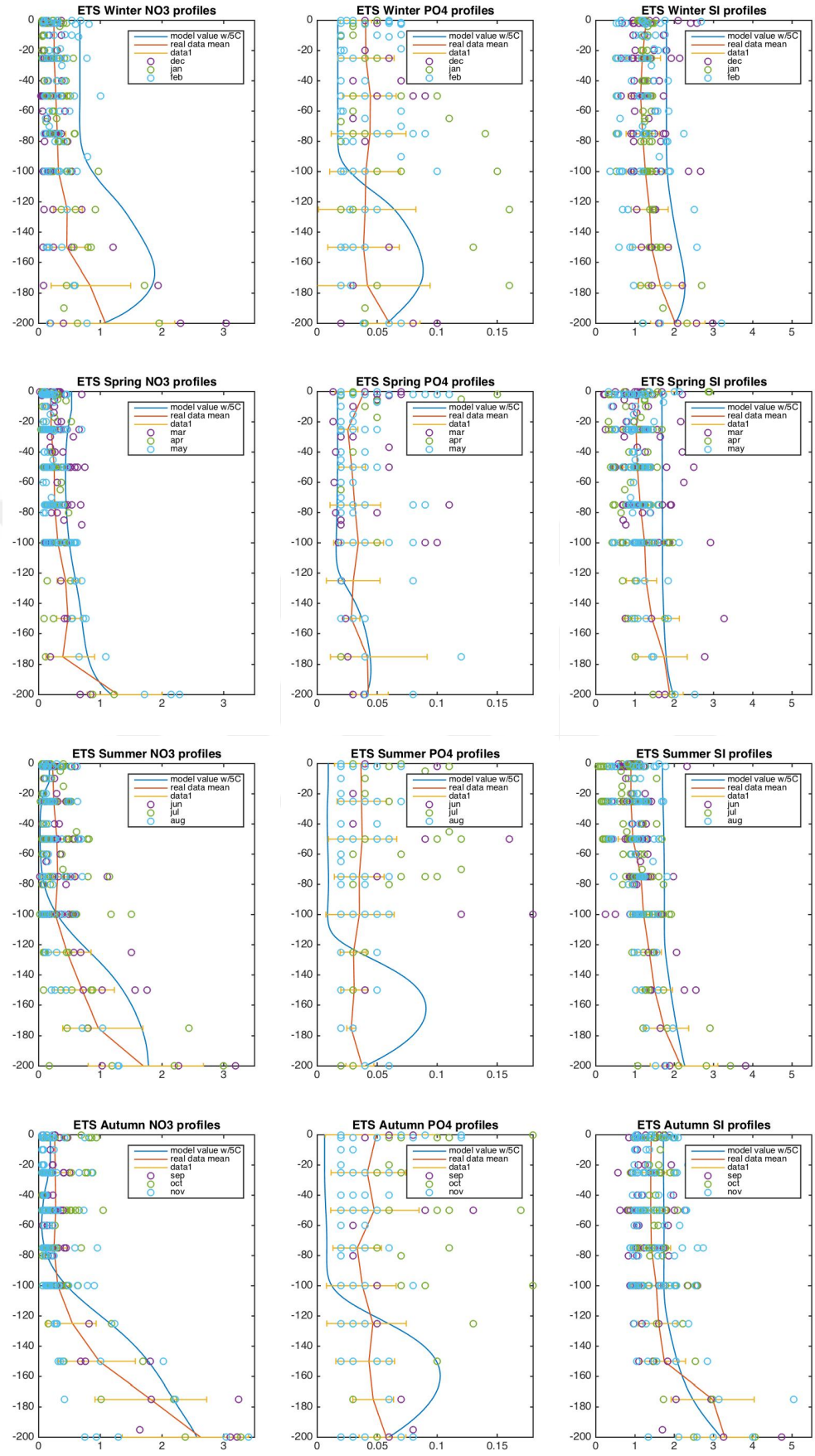

Figure 18. Comparison of model results vs field data of ETS, using 2nd T-func. (yellow horizontal lines indicate error bars)

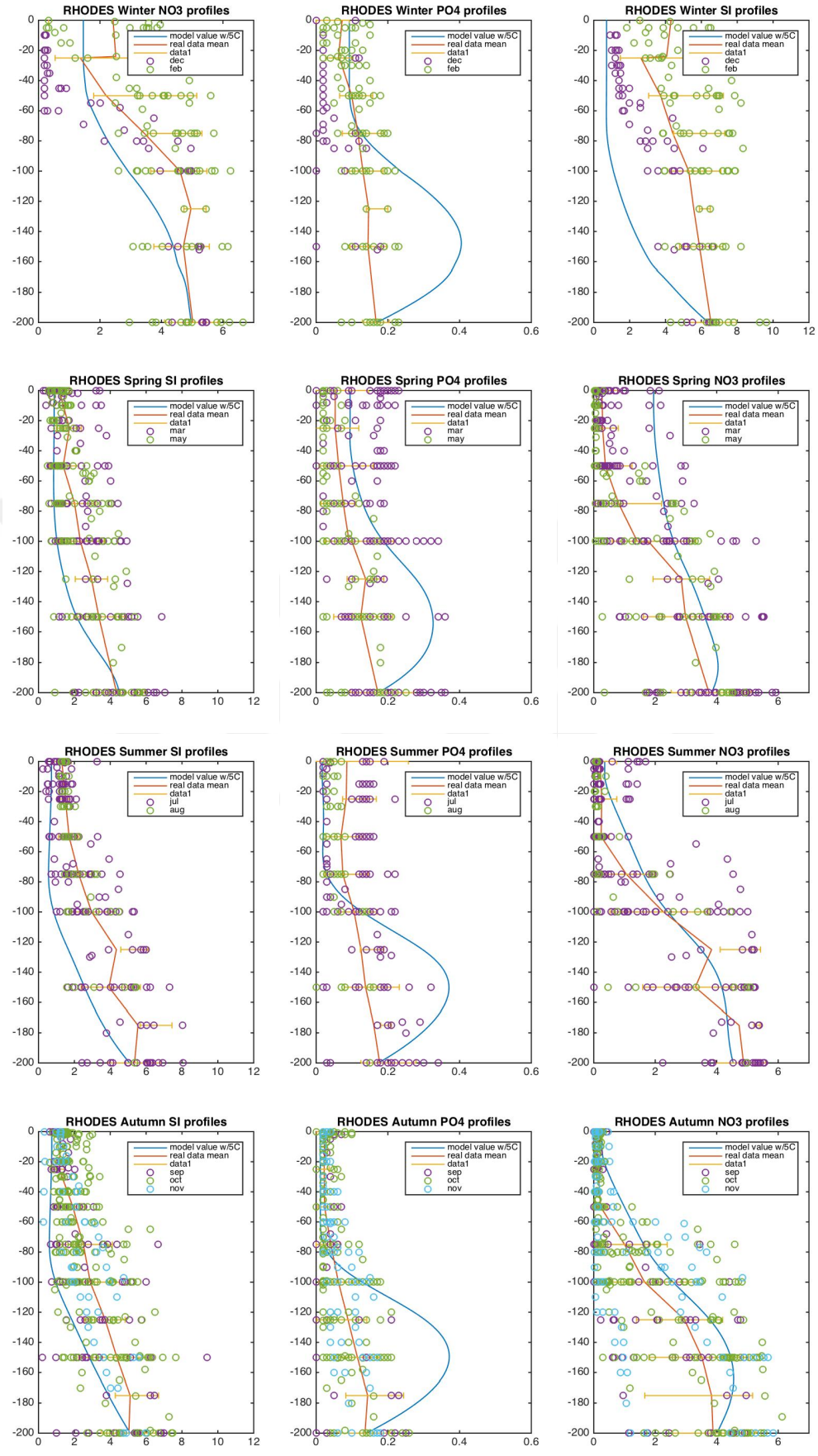

Figure 19. Comparison of model results vs real data of Rhodes Basin, using 2nd T-func. (yellow horizontal lines indicate error bars)

With Tfunc 2, at ETS and Rhodes DON and DOP estimations were also improved (Figure 20). In winter, with the mixing of the water column, dissolved organic material distributed over the water column nearly uniformly inside the mixed layer. As the winter mixing vanishes, there is an accumulation of the values due to sinking organic material from upper and mid layers of the water column. This accumulation occurs strongest in the Rhodes upwelling area since both biomasses of lower trophic species and zooplankton are higher in this area.

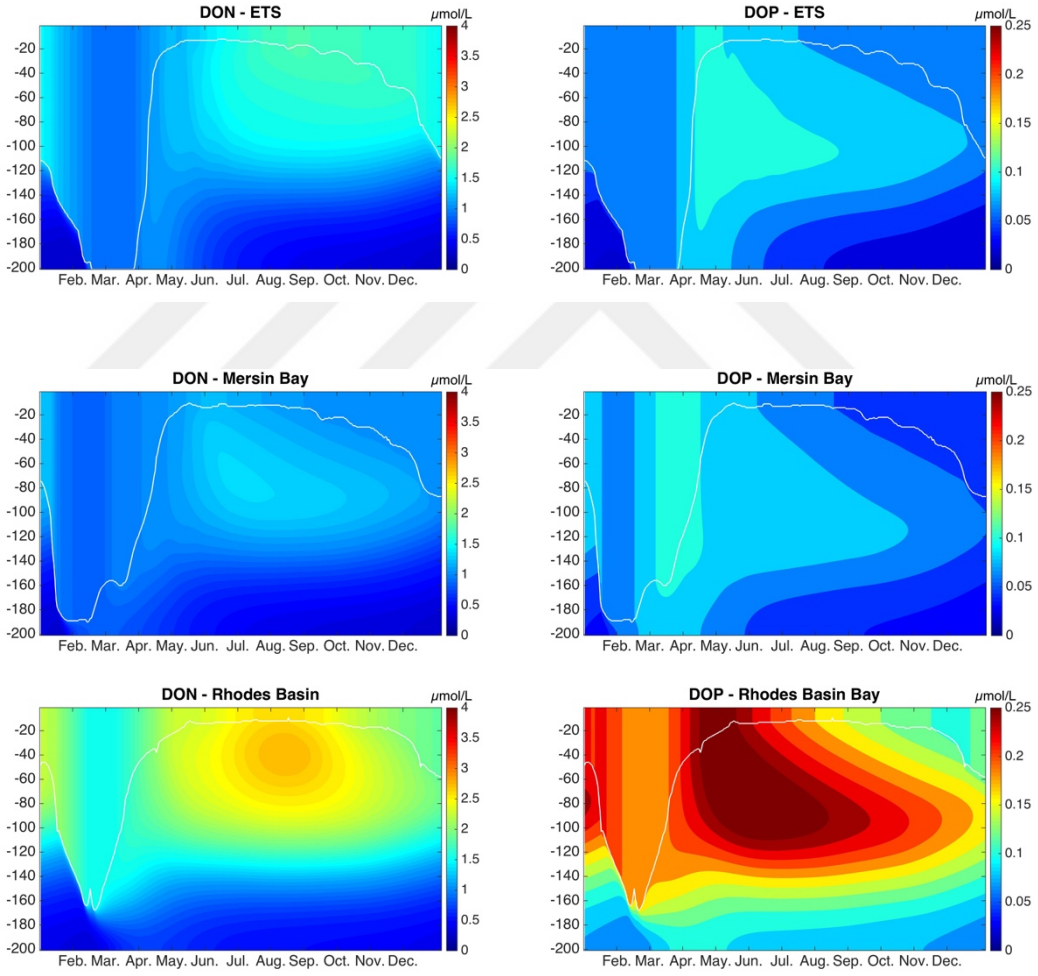

Figure 20. Depth-time distribution of model simulations for DON and DOP values, for ETS (a, b), Offshore waters of Mersin Bay (c, d), Rhodes Upwelling region (e, f), – white line indicates mixed layer depth

4.1.3. Effect of recycled nutrients on primary production

In oligotrophic waters, when nutrient availability is insufficient for production, the percentage of the support of recycled nutrients for PP is higher. To quantify the contribution of the effect of remineralization on primary production, transfers from detritus to DOM, Si, and from DOM to NH_4 and PO_4 are ceased (Figure 21).

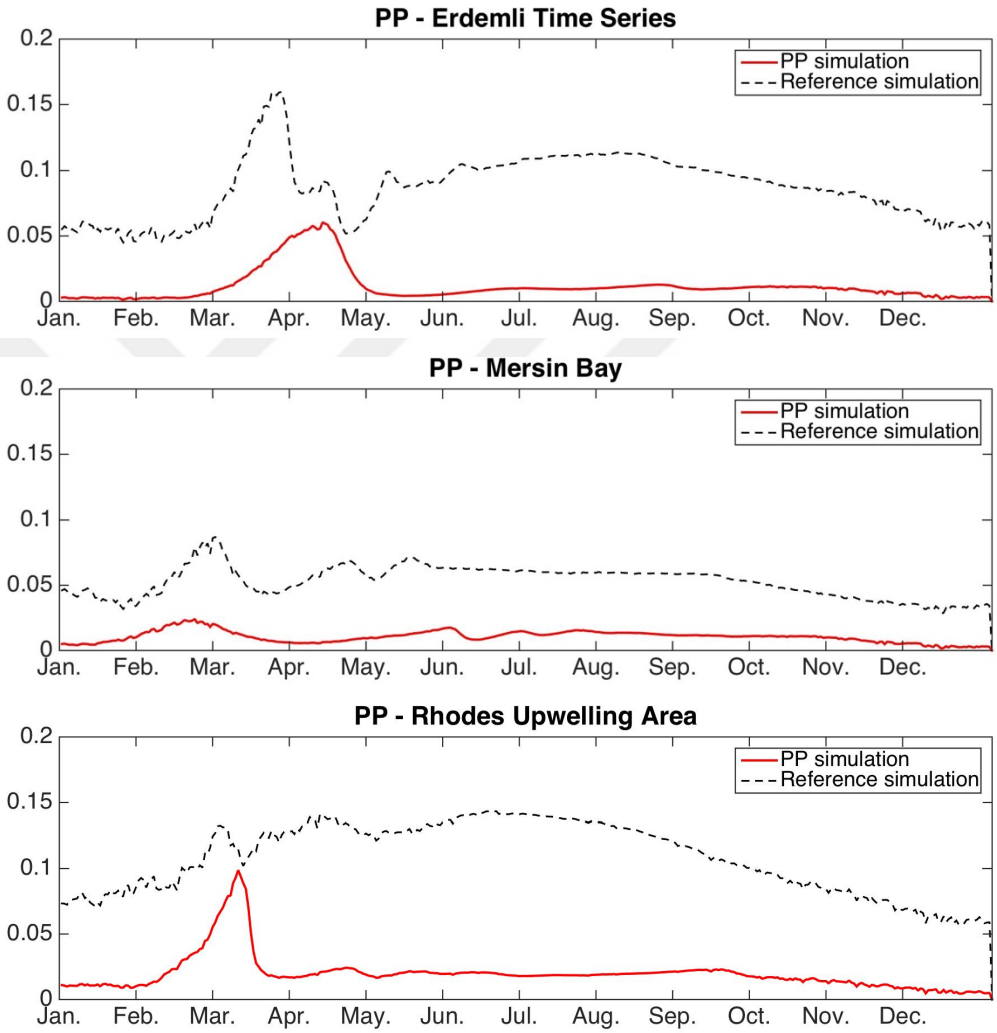

Figure 21. Primary production without nutrients recycled (red line) in comparison with reference run estimates (dashed line)

In Mersin Bay, nutrients are provided from deep waters to the euphotic zone with winter mixing, which gives rise to an increase in primary production. However, due to this increase in PP, nutrients are quickly utilized, the concentration of nutrients decreased sharply. After this, the system became more dependent on recycled nutrients. The contribution of recycled nutrients to PP is 78% in a year. This

contribution decreases with winter mixing to 65% when the nutrient input occurs with winter mixing, and the rest of the year is about 91%.

In Erdemli this value is 86%. Percentages were lowest during early spring than the remaining of the year, around 65% and 91% respectively. In this site, besides bottom waters, the influence of river inputs illustrated which decreased the dependency on recycled nutrients in the spring season.

In Rhodes basin, Regenerated nutrients covered 81% of the production supply of this site. In winter this ratio reduces to 58% and whole year mean value is 84.985%. There is an increase in winter mixing, and since the input is higher than other areas, production depending on ambient nutrients is greater but these are utilized quickly, and there is a sharp decrease in late March. Also since the rest of the year, nutrients are carried to the upper layers, production without the support of remineralized nutrients are higher in Rhodes Basin. Temperature and the mixed layer in winter and thermocline in summer variables have the greatest impact on the growth of the species as well as the nutrient distribution and remineralization.

4.2. Reference model-data comparison

The only constraints of the reference model run were boundary and initial nutrient fields and the physical drivers and it was expected to evolve to reproduce the observed nutrient fields. Because rivers at the costal ETS station area introduce a high amount of Silicate and other macronutrients to the system, diatom species was expected to grow in higher biomass. Also, past studies conducted in shelf waters indicated diatom as an important species, reaching high biomass values throughout the year. Despite the model successfully captured the seasonal variability and magnitudes of nutrients, the biomass of diatoms was low compared to the measurements of Uysal et al. (2008) in Cilician Basin. To eliminate this discrepancy, growth rate of diatoms in the model was increased fractionally.

Phosphate concentrations were slightly underestimated in the upper layers and slightly overestimated at 120 – 180 m contour in all regions as shown in Figure 22

for ETS, in Figure 23 for Mersin Bay and Figure 24 for Rhodes Basin. As described in section 4.2.2, this increase is thought to be mainly resulted from remineralization rates of phosphate from DOP that is weak to demonstrate the area's characteristics. Another but minor reason for underestimation in the water column could be the measurement bias. In Eastern Mediterranean, phosphate values are too low and occasionally fall below the detection limit (0.02 μg/L). These were recorded as 0.02 μg/L even if the real value was below, which made the mean in-situ profiles slightly elevated. However, NO_3 and Si values in both sites were simulated successfully (Figure 22).

According to both data and model simulations, in all regions, in late January – early February with the extensive mixing of the water column, there is a high amount of nutrient input from the deeper layers. Due to the upwelling property of the region, mixed layer thickness in the core of the Rhodes Gyre is shallow at around 170 – 180 m from the surface, whereas in the Cilician Basin it is deeper, during winter reaching down below 200 m in ETS stations. Starting through the end of the mixing season, nutrients that introduced into the euphotic layer are rapidly utilized and depleted by the species resulting in a sharp decrease in nutrient concentrations. As water temperature increases, strong thermocline forms around ~10 – 20 m in all regions from late spring until the end of the summer. In warm seasons, bottom nutrient input into the biogenic layer is ceased in both shelf and offshore waters of the Cilician Basin and due to the sharp thermocline, there is less interaction of surface with the mid-layers.

In Mersin Bay there is limited new nutrient source to the system, except for the atmospheric input which has high N: P nutrient ratios. Because the system is already phosphate limited, such input is thought to be further deteriorating the limitation of phosphate. ETS site is exposed to new nutrient inputs with increased debris of river discharges at the beginning of the spring season, and atmospheric input. River discharges introduce silicate and phosphate into the coastal areas which lack in offshore waters. At the core of the Rhodes Cyclonic Gyre, due to upwelling, nutricline is located at the base of the euphotic zone during the whole year, introducing steady new nutrient support to the system.

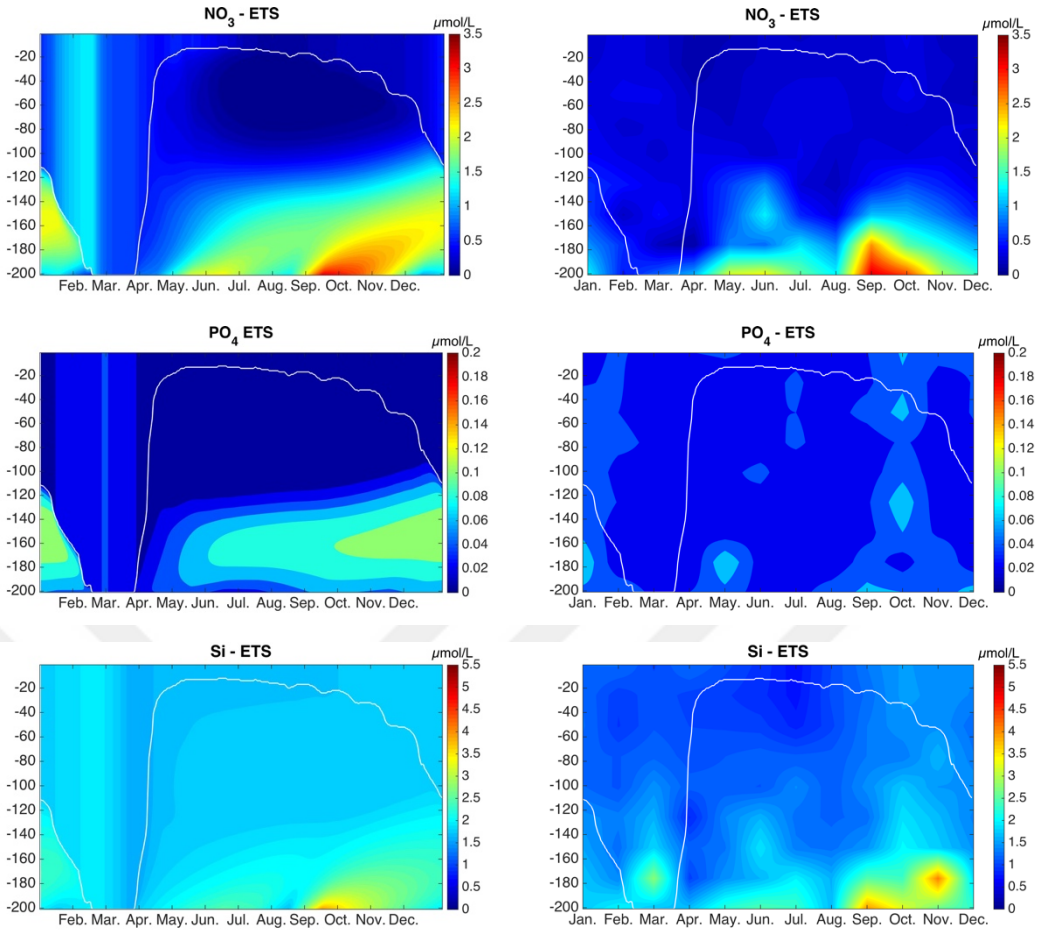

Figure 22. Depth-time distribution of nutrients derived from model run (left) and in-situ (right) data for ETS– white line indicates mixed layer depth

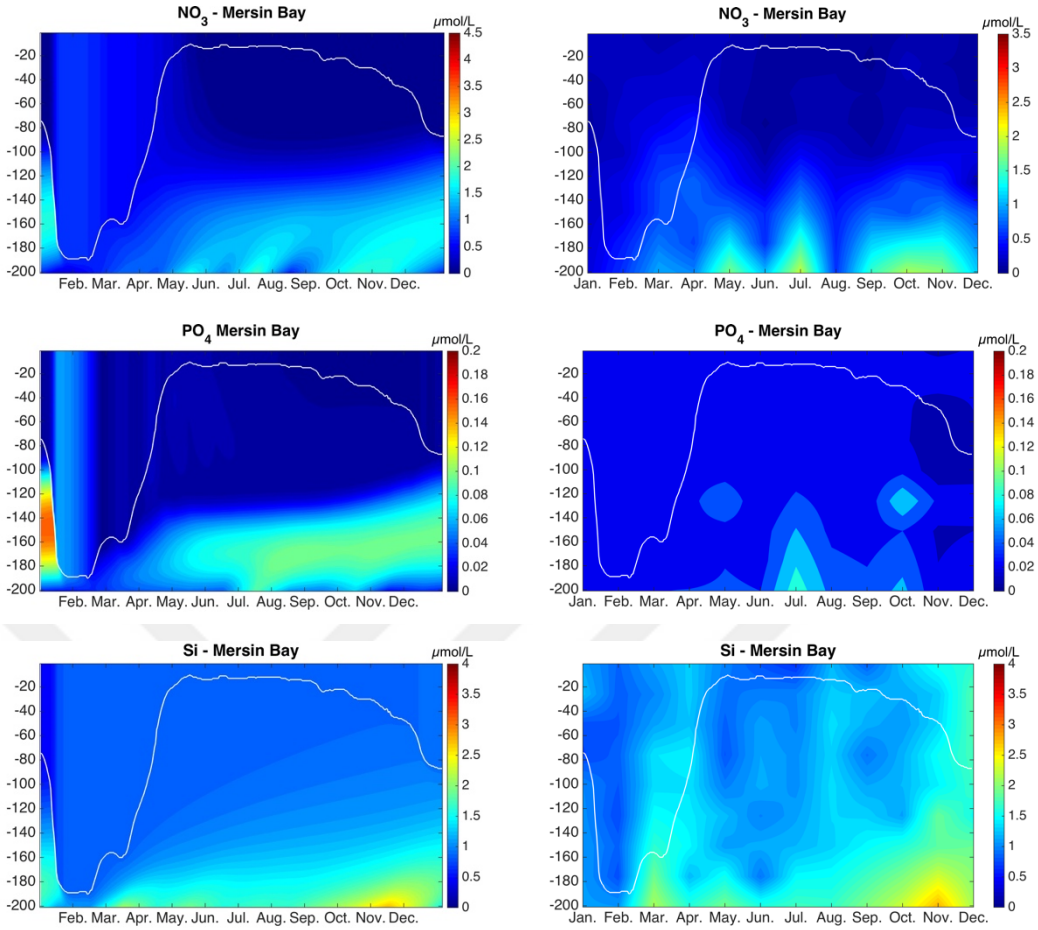

Figure 23. Depth-time distribution of nutrients derived from model run (left) and in-situ (right) data for Mersin Bay – white line indicates mixed layer depth

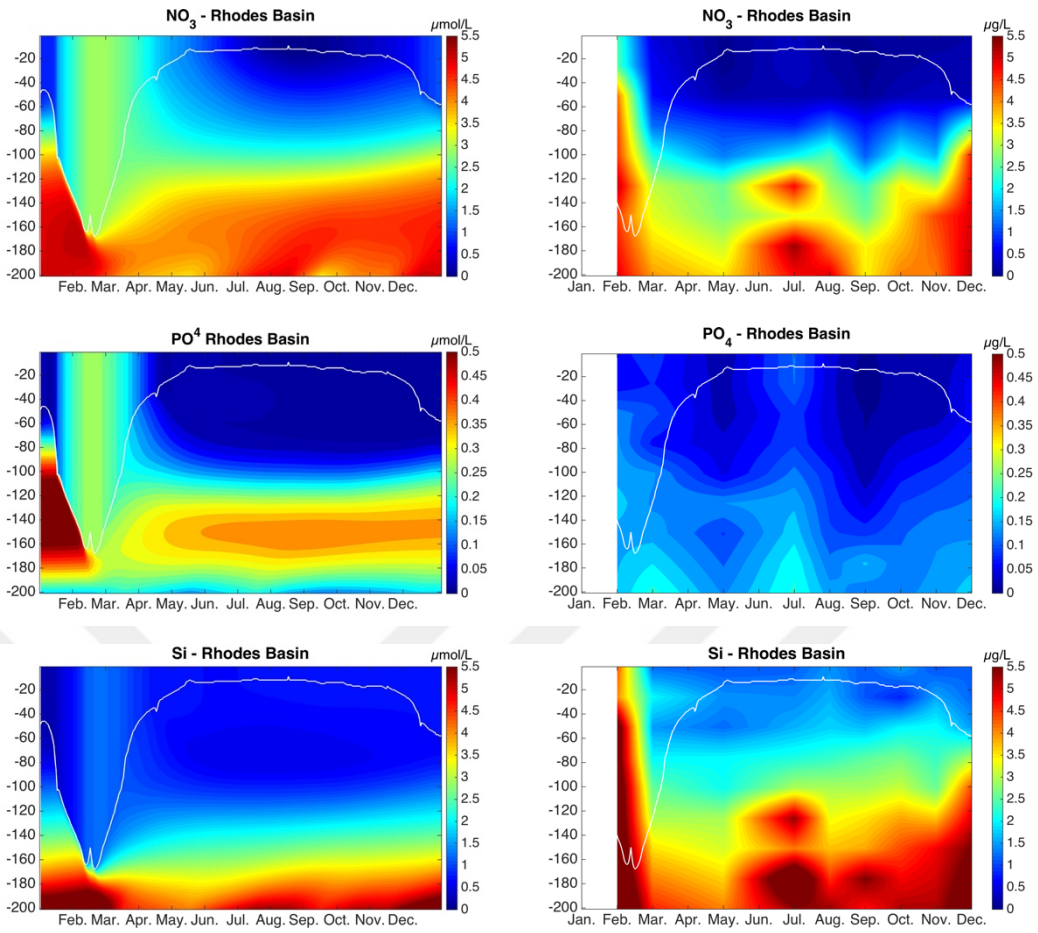

Figure 24. Depth-time distribution of nutrients derived from model run (left) and in-situ (right) data for Rhodes Basin

Chl-a estimations of the model are important indicators of the ecosystem because these dynamics are a reflection of the characteristics of the species distribution and behavior also primary production. For this aim, seasonally averaged profiles of model simulation and in-situ data and point measurements of chl-a in the water column are used for comparison. The model results successfully followed the mean chl-a values calculated from the real station data points and deviations fell within the error bars which calculated for each 25 m (Figure 25, Figure 26, Figure 27).

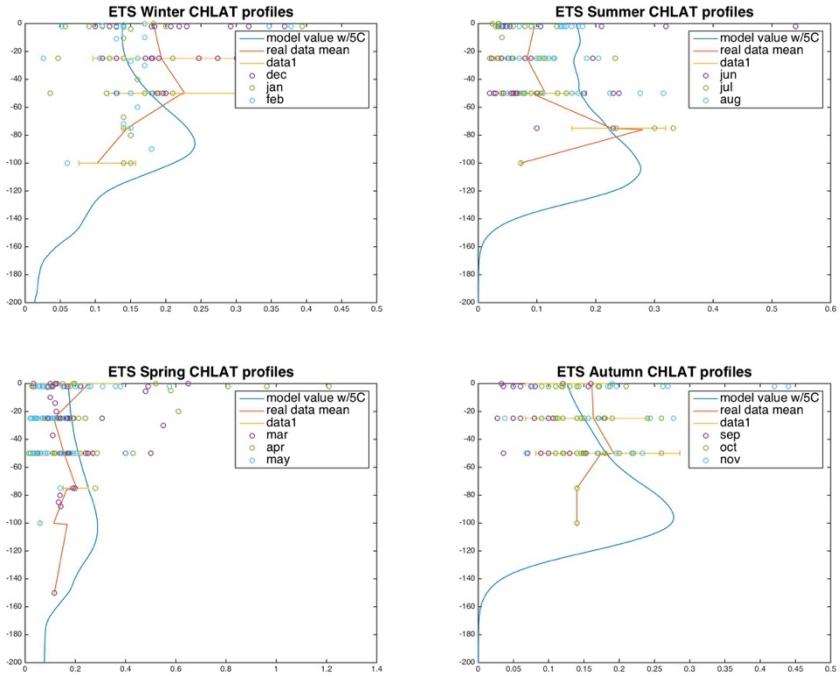

Figure 25. ETS seasonally-averaged Chl-a profile comparisons - horizontal lines indicate error bars from the mean data at depth

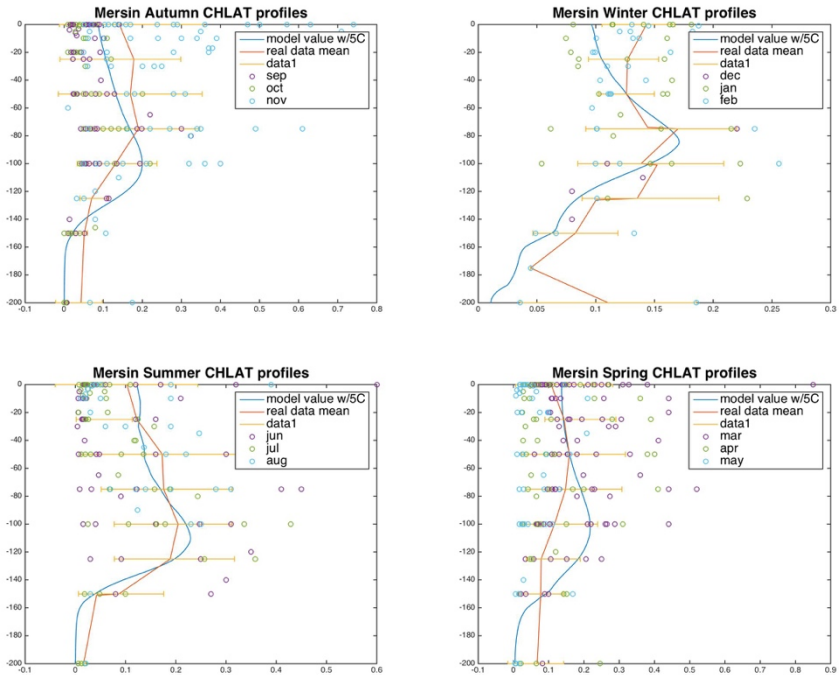

Figure 26. Mersin Bay seasonally-averaged Chl-a profile comparisons – horizontal lines indicate the errorbars from the mean data at depth.

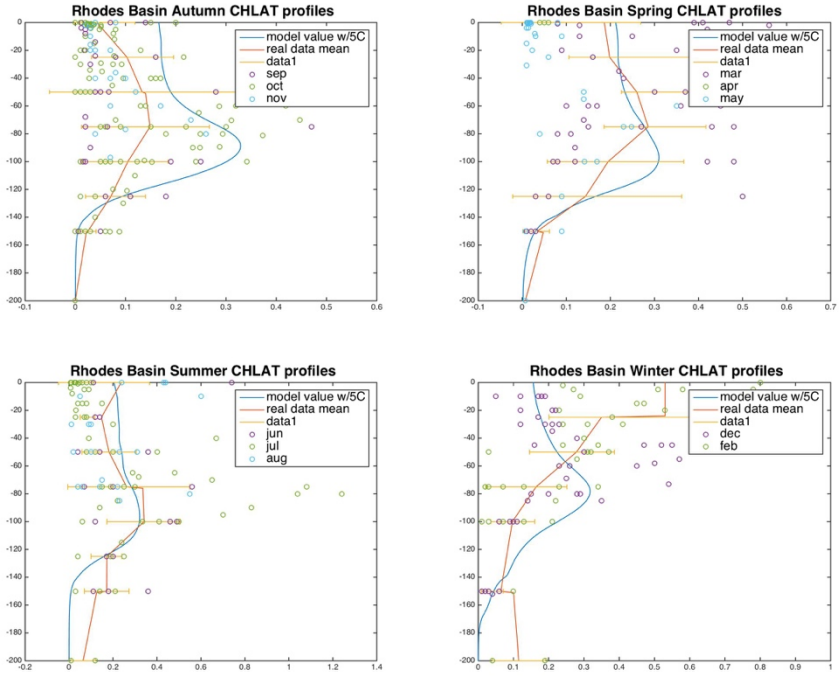

Figure 27. Rhodes Basin seasonally-averaged Chl-a profile comparisons – horizontal lines indicate error bar from the mean data at depth

4.3. Light field

Light penetration to the water column and photic zone are important factors on the growth of the species and primary production. As mentioned in section 3.3, surface data obtained from ECMWF were scattered into the water column by a light module of the model. For model validation light data for Mersin is used because this is the region of most available data of the light field. Model results are successful in reproducing the light penetration in depth (Figure 29). As can be observed from the real measuremens, shown in Figure 28, light penetration in depth increases in summer months as the radiation increases in summer months. In winter months, with the effect of the stirred particles by winter mixing also prevents further penetration of UV lights.

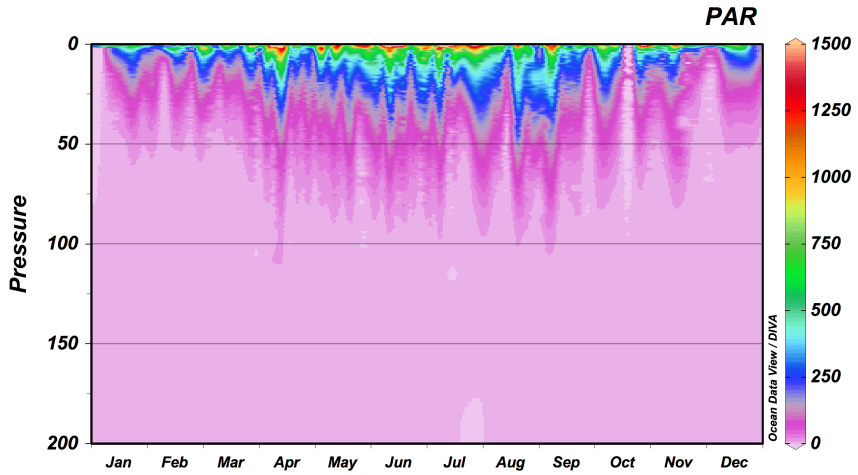

Figure 28. Photosynthetically active radiation from sensor measurements (Watt/m^2)

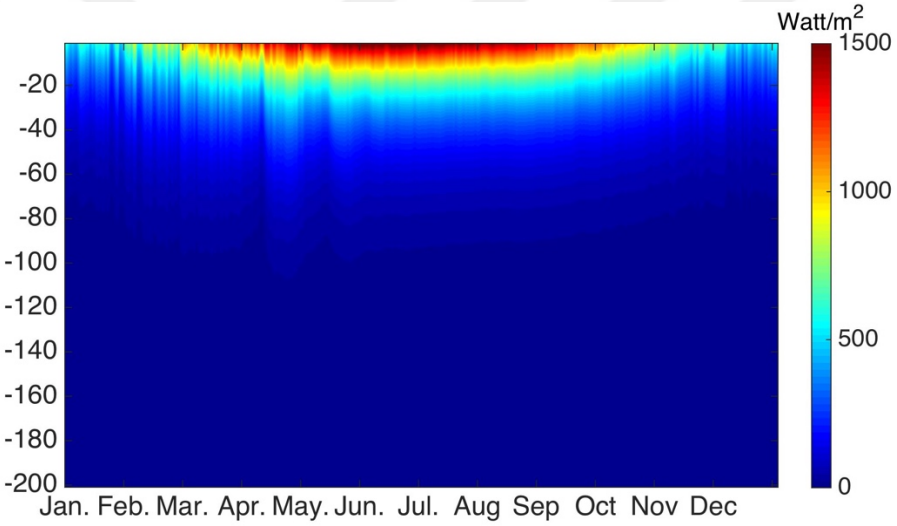

Figure 29. Model estimations on photosynthetically active radiation (Watt/m^2)

4.4. Species composition, Chl-a and Primary Production

Nutrient flux and physical conditions in the water column were quite well reproduced by the model in previous sections. Using reference model, species composition, Chl-a, primary production and further implications will be discussed in this part.

4.4.1. Species composition

In all stations, water temperature and winter mixing have a significant impact on species growth rate, as well as chemical and physical setting of the ecosystem. Starting from late January until early April, winter mixing occurs in the water column at different depths on all sites which carry nutrient – rich, deep water to the upper layers. Since the production is highly P-limited in Northern Levantine, such nutrient inputs temporarily drive the system into a highly productive period. Larger cell-sized species (autotrophic eukaryotes, diatoms) cellular stoichiometry are close to the classical Redfield Ratio which makes them more sensitive to N:P deviations in the water column. Whereas small cell-sized (*Synechococcus*, *Prochlorococcus*) species have higher N:P stoichiometry and survive better in nutrient-limited environments due to their adaptation on the limiting nutrient (Bertilsson, Berglund, Karl, & Chisholm, 2003; Leonardos & Geider, 2004). *Synechococcus* also grow better on temperate mediums (Uysal & Koksalan, 2010)

In Erdemli coast, nutrients are introduced to the system through the river discharge especially with its increased volume during spring (Figure 30). These inputs feed the system to the point where P-limitation lessens, and ecosystem slightly switches from oligotrophic level to mesotrophy. Similarly, in Rhodes upwelling area, nutrient input provided from deep layers' yields decreased N:P ratios in upper layers whole year and gave a chance for growth of species (Figure 32).

During winter mixing, large diatoms, and autotrophic eukaryotes dominated the system with a rapid increase in their biomass in ETS site. In late April when the nutrients in the water depleted and P-limitation severed especially at surface water, the biomass of these species decreased. In summer, strong stratification formed about 20 m from the surface, the transfer from the upper layer with the medium layers weakened and nutrients in the surface are trapped in the thermocline. Their small cell size and low sinking rate, kept cyanobacteria suspended in the photic zone. Through the summer, also with the effect of the increased temperature, *Synechococcus* and *Prochlorococcus* grow better due to their better adaptation to P-limitation. These species became dominant at the surface 0 – 100 m starting from May. The presence

of autotrophic eukaryotes formed In 80 – 140 m depth band. Since they thrive for phosphate and their cell size is larger, their population increased with depth where the nutrient availability is higher. Their abundance depth slightly shallow from mid-summer to autumn due to increased recycled nutrients resulted from the increase in population in the upper column of the water (i.e. mortality, zooplankton excretion, respiration) (Figure 30).

Since Cilician Basin offshore waters are oligotrophic, high N:P values limited the growth of larger cell sized species. Diatom growth limited and autotrophic eukaryotes were most abundant during late February to May in 0-180 m from the surface (Figure 31). Spring bloom dominated by autotrophic eukaryotes reached its maximum levels in March, resulted in a quick depletion of nutrients in upper layers and water returned to its initial phosphate limited form which can also be tracked from nutrient profiles.

In spring – summer season, the location of highest biomass concentrations of Mersin Bay is illustrated deeper than ETS, around 110 – 140 m, since the nutrient availability constrained in upper layers. Since *Synechococcus* doesn't compete with larger species in early spring, their population increases in April, became the dominant species in the upper 100 – 120 m of the water column. Since *Prochlorococcus* grow well on ammonium (Moore, Post, Rocap, & Chisholm, 2002), their biomass increased as the organic compound and recycled ammonium grown in surface waters in late summer – autumn in the upper part of the water column.

Highest biomass values for diatoms and autotrophic eukaryotes calculated in Rhodes upwelling region (Figure 32).In contrast, *Synechococcus* and *Prochlorococcus* abundance were lowest in this area among 3 regions. Autotrophic eukaryotes were the most abundant species throughout the year from the surface to ~ 120 m. Diatoms were most abundant following the winter mixing depth and from April their biomass placed between 70 – 120 m depth. These results are consistent with the literature. Using the cell concentration data obtained in 1986 – 1987 POEM cruises, Siokou-Frangou et. al. (1998) found that the dominant species were diatom*s* during spring season in the Rhodes Basin. Diatom and autotrophic eukaryotes abundance depth

were shallowest comparing to other regions since in this area deep waters were upwelled bringing rich nutrients to the upper layer.

Zooplankton population followed the abundance of primary producers. At ETS small zooplankton grew in spring – summer seasons in the upper 60 – 70 m depth whereas large zooplankton population increased in April following the diatom growth. In offshore waters of Mersin Bay small zooplankton grew in spring, however large zooplankton biomass was too low because almost no diatom biomass was estimated by the model. In Rhodes upwelling area highest zooplankton biomasses were calculated. From spring to autumn, small zooplankton was abundant in the first 80 m of the water column. Large zooplankton species growth was highest in spring, then followed the abundance of diatom and small zooplankton biomasses.

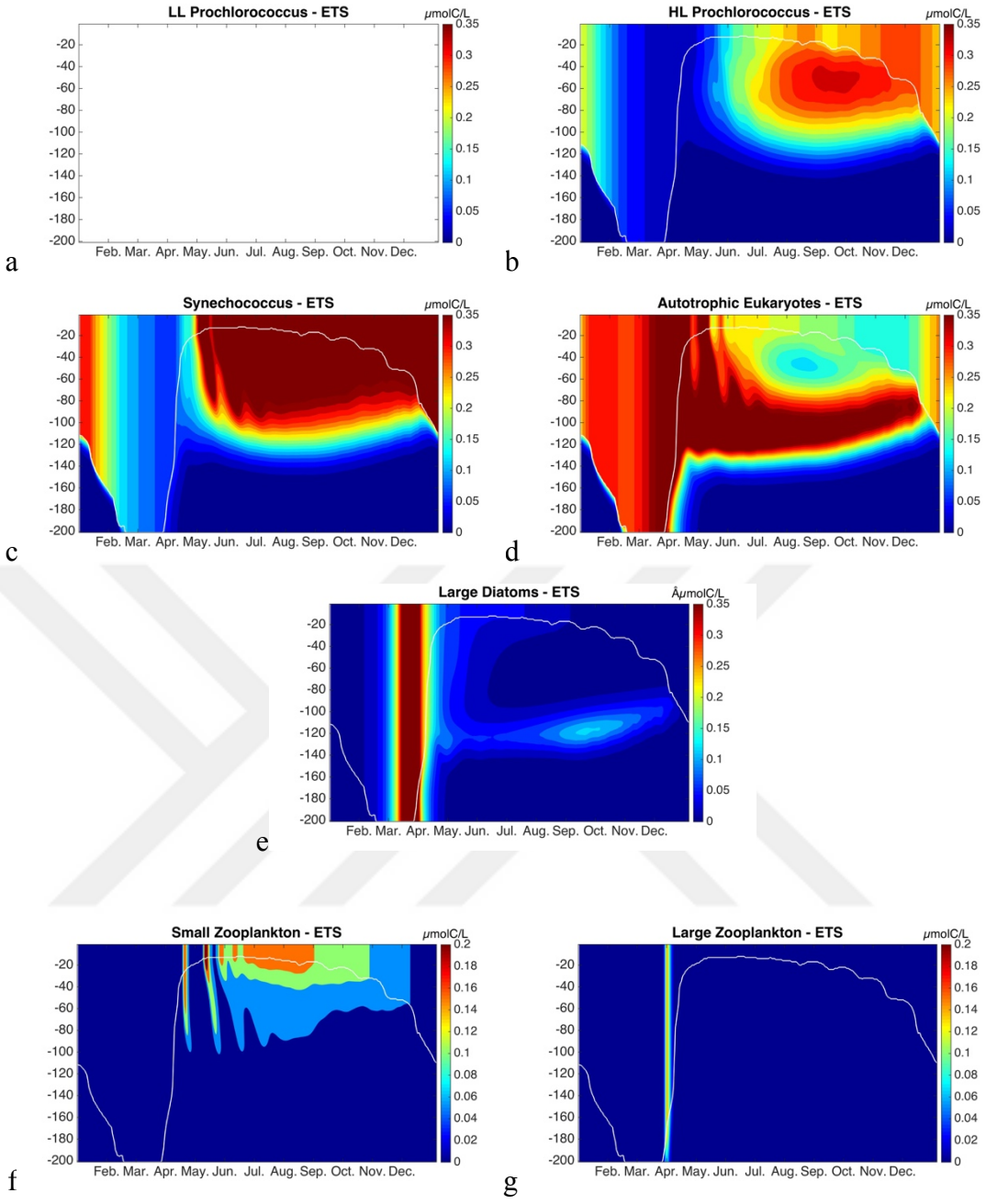

Figure 30. Yearly distributions of biomass (µmolC/L) of low light adapted *Prochlorococcus*, high light adapted *Prochlorococcus*, *Synechococcus*, autotrophic eukaryotes, diatoms and zooplankton groups in ETS site – White lines indicate the mixed layer depth

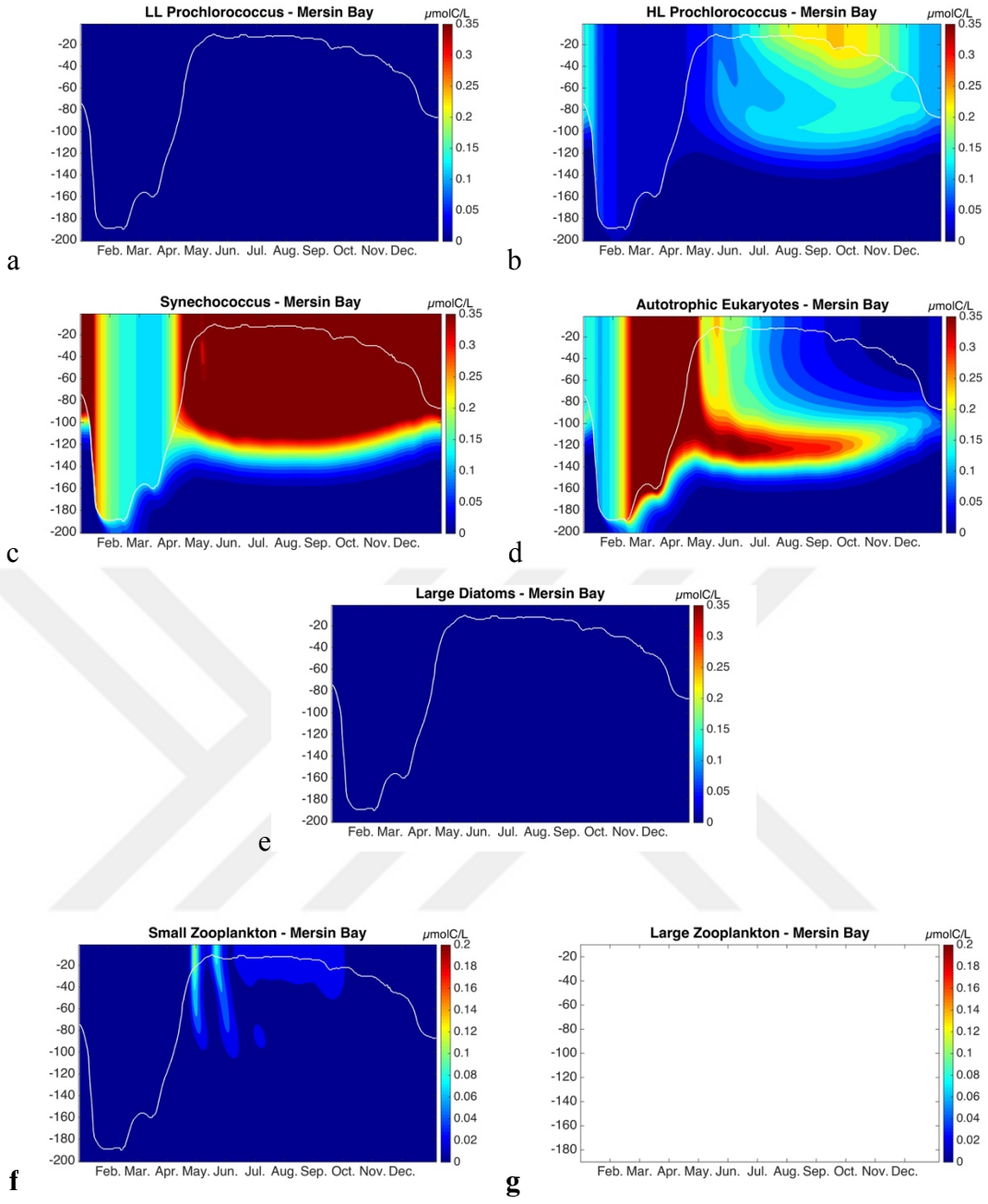

Figure 31. Yearly distributions of biomass (µmolC/L) of low light adapted *Prochlorococcus*, high light adapted *Prochlorococcus*, *Synechococcus*, autotrophic eukaryotes, diatoms and zooplankton groups in Mersin Bay offshore waters in depth – White lines indicate the

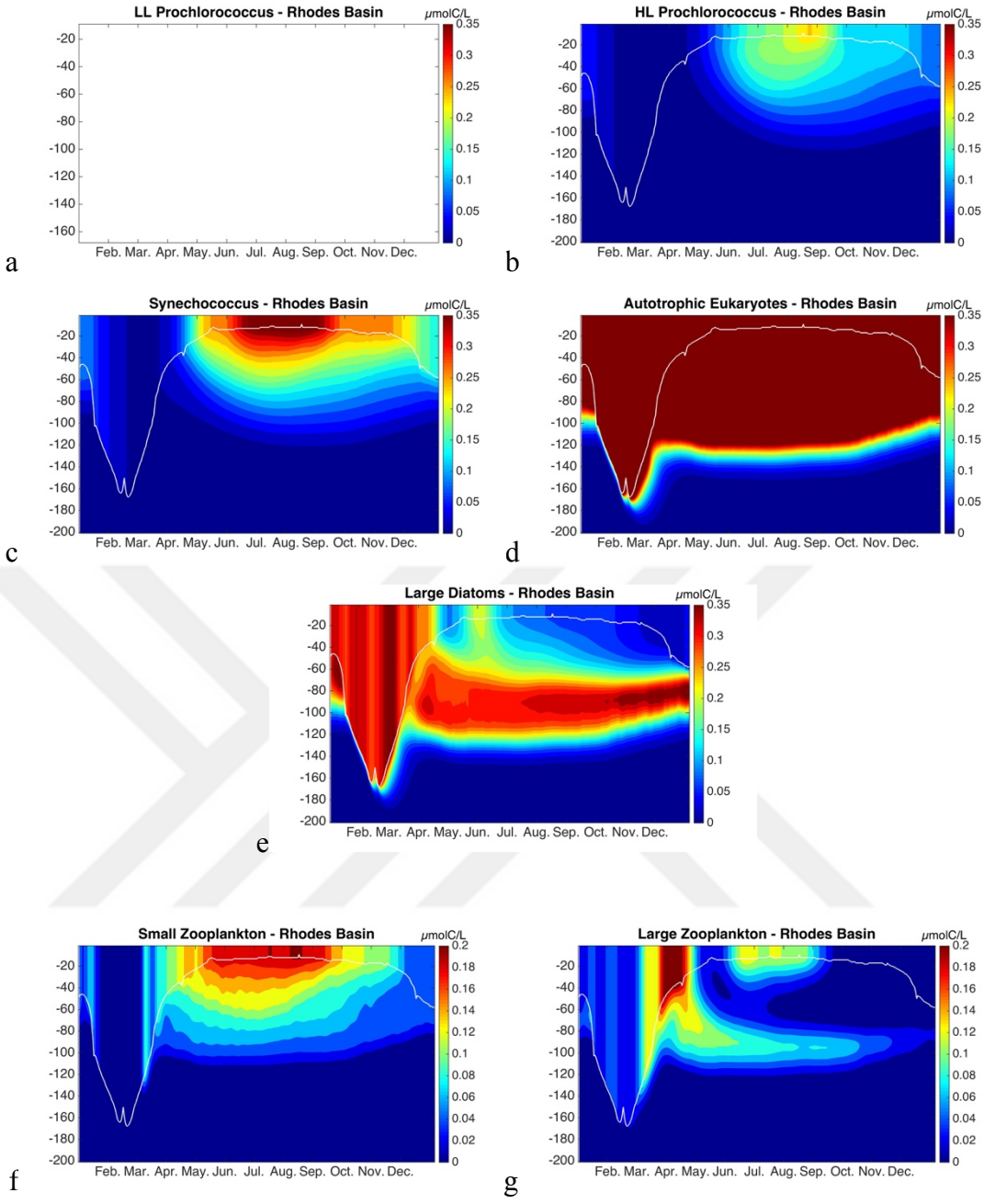

Figure 32. Yearly distributions of biomass (µmolC/L) of low light adapted *Prochlorococcus*, high light adapted *Prochlorococcus*, *Synechococcus*, autotrophic eukaryotes, diatoms and zooplankton groups in Rhodes Basin waters – White lines indicate the mixed layer depth

4.4.2. Chl-a & primary production

Modelled chlorophyll-a concentrations and primary production values during the year were highest in Rhodes upwelling area and followed by ETS and Mersin Offshore stations (Figure 33). In Rhodes area, highest chlorophyll-a values estimated as ~ 0.35 µg/L in March took place in depth between ~ 60 - 140 m from the surface. After winter mixing vanishes, chlorophyll at depth followed the pattern of autotrophic eukaryote and diatom abundances. Nutricline is located at the base of the euphotic zone in Rhodes Gyre due to upwelling of deep waters, leading to more pronounced deep chlorophyll maximum which took place between 70 – 120 m during spring – autumn period. Primary production was also the highest in Rhodes area, maximum value calculated as ~ 0.35 µmolCL^{-1} was at the beginning of the spring and June – September period. Total primary production is calculated as 7919 µmolCL^{-1}yr^{-1}.

For Erdemli coast, integrated chlorophyll-a concentration reached ~ 0.4 µg/L during the second half of the winter mixing. After the end of the winter mixing, lower values were illustrated between depth 80 – 130 m depths (Figure 33).Primary production values were peaked at 2 periods; one is at the beginning of April, and the other was between May – October maximum values were ~ 0.30 µmolC L^{-1}. Annual primary production was 6335 µmolCL^{-1}yr^{-1}. The intensity and depth of the spring bloom occurring during late March to early April in ETS were highest which made us conclude that the model catches the riverine effects on primary production, which characterized by an increase as the river input is high in spring.

Lowest primary production and chl-a values obtained for Mersin Bay offshore waters as the annual value of 3865 µmolCL^{-1}yr^{-1}. Chlorophyll – a Concentrations barely reach ~ 0.254 µg/L in March between 100 – 160 m and ~ 0.2 µg/L during spring – autumn seasons at depth ~ 120 m. Highest production calculated as 0.15 µmolCL^{-1} in March and 0.01 µmolCL^{-1} in the upper water column in spring – summer seasons

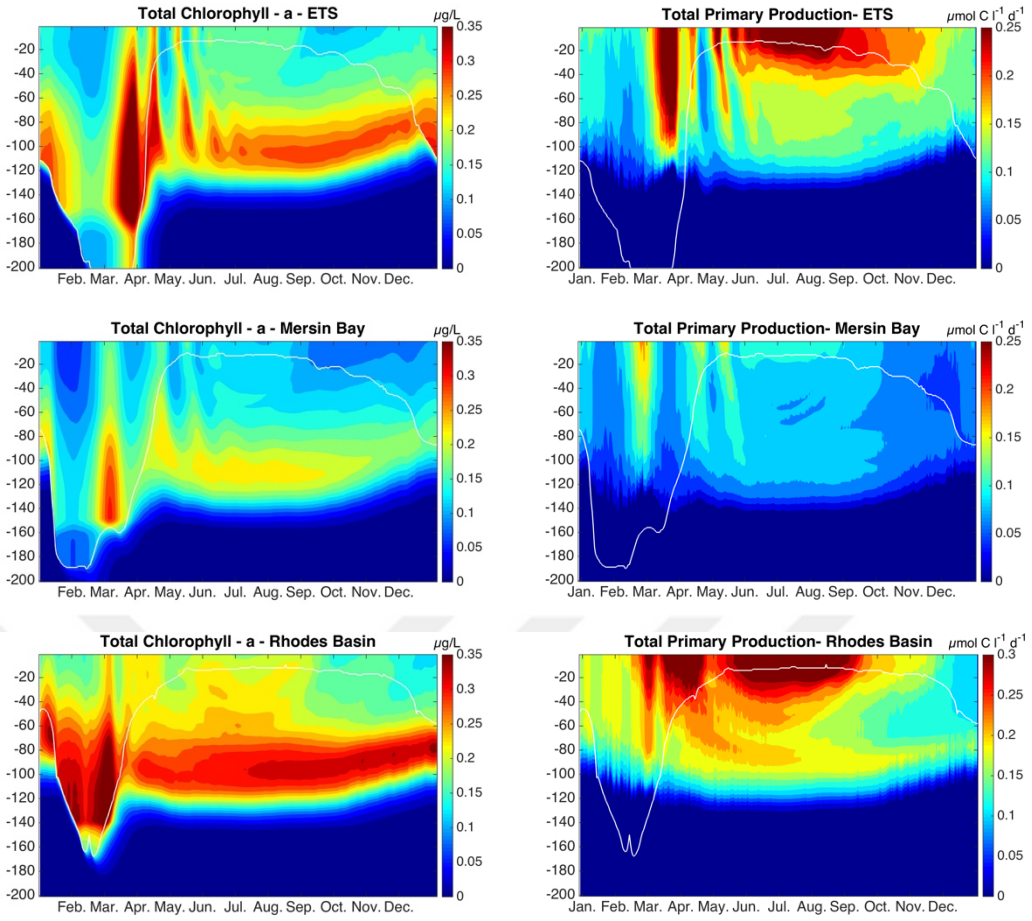

Figure 33. Chl-a and Primary production of ETS, Offshore waters of Mersin Bay and Rhodes upwelling area - white lines indicate mixed layer depth

Since chl-a are more active in light, even though more chl-a values observed in deeper layers in winter, production tends to be in surface layers. As well as light availability, size and C/Chl-a ratio of species also responsible for that difference in pattern between Chl-a and primary production. Species contribution to chl-a and primary production is discussed below.

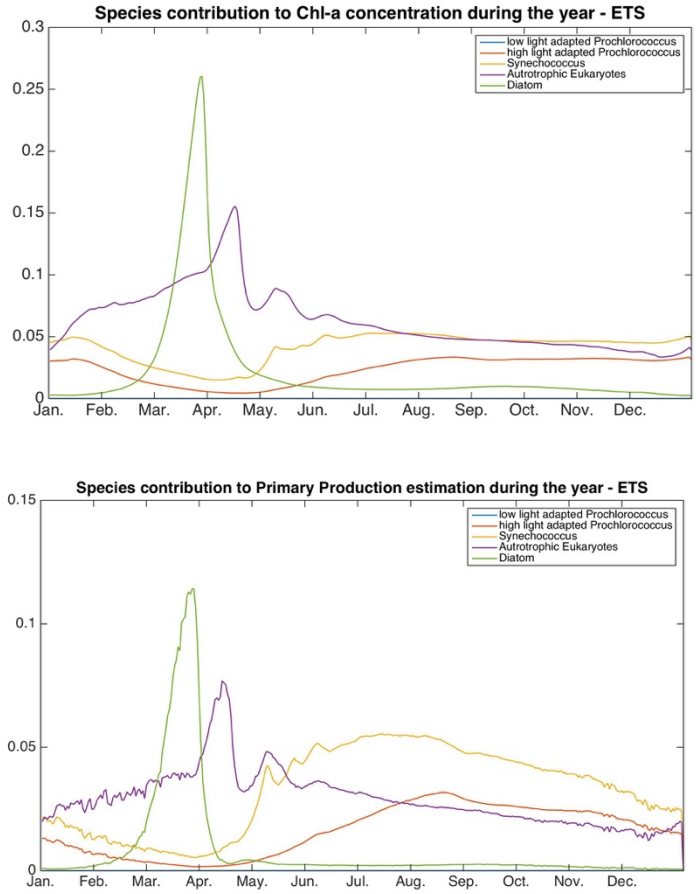

Figure 34. Species contribution to Primary Production estimation – ETS

During spring bloom period, highest contribution to chl-a and primary production concentrations was from autotrophic eukaryotes followed by diatoms with percentages around 48% and 35%, respectively in ETS (Figure 34). Rest of the year, *Synechococcus* was dominant providing 46% primary production while autotrophic eukaryotes were dominant in the contribution of chl-a with and 59% contribution. Considering the whole year, *Synechococcus* and autotrophic eukaryotes have the highest participation on chl – a (27% and 42%) and primary production (37% and 34%, respectively.)

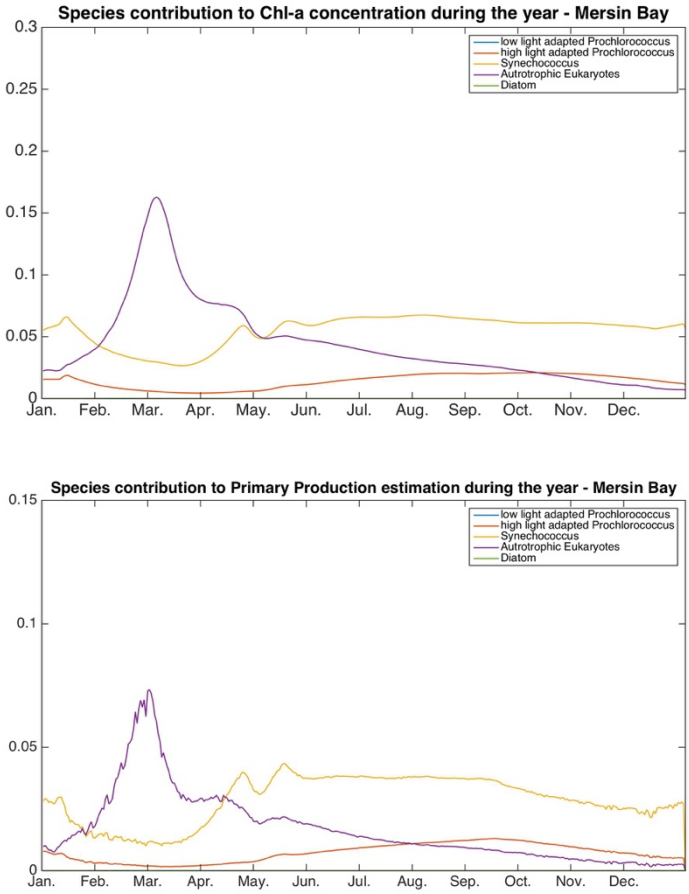

Figure 35. Species contribution to Primary Production estimation - Mersin Bay

Similar to ETS, in Mersin Bay *Synechococcus* and autotrophic eukaryotes species had the highest contribution throughout the year (Figure 35). In contrast, diatom species' population didn't grow well. *Synechococcus* contribution to chl-a and primary production participation were highest, 48% and 54% respectively. Autotrophic eukaryotes were the second most dominant species with 31% on primary production and 38.73% in chl – a.

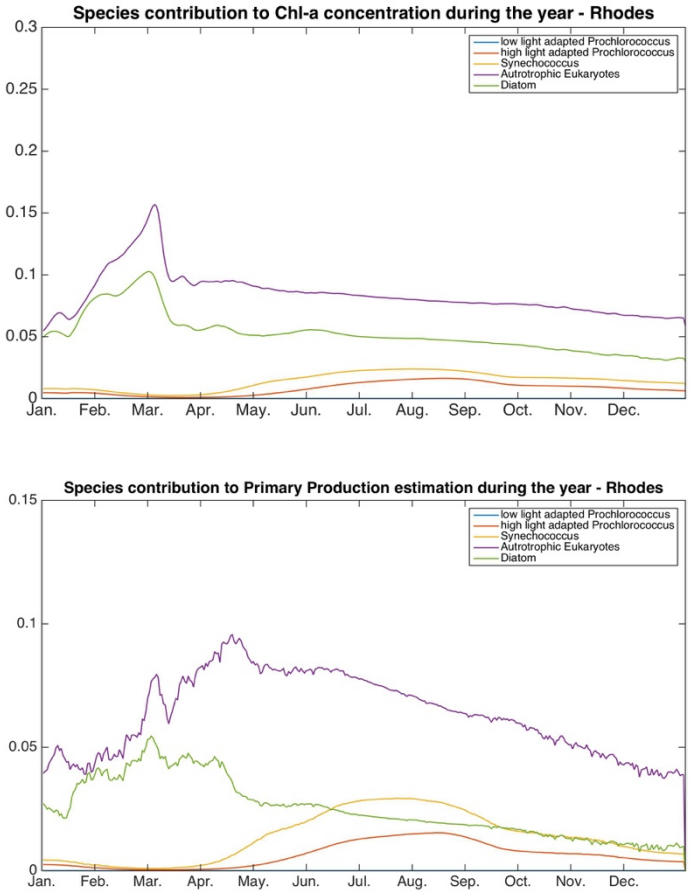

Figure 36. Species contribution to Primary Production estimation - Rhodes Basin

In Rhodes area, most dominant species contributing to chl-a abundance and primary production were autotrophic eukaryotes and diatoms (Figure 36). Their contribution to primary production was 57% and 38% and on chl – a 53% and 33% during the whole year. Their contribution increases during the winter mixing period and decreases between spring – autumn. The growth of the *Synechococcus* and *Prochlorococcus* were lowest in this area, providing just 16% and 7% of primary production, respectively.

The result for *Synechococcus* was consistent with the result found in Denis et al. (2010) which considered Rhodes Basin as low in concentration of *Synechococcus* and find its contribution to total biomass as 15%. They also found *Prochlorococcus* contribution was as low as 1.2 %, as our calculation were a slightly higher.

4.5. Nutrient Limitation in the Northern Levantine Basin

Mediterranean Sea is widely known as highly phosphate limited oligotrophic ecosystem. However, there is evidence from some of the studies that show, during few months, nitrate can be limiting or co-limiting nutrient on the production in Mediterranean. (Krom et al., 1991; Selmer, Ferrier-Pages, Cellario, & Rassoulzadegan, 1993). An analyses carried out to understand if the nitrogen-phosphorus co-limitation similar to the Northeastern Mediterranean Basin occur even if for a shorter time interval and with lesser intensity in Eastern Mediterranean. Uptake of both NO3 and NH4 and species' cellular stoichiometry of N and P were examined as proxies of nitrogen limitation on production,

In all regions, during late winter – early spring period NO_3 uptake was higher where in summer NH_4 uptake increases. This increase was highest in Rhodes upwelling area and lowest in Mersin Bay.

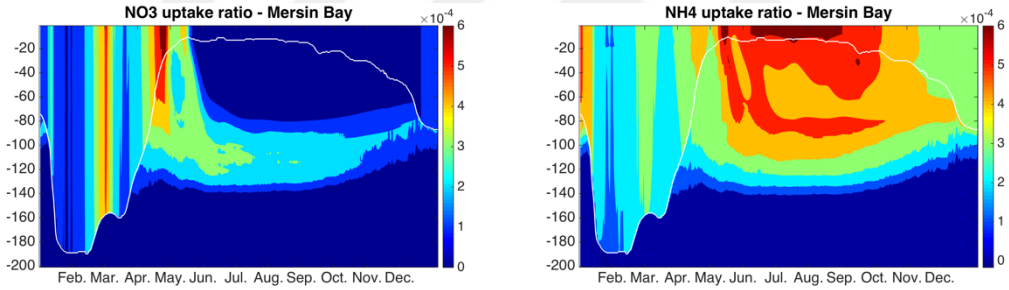

Figure 37. NO3, NH4 uptake in ETS

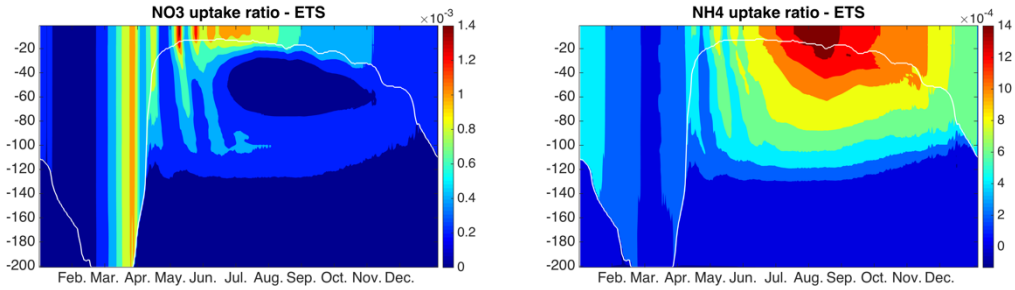

Figure 38. NO3, NH4 uptake in ETS

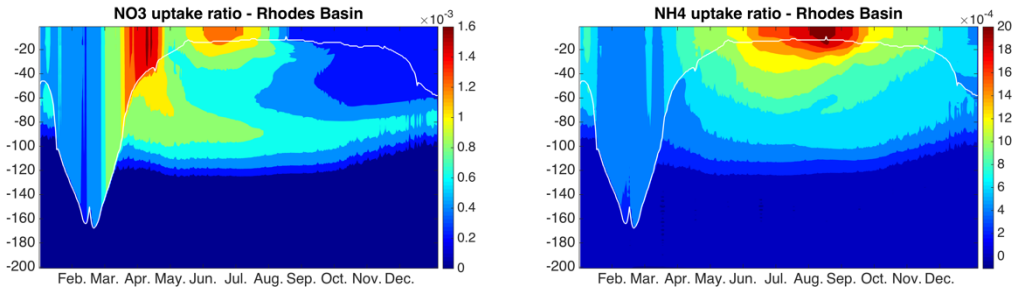

Figure 39. NO3, NH4 uptake in Rhodes Basin

Species cellular N:C, P:C and Si:C ratios are calculated to see if any of these nutrients limit the productivity. Each species has maximum allowed capacity of nutrients in the model. If the species couldn't reach this maximum value in their cells, then that nutrient is limiting for that species (maximum value falls in red color in Figure 40, Figure 41, and Figure 42). In Mersin Bay from spring to autumn, since their cells P:C ratio didn't reach the maximum value, we concluded phosphate limited the growth of *Synechococcus* growth between 0 – 120 m depth interval. Phosphate also was a limiting nutrient for autotrophic eukaryotes and diatoms starting from the surface to 120 – 130m depth. However, in this area nitrogen also seemed to limit the productivity of autotrophic eukaryotes during summer – autumn and of large diatoms from early – summer to fall period. Silicate was not a limiting nutrient for diatoms since this species is already limited by phosphorus and nitrogen.

In ETS, during winter mixing, all species were at their maximum N:C and P:C capacity. During spring – autumn period, upper ~ 120 m of the water column was depleted in phosphorus for the needs of autotrophic eukaryotes and diatoms. Similar to Mersin Bay, diatom species seemed to be slightly limited by nitrogen during July – October.

Model results suggest that there was no nutrient limitations for *Prochlorococcus* and *Synechococcus* species at Rhodes basin because they all reach their maximum N:C and P:C values. However, starting from the beginning of April species couldn't reach the maximum capacity of P:C, which implies there is a phosphate limitation for autotrophic eukaryotes and diatoms in upper ~ 80 m of the water column. Silicate was not a limiting factor for modelled diatom.

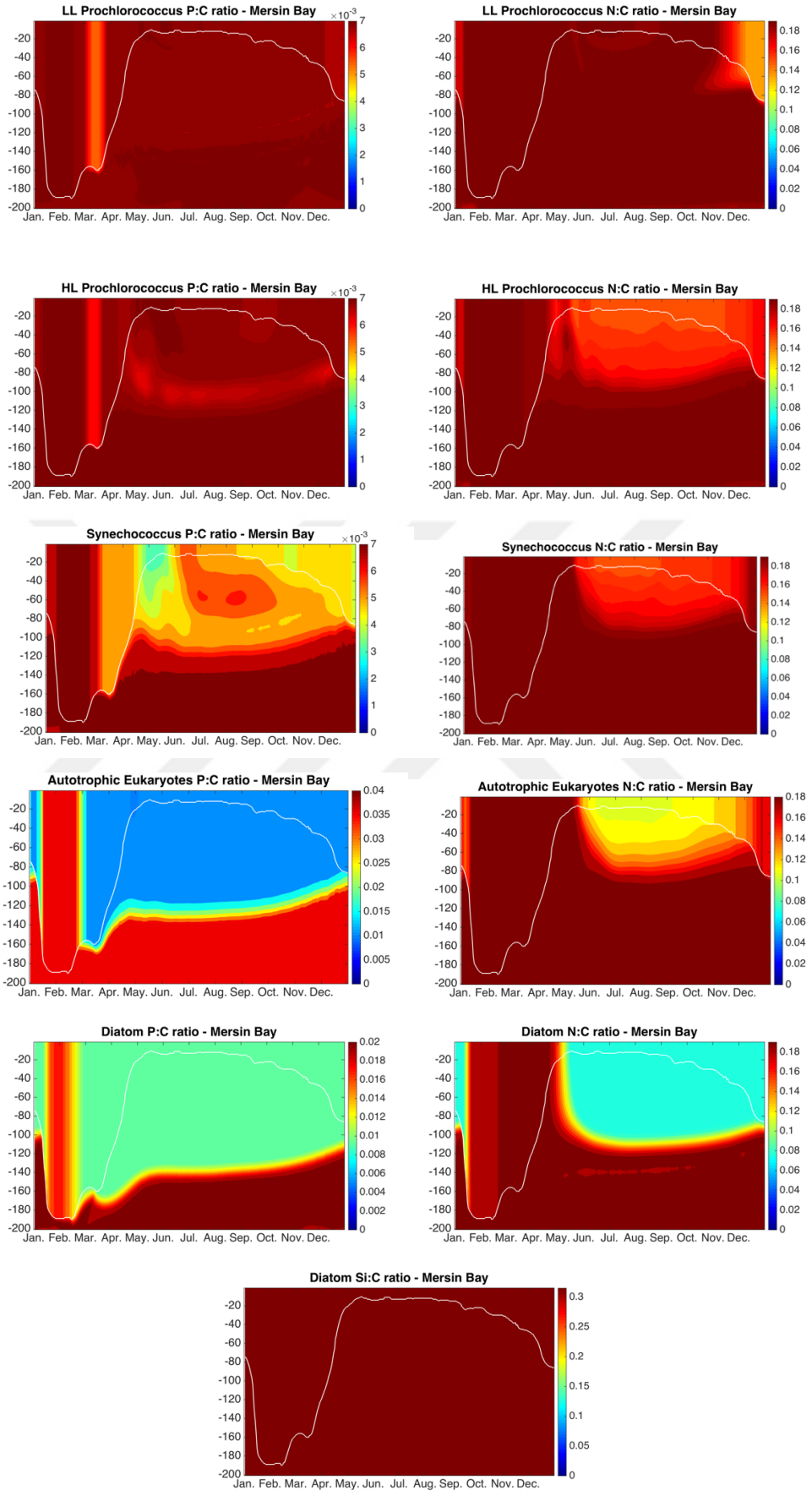

Figure 40. Cellular N:C, P:C and Si:C ratios of species in Mersin Bay

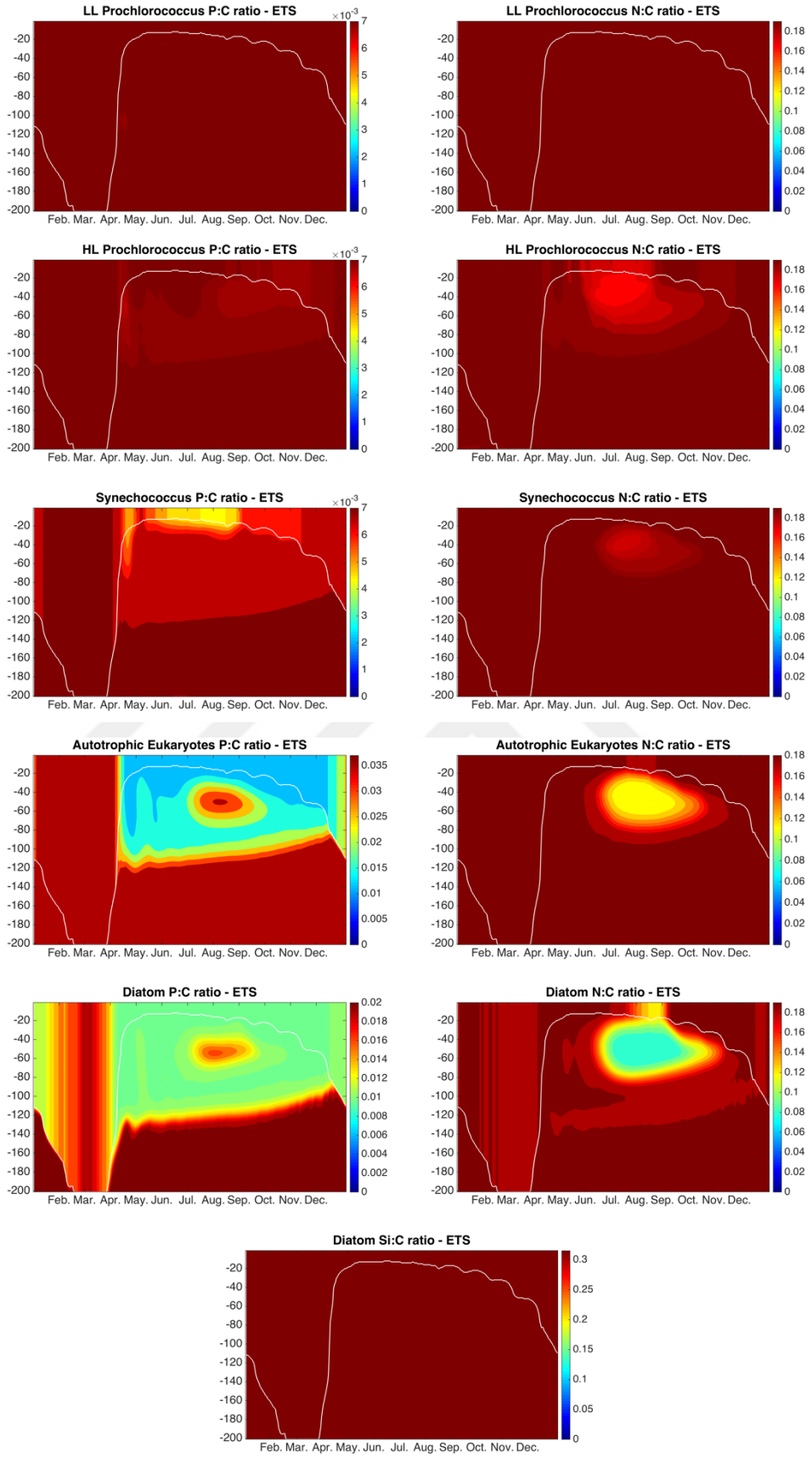

Figure 41. Cellular N:C, P:C and Si:C ratios of species in ETS

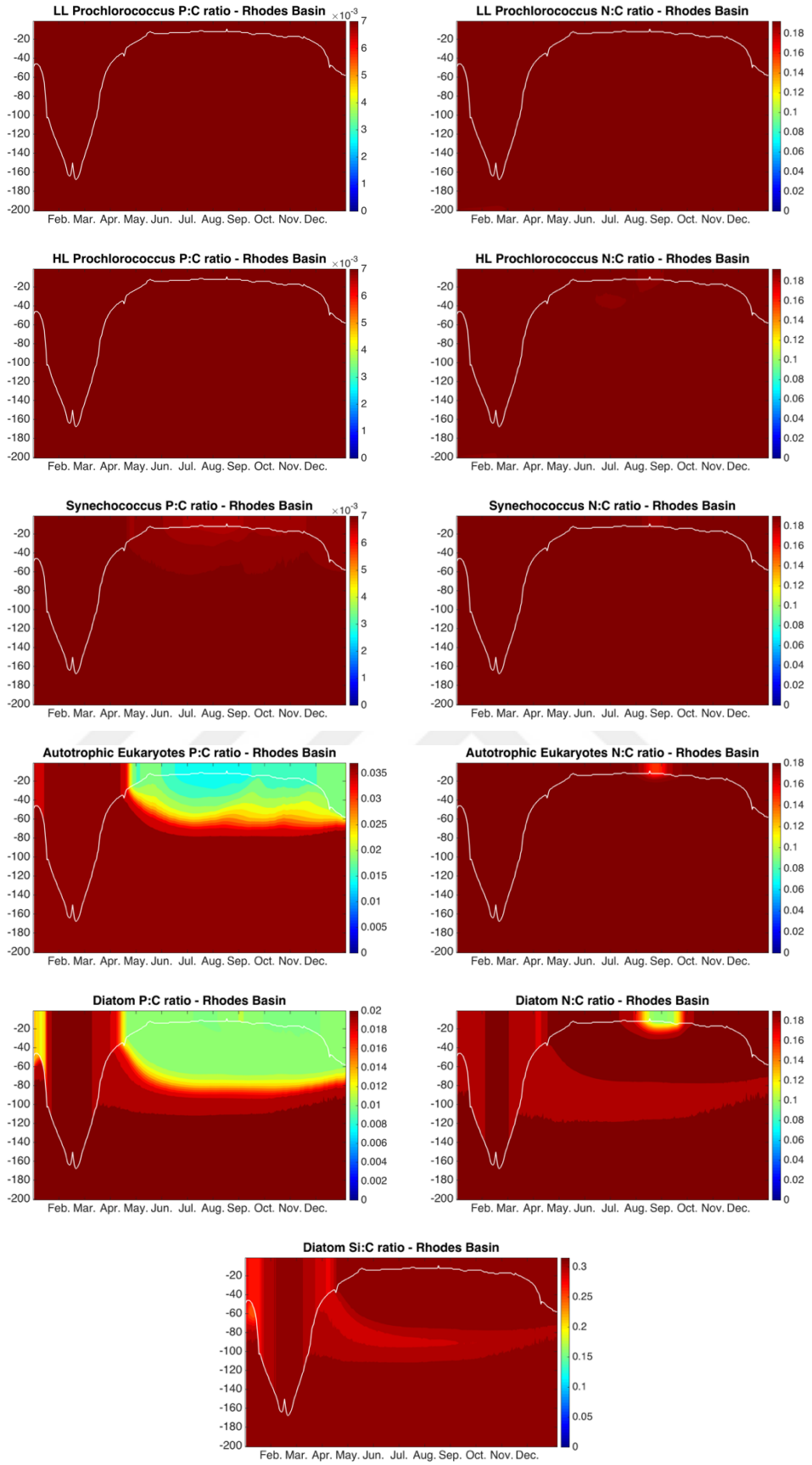

Figure 42. Cellular N:C, P:C and Si:C ratios of species in Rhodes upwelling area.

CHAPTER 5

CONCLUDING REMARKS

In this thesis, 3 areas with distinctive characteristics as physical conditions and nutrient contents, in oligotrophic Northern Levantine Basin are analysed. Because the system is oligotrophic, any nutrient input to the system causes an alteration in the ecosystem structure. Model results illustrate the effects of nutrient dynamics on primary production.

Winter mixing had a high impact in all areas causing a great increase of nutrients in the mixed layer. The thickness of this layer was shallowest in Rhodes area due to upwelling of waters, and deeper in Cilician. In all regions, remineralization of nutrients was of great importance in primary production. Recycled nutrients were found responsible more than 75% of primary production for all regions. This percentage were lowered during winter mixing.

Deep Chlorophyll Maximum is a characteristic of oligotrophic eastern Mediterranean Sea, and in all sites, this feature is illustrated. However, in Rhodes upwelling area, this depth was shallower and more pronounced due to the upwelling of deep waters with high nutrient contents to the euphotic zone. Since the nutrients were introduced to the system with upwelling upper layers, the growth of autotrophic eukaryotes and diatoms growth were in higher levels

In Rhodes upwelling area, annual primary production was estimated as 7919 μmol C $L^{-1}yr^{-1}$. Spring bloom observed in March earlier than ETS. Even though primary production estimate of ETS (6335 μmol C $L^{-1}yr^{-1}$) was not as high as Rhodes area, intensity and depth of the spring bloom were highest due to riverine input to the area

in late March to early April. Lowest primary productivity observed in offshore waters of Mersin Bay have the lowest annual budget as 3865 μmol C $L^{-1}yr^{-1}$.

Smaller sized species (*Synechococcus* & *Prochlorococcus*) were more abundant in oligotrophic Mersin Bay offshore waters. In Mersin Bay, the contribution of *Synechococcus* was greatest where autotrophic eukaryotes were the second highest primary production ratio. Diatoms only grew at coastal and upwelling areas. At the ETS site, autotrophic eukaryotes and *Synechococcus* were important primary producers, on the other hand, diatom species had great contribution during the winter period. In Rhodes, a little activity of *Synechococcus* and *Prochlorococcus* species simulated, whereas autotrophic eukaryotes and diatom species production were highest.

Phosphate was found to be the limiting nutrient in all regions especially for diatom and autotrophic eukaryotes. However, based on model results, N is also considered to be a co-limiting nutrient for autotrophic eukaryotes and large diatom*s*, in the summer season, in offshore waters of Mersin Bay. This situation is partly valid for diatom species in ETS. Si was not observed as a limiting nutrient for large diatoms.

To interpret the characteristics of the ETS area, only nutrients from boundaries were used to constrain the model. However, considering that significant riverine and atmospheric input fluctuations occur inter-annually, monthly and even weekly basis, comprehensive studies should be carried out to monitor sensitive dynamics of the system which is off the interest of this thesis.

Another important debate is on the physical conditions of the Rhodes gyre area. During harsh winter conditions (Napolitano et al., 2000; Yilmaz & Tugrul, 1998) (and especially those based on POEM Results, 1992) in the core of the Rhodes Cyclonic Gyre, with the effect of cooling events of intense winter conditions, winter mixing breaks the stratification and water column becomes uniform in structure, i.e. uniform temperature and salinity profiles were observed. The occurrence of the chimney formation observed for a very short time interval – several days – during late January to early February. However, visualizing the 26-years CTD data used for this study (which was considered as dense enough to cover the winter season), no

such a structure was observed except for a few days on winter of years 1992 – 1993 that were reported as extreme cold years in literature resulted from Pinatubo volcanic eruption (Fasullo et al., 2016). Hence, we conclude that either such event couldn't be captured by the data collection period of relevant cruises, or this structure occurs only in exceptionally harsh winter conditions. To solve this dilemma, spatially and temporarily broader monitoring need to be done.

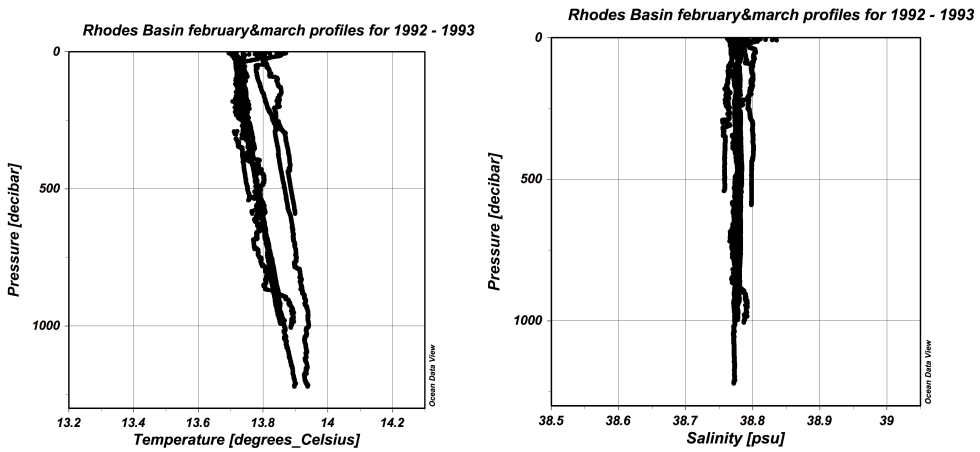

Figure 43. Rhodes Basin profiles for 1992 – 1993

Lastly, as mentioned in Chapter 4.1, to further calibrate the model and to fit the Mediterranean Sea environment, more identifying temperature-dependent remineralization function should be used. The Mediterranean Sea displays distinctive features comparing to other oceans and by this means it requires a proper approach to numerically interpret the remineralization rates.

REFERENCES

Akyüz, E.F., 1957. Observations sur le rouget barbet (Mullus barbatus) du Golfe d'Iskenderun et son milieu. Proc. gen. fish. counc. Med., 4: 305--326.

Antoine, D., & Morel, A. (1995). Observations, Algal pigment distribution and primary production in the eastern Mediterranean as derived from coastal zone color scanner. *Journal of Geophysical Research*. http://doi.org/10.1029/95jc00466

Bertilsson, S., Berglund, O., Karl, D. M., & Chisholm, S. W. (2003). Elemental composition of marine *Prochlorococcus* and *Synechococcus*: Implications for the ecological stoichiometry of the sea. *Limnology and Oceanography*, *48*(5), 1721–1731. http://doi.org/10.4319/lo.2003.48.5.1721

Béthoux, J. P., & Copin-Montégut, G. (1986). Biological fixation of atmospheric nitrogen in the Mediterranean Sea. *Limnology and Oceanography*, *31*(6), 1353–1358. http://doi.org/10.4319/lo.1986.31.6.1353

Bethoux, J. P., Morin, P., Madec, C., & Gentili, B. (1992). Phosphorus and nitrogen behaviour in the Mediterranean Sea. *Deep Sea Research Part A, Oceanographic Research Papers*, *39*(9), 1641–1654. http://doi.org/10.1016/0198-0149(92)90053-V

Carter D. 8., 1956. The water balance of the Mediterranean and Black Seas, Pub!. Climatol. Centerton, N.J., Drexel Inst. Technol., Lab. Climatol. 9, 123-175.

Christian, J. R., & Karl, D. M. (1995). Bacterial ectoenzymes in marine waters: Activity ratios and temperature responses in three oceanographic provinces. *Limnology and Oceanography*, *40*(6), 1042–1049. http://doi.org/10.4319/lo.1995.40.6.1042

Collins, M. B., & Banner, F. T. (1979). Secchi disc depths, suspensions and circulation, northeastern Mediterranean Sea. *Marine Geology*, *31*(1–2), M39–M46. http://doi.org/10.1016/0025-3227(79)90051-3

Denis, M., Thyssen, M., Martin, V., Manca, B., Vidussi, F. (2010). Ultraphytoplankton basin-scale distribution in the Eastern Mediterranean Sea in winter: link to hydrodynamism and nutrients. Biogeosciences 7:2227 - 2244.

doi:10.5194/bg - 7 - 2227 - 2010

Dogan-Saglamtimur, N., Tugrul, S., 2004. Effects of riverine nutrients on coastal water ecosystems: a case study from the Northeastern Mediterranean shelf. Fresenius Environ. Bull. 13, 1288–1294.

D'Ortenzio, F. (2005). Seasonal variability of the mixed layer depth in the Mediterranean Sea as derived from in situ profiles. *Geophysical Research Letters*, *32*(12), L12605. http://doi.org/10.1029/2005GL022463

Ediger, V., Evans, G., & Ergin, M. (1997). Recent surficial shelf sediments of the Cilician Basin (Turkey), northeastern Mediterranean. *Continental Shelf Research*, *17*(13), 1659–1677. http://doi.org/10.1016/S0278-4343(97)00030-7

Engel, I. (1967) Currents in the Eastem Mediterranean. International Hydrographic Review, 44, 23-40.

Fasullo, J. T., Nerem, R. S., Hamlington, B., Church, J. A., Stocker, T. F., Nerem, R. S., … Church, J. A. (2016). Is the detection of accelerated sea level rise imminent? *Scientific Reports*, *6*(April), 31245. http://doi.org/10.1038/srep31245

Franks, P. J. S., Wroblewski, J. S., & Flierl, G. R. (1986). Behavior of a simple plankton model with food-level acclimation by herbivores. *Marine Biology*, *91*(1), 121–129. http://doi.org/10.1007/BF00397577

Koçak, M., Kubilay, N., Tuğrul, S., & Mihalopoulos, N. (2010). Long-term atmospheric nutrient inputs to the Eastern Mediterranean: sources, solubility and comparison with riverine inputs. *Biogeosciences Discussions*, *7*(4), 5081–5117. http://doi.org/10.5194/bgd-7-5081-2010

Krom, M. D., Emeis, K. C., & Van Cappellen, P. (2010). Why is the Eastern Mediterranean phosphorus limited? *Progress in Oceanography*, *85*(3–4), 236–244. http://doi.org/10.1016/j.pocean.2010.03.003

Krom, M. D., N., K., & L.I., G. (1991). Phosphorus limitation of primary productivity in the eastern Mediterranean Sea. *Limnol. Oceanogr*, *36*(3), 424–432. http://doi.org/10.4319/lo.1991.36.3.0424

Krom, M. D., Woodward, E. M. S., Herut, B., Kress, N., Carbo, P., Mantoura, R. F. C., … Zodiatis, G. (2005). Nutrient cycling in the south east Levantine basin of the eastern Mediterranean: Results from a phosphorus starved system. *Deep-Sea Research Part II: Topical Studies in Oceanography*, *52*(22–23), 2879–2896. http://doi.org/10.1016/j.dsr2.2005.08.009

Lascaratos, A., Williams, R. G., & Tragou, E. (1993). A mixed-layer study of the

formation of Levantine intermediate water. *Journal of Geophysical Research*, *98*(October 2012), 14739. http://doi.org/10.1029/93JC00912

Leonardos, N., & Geider, R. J. (2004). Responses of elemental and biochemical composition of Chaetoceros muelleri to growth under varying light and nitrate:phosphate supply ratios and their influence on critical N : P. *Limnology and Oceanography*, *49*(6), 2105–2114. http://doi.org/10.4319/lo.2004.49.6.2105

Lionello, P., Malanotte-Rizzoli, P., Boscolo, R., Alpert, P., Artale, V., Li, L., … Xoplaki, E. (2006). The Mediterranean climate: An overview of the main characteristics and issues. *Developments in Earth and Environmental Sciences*, *4*(C), 1–26. http://doi.org/10.1016/S1571-9197(06)80003-0

Ludwig, W., Dumont, E., Meybeck, M., & Heussner, S. (2009). River discharges of water and nutrients to the Mediterranean and Black Sea: Major drivers for ecosystem changes during past and future decades? *Progress in Oceanography*, *80*(3–4), 199–217. http://doi.org/10.1016/j.pocean.2009.02.001

Malanotte-rizzoli, P., & Hecht, A. (1988). Large-scale properties of the . Eastern Mediterranean : a review. *Oceanologica Acta*, *11*, *n4*(4), 323–335. http://doi.org/10.1016/S0967-0645(99)00020-X

Malanotte-rizzoli, Paola, V. N. E. (1998). *The Eastern Mediterranean as a Laboratory Basin for the Assessment of Contrasting Ecosystems*. (P. Malanotte-Rizzoli & V. N. Eremeev, Eds.)*NATO Science Series* (Vol. 53). Dordrecht: Springer Netherlands. http://doi.org/10.1007/978-94-011-4796-5

Marullo, S. (2003). Variability of Rhodes and Ierapetra Gyres during Levantine Intermediate Water Experiment: Observations and model results. *Journal of Geophysical Research*, *108*(C9), 8119. http://doi.org/10.1029/2002JC001393

Milliff, R. F., & Robinson, A. R. (1992). Structure and Dynamics of the Rhodes Gyre System and Dynamical Interpolation for Estimates of the Mesoscale Variability. *Journal of Physical Oceanography*. http://doi.org/10.1175/1520-0485(1992)022<0317:SADOTR>2.0.CO;2

Moore, L. R., Post, A. F., Rocap, G., & Chisholm, S. W. (2002). Utilization of different nitrogen sources by the marine cyanobacteria *Prochlorococcus* and *Synechococcus*. *Limnology and Oceanography*, *47*(4), 989–996. http://doi.org/10.4319/lo.2002.47.4.0989

Napolitano, E., Oguz, T., Malanotte-Rizzoli, P., Yilmaz, A., & Sansone, E. (2000). Simulations of biological production in the Rhodes and Ionian basins of the

eastern Mediterranean. *Journal of Marine Systems*, *24*(3–4), 277–298. http://doi.org/http://dx.doi.org/10.1016/S0924-7963(99)00090-1

Nielsen J. N., 1912. Hydrography of the Mediterranean and adjacent waters, Rep. Dan. Oceanogr. Exped. 1908-1910, 77-192.

Onken, R., & Yuce, H. (2000). Winter circulation and convection in the Antalya Basin (Eastern Mediterranean). *Journal of Physical Oceanography*, *30*(5), 1099–1110. http://doi.org/10.1175/1520-0485(2000)030<1099:WCACIT>2.0.CO;2

Ovchinnikov, I. M. (1966) Circulation in the surface intermediate of the Mediterranean. Oceanology 6, 48-57.

Ovchinnikov, I.M. & Plakhin, A. (1984) Fonnation of the Intennediate Waters of the Mediterranean Sea in the Rhodes Cyclonic Gyre, Oceanology, 24, 317-319.Ozsoy E., Latif H. A., Unluata U., 1981. On the formation of Levantine Intermediate Water, Rapp. Comm. Inter. Mer Médit., 27, 51-65.

Özsoy, E., Hecht, a., & Ünlüata, Ü. (1989). Circulation and hydrography of the Levantine Basin. Results of POEM coordinated experiments 1985–1986. *Progress in Oceanography*, *22*, 125–170. http://doi.org/10.1016/0079-6611(89)90004-9

Özsoy, E., Hect, A., Unluata, U., Brenner, S., Oguz, T., Bishop, J., Latif, M.A., Rosentraub, Z., 1991. A review of the Levantine Basin circulation and its variability during 1985–1988. Dyn. Atmos. Oceans 15, 421–456.

Özsoy, E., Hecht, a., Ünlüata, Ü., Brenner, S., Sur, H. I., Bishop, J., … Oğuz, T. (1993). A synthesis of the Levantine Basin circulation and hydrography, 1985–1990. *Deep Sea Research Part II: Topical Studies in Oceanography*, *40*(6), 1075–1119. http://doi.org/10.1016/0967-0645(93)90063-S

Pollak M. 1., 1951. The sources of deep water of the eastern Mediterranean Sea, J. Mar. Res., 10, 128-152.

Pujo-Pay, M., Conan, P., Oriol, L., Cornet-Barthaux, V., Falco, C., Ghiglione, J. F., … Prieur, L. (2011). Integrated survey of elemental stoichiometry (C, N, P) from the western to eastern Mediterranean Sea. *Biogeosciences*, *8*(4), 883–899. http://doi.org/10.5194/bg-8-883-2011

Robinson, A. R., Hecht, A., Michelato, A., Roether, W., Theocharis, A., Unliiata, U., … POEM group. (1992). General circulation of the Eastern Mediterranean. *Earth-Science Reviews*, *32*(4), 285–309.

http://doi.org/http://dx.doi.org/10.1016/0012-8252(92)90002-B

Roether, W., Roussenov, V. M., & Well, R. (1994). A tracer study of the thermohaline circulation of the eastern Mediterranean. *Ocean Processes in Climate Dynamics: Global and Mediterranean Examples*, 371–394.

Salihoglu, B., Garçon, V., Oschlies, a., & Lomas, M. W. (2008). Influence of nutrient utilization and remineralization stoichiometry on phytoplankton species and carbon export: A modeling study at BATS. *Deep Sea Research Part I: Oceanographic Research Papers*, *55*(1), 73–107. http://doi.org/10.1016/j.dsr.2007.09.010

Salihoğlu, İ., Saydam, C., Baştürk, Ö., Yilmaz, K., Göçmen, D., Hatipoğlu, E., & Yilmaz, A. (1990). Transport and distribution of nutrients and chlorophyll-a by mesoscale eddies in the northeastern Mediterranean. *Marine Chemistry*, *29*, 375–390. http://doi.org/10.1016/0304-4203(90)90024-7

Salihoglu, B., Garçon, V., Oschlies, a., & Lomas, M. W. (2008). Influence of nutrient utilization and remineralization stoichiometry on phytoplankton species and carbon export: A modeling study at BATS. *Deep Sea Research Part I: Oceanographic Research Papers*, *55*(1), 73–107. http://doi.org/10.1016/j.dsr.2007.09.010

Salihoğlu, B., 2005. Modeling the effects of physical and biogeochemical processes on phytoplankton species and carbon production in the equatorial pacific ocean. Ph.D. Thesis, Old Dominion University, Norfolk, Virginia, United States.

Selmer, J.-S., Ferrier-Pages, C., Cellario, C., & Rassoulzadegan, F. (1993). New and regenerated production in relation to the microbial loop in the NW Mediterranean Sea. *Marine Ecology Progress Series*, *100*(1–2), 71–83. http://doi.org/10.3354/meps100071

Siokou-Frangou I, Gotsis-Skretas O, Christou ED, Pagou K (1999). Plankton characteristics in the Aegean, Ionian and NW Levantine Seas. In: Malanotte-Rizzoli P, Eremeev VN (eds) The Eastern Mediterranean as a laboratory basin for the assessment of contrasting ecosystems. Kluwer, Dordrecht, pp 205–223

Ünlüata, Ü., Oguz, T., & Özsoy, E. (1983). Blocking of steady circulation by coastal geometry. *Journal of Physical Oceanography*, *13*(6), 1055–1062. http://doi.org/10.1175/1520-0485(1983)013<1055

Uysal, Z., & Koksalan, I. (2010). *Synechococcus* dynamics in the Levantine basin shelf waters (northeastern Mediterranean). *Mediterranean Marine Science*,

11(2), 277–294.

Uysal, Z., & Köksalan, I. (2006). The annual cycle of *Synechococcus* (cyanobacteria) in the northern Levantine Basin shelf waters (Eastern Mediterranean). *Marine Ecology*, *27*(3), 187–197. http://doi.org/10.1111/j.1439-0485.2006.00105.x

Uysal, Z. et al., 2008. Kilikya baseni kıyısal ekosisteminde dolaşım, taşınım ve ötrofikasyon araştırmaları (Cilician basin coastal ecosystem circulation, transportation and eutrophication research). TUBİTAK 104Y277 kodlu proje. Proje raporu. 522 s. In Turkish.

Wüst, G. (1961). On the vertical circulation of the Mediterranean Sea. *Journal of Geophysical Research*, *66*(10), 3261. http://doi.org/10.1029/JZ066i010p03261

Yilmaz, A., & Tugrul, S. (1998). The effect of cold- and warm-core eddies on the distribution and stoichiometry of dissolved nutrients in the northeastern Mediterranean. *Journal of Marine Systems*, *16*(3–4), 253–268. http://doi.org/10.1016/S0924-7963(97)00022-5

Yücel, N., 2013. Monthly changes in primary and bacterial productivity in the north-eastern Mediterranean shelf waters, PhD dissertation, Institute of Marine Sciences, METU, Mersin, Turkey

Yilmaz, A. Z., & Besiktepe, S. (2010). Annual variations in biochemical composition of size fractionated particulate matter and zooplankton abundance and biomass in Mersin Bay, NE Mediterranean Sea. *Journal of Marine Systems*, *81*(3), 260–271. http://doi.org/10.1016/j.jmarsys.2010.01.002

Zohary, T., Herut, B., Krom, M. D., Fauzi C. Mantoura, R., Pitta, P., Psarra, S., … Malcolm S. Woodward, E. (2005). P-limited bacteria but N and P co-limited phytoplankton in the Eastern Mediterranean—a microcosm experiment. *Deep Sea Research Part II: Topical Studies in Oceanography*, *52*(22–23), 3011–3023. http://doi.org/10.1016/j.dsr2.2005.08.011